AN EXPERIMENTAL STUDY OF THE MERIDIONAL TEMPERATURE DISTRIBUTION AND ENERGY TRANSFORMATION IN THE LOWER STRATOSPHERE

by

LI PENG

B.S., National Taiwan University
(1960)
M.A., University of California
(1962)

SUBMITTED IN PARTIAL FULFILLMENT
OF THE REQUIREMENTS FOR THE
DEGREE OF DOCTOR OF
PHILOSOPHY
at the
MASSACHUSETTS INSTITUTE OF
TECHNOLOGY
January, 1965

Signature of Author . . . . . .
Department of Meteorology, 19 January 1965

Certified by. . . . . .
Thesis Supervisor

Accepted by . . . . . .
Chairman, Departmental Committee on Graduate Students

AN EXPERIMENTAL STUDY OF THE MERIDIONAL TEMPERATURE DISTRIBUTION AND ENERGY TRANSFORMATION IN THE LOWER STRATOSPHERE

by

Li Peng

Submitted to the Department of Meteorology on 19 January 1965 in partial fulfillment of the requirements for the degree of Doctor of Philosophy

ABSTRACT

A highly simplified model based on the quasi-geostrophic approximation is employed to investigate the meridional temperature profile in the lower stratosphere and its relation to the energy transformations. An equator-to-pole temperature increase is reproduced in the model with an external heating function which heats the atmosphere in low latitudes and cools the atmosphere in high latitudes in each layer. The magnitude of the equator-to-pole temperature increase is comparable to the observed value. The major process responsible for the equator-to-pole temperature increase is found to be the up-gradient transport of heat due to large-scale eddies. It is found that the up-gradient heat transport in the upper layer takes place generally when eddy kinetic energy is converted into eddy available potential energy in the upper layer and eddy available potential energy is converted into eddy kinetic energy in the lower layer. In other words the up-gradient heat transport in the upper layer is due to the passive nature of the upper layer. There is an indication that there exists a critical value of the ratio of the latitudinal differential heating in the upper layer to the latitudinal differential heating in the lower layer, which may be a function of other parameters, such that above the critical value no equator-to-pole temperature increase can be maintained in the upper layer. Below the critical value, the magnitude of the equator-to-pole temperature increase does not seem to depend significantly upon the upper layer differential heating.

The mean energy transformations in the upper layer are in good agreement with the observations in the lower stratosphere. The non-adiabatic effect dissipates eddy and zonal available potential energies. The former receives its supply from the latter, and the latter receives its supply from the eddy kinetic energy which receives its supply from the lower layer.

Thesis Supervisor: Edward N. Lorenz
Title: Professor of Meteorology

ACKNOWLEDGEMENTS

The author is very grateful to Professor Edward N. Lorenz for his continual interest and advice during the course of this study, Professors Victor P. Starr and Reginald E. Newell for their support, encouragement and interesting discussions.

The author is indebted to Mrs. Barbara Goodwin for her help in preparing the manuscript, Miss Ruth Benjamin for typing the manuscript, and Miss Isabel Kole for drafting the figures.

Thanks are also due to the MIT computation center for making available their IBM computer without which this study would not have been possible, and to Mrs. Judy Copeland for her assistance in programming the computation.

TABLE OF CONTENTS

LIST OF TABLES

LIST OF FIGURES

1. INTRODUCTION

One of the most interesting features of the thermal structure of the atmosphere is the positive meridional temperature gradient in the lower stratosphere, i.e., the temperature in the lower stratosphere increases as one passes from lower latitudes to higher latitudes. This temperature gradient is apparently contrary to the distribution of solar radiation and to the distribution of terrestrial long wave radiation. Ever since it was discovered meteorologists have searched for a satisfactory explanation of its existence. However, as the atmosphere is radiative, heterogeneous and constantly in motion and the processes related to the temperature distribution are very complex, a lack of coherent and quantitative understanding of the positive meridional temperature gradient is still felt at the present time.

Presumably, the temperature of any part of the atmosphere ultimately depends upon external and imbedded heat sources. It is then natural that in searching for the causes of the positive meridional temperature gradient in the lower stratosphere, meteorologists first looked into the imbedded heat sources of that part of the atmosphere. In 1943 Möller suggested that the overlapping of the ozone band at 14 μ and the carbon dioxide band at 14 μ might be responsible for the positive temperature gradient. As the total amount of ozone increases with

increasing latitude, its sheltering effect also increases and a lesser amount of carbon dioxide emission leaves the atmosphere. Accordingly the temperature of the stratosphere could increase with increasing latitude. Quantitatively speaking, however, the intensity of the 14 μ band of ozone is much too weak to cause the observed large positive temperature gradient. In 1946, Dobson and others presented a theory of radiative equilibrium in which effects of the 9.6 μ band of ozone and the 15 μ band of carbon dioxide as well as the long wave radiation by water vapor were included. They attributed the observed positive temperature gradient to the fact that the amount of ozone, or the ratio of ozone to water vapor, is greater over the polar regions than the equator. Although Dobson's discussion is still qualitative it seems more acceptable than Möller's. Goody (1949) presented a theory which seemed quite contrary to the idea of Dobson's group. According to Goody, ozone supplies no greater heating effect in the arctic than in the tropics despite the increase of ozone concentration with latitude; the observed positive temperature gradient is a result of a balance between the heating effect of carbon dioxide and the cooling effect of water vapor. Although Goody's explanation and Dobson's are different from each other, they both lead us to the conjecture that the observed positive temperature gradient in the lower stratosphere could be satisfactorily explained by radiative equilibrium

theory if the combined effect of all absorbing gases were considered. To verify the conjecture requires of course further extensive studies of the properties and the distributions of the atmospheric constituents. A more immediate question, however, is, "Is the atmosphere in radiative equilibrium?" Despite the fact that radiation is believed to be the main factor governing the temperature of the stratosphere, a study of the heat budget of the stratosphere by Ohring (1958) indicates that the stratosphere is not in radiative equilibrium. In fact, it was found that the radiative processes tended to heat the stratosphere in lower latitudes and to cool it in higher latitudes.

The remarkable differences among the results of the investigators led Manabe and Möller (1961) to a quantitative study of the radiative equilibrium and the heat budget of the atmosphere. They took into consideration the effects of the absorption of solar radiation by water vapor carbon dioxide and ozone as well as those of long wave radiation of these three gases. With the available information on the distribution and the absorption coefficients of these gases they computed, using a 9 -level model, the distribution of radiative equilibrium temperature for various latitudes and various seasons, and the distribution of the radiative heat budget. Their results show the following:

1. The lower stratosphere is not in radiative equilibrium. The net radiative effect results in a very weak heating in low latitudes and a

rather strong cooling in high latitudes.

2. The computed temperature of radiative equilibrium at the 18-km level, where the observed annual mean temperature increases about 20^{o}C from equator to pole, increases only slightly ($\sim 7^{o}$C) from equator to pole both in summer and spring but decreases monotonically in winter and fall. Furthermore, the net effect of the radiative processes could barely maintain the temperature at the 18-km level approximately constant with latitude even though the observed temperatures are given for all other levels. Hence the net radiative effect can hardly explain the sharp latitudinal temperature increase observed in the lower stratosphere. These results were further confirmed by Manabe and Strickler (1964) in their study of "thermal equilibrium" of the atmosphere with convective adjustments.

In the above mentioned radiative studies the motion of the atmosphere was completely neglected. Such an approximation is, of course, convenient but not adequate. Since radiative heating is generally very slow in the region we are concerned with compared with the adiabatic heating associated with the atmospheric motions, it is rather easy to intuitively convince ourselves that the role of atmospheric motions in redistribution of heat energy is indispensible. The result of Manabe and Möller just prove the point. However, taking full account of dynamical and kinematical effects in the discussion of temperature distribution in the lower stratosphere is of great difficulty. In the past only

some postulations and brief discussions of certain transport mechanisms have been made. Early in 1949, Brewer's study of helium and water vapor distribution led him to propose a meridional circulation in which air entered the stratosphere at the equator, traveled northward toward the pole and sank into the troposphere in high latitudes. He pointed out that such a meridional circulation could account for the observed temperature distribution in the lower stratosphere. Similar types of mean meridional circulations were suggested by many others through studies of various tracer substances. As Brewer realized, however, the proposed circulation cannot meet the balance requirement of angular momentum. A recent observational study by Oort (1962) shows that Brewer's proposed circulation does not agree with the directly observed mean meridional circulation in the lower stratosphere which in fact, tends to destroy the observed temperature gradient. On the other hand, a very interesting feature was reported by White in 1954, namely, that the heat transport by large-scale eddies at 100-mb level is northward and up the zonally averaged temperature gradient, i.e., from the latitudes of lower zonally averaged temperature to the latitudes of higher zonally averaged temperature. Recent studies of the IGY data (e.g., Murakami, 1962; Peng, 1963) have shown that up-gradient heat transport due to large-scale eddies is a general feature in the whole lower stratosphere. This certainly leads us to the idea that the up-gradient heat transport may be a major factor in

maintaining the positive meridional temperature gradient in the lower stratosphere, since it implies a convergence of heat in high latitudes and a divergence of heat in low latitudes if no heat flow crosses the equator. The idea is supported by recent observational studies (e. g. , Oort, 1964). Then, we are led to a more fundamental question: Why are the large-scale atmospheric motions so organized that horizontal eddy heat transport is on the average up-gradient in the lower stratosphere but down-gradient in the troposphere?

From an energy point of view the meridional temperature gradient is closely related to zonal available potential energy. Any variation of the latter necessarily changes the former. An up-gradient heat transport due to large-scale eddies is just another way of saying a conversion from eddy available potential energy to zonal available potential energy. The above fundamental question as well as the question of the positive meridional temperature gradient in the lower stratosphere may thus be regarded as a part of the problem of energy balance in the atmosphere.

The energy balance in the atmosphere or, more precisely, in the troposphere has long been studied theoretically, observationally, and experimentally. The universally accepted energy cycle may be stated as follows. The net meridional differential heating of the atmosphere by its environment results in a continual generation of zonal available potential energy. This energy is converted into eddy available

potential energy by the eddies. Some of this eddy available potential energy may be radiatively dissipated, the remainder is converted into eddy kinetic energy by baroclinic processes. This eddy kinetic energy is partly dissipated by friction and partly converted into zonal kinetic energy by barotropical processes. Most of this zonal kinetic energy is dissipated by friction; only a small residue of it is converted into zonal potential energy again by meridional circulation.

Although the above energy cycle represents the spatial and time mean of the energy flow in the whole atmosphere, it may not be taken to represent the energy flow in a single layer such as the lower stratosphere. The classical view is this: the lower stratosphere is an inert, passive layer wherein any tendency toward direct convective action is suppressed by the existing large hydrostatic stability. The needed kinetic energy supply for maintaining the motion in the layer must originate in more active neighboring layers.

During the past few years sufficient data have been produced in the IGY program and by other sources to allow observational studies of the stratospheric general circulation and attempts to verify the classical concept of the stratosphere have been made by several authors (e. g., Barnes 1963, Oort, 1964). A most important one is the study by Oort based on one year of data of the IGY. It was found that during

that one year period the lower-stratospheric eddy processes, on the average, extracted energy from the eddies in favor of the zonal flow, converted eddy kinetic energy into eddy potential energy, and transformed eddy potential energy into zonal potential energy which subjected itself to radiative dissipation. Hence Oort concludes that the classical concept has been confirmed. The so-called adiabatic method was used to compute the individual change of pressure in Oort's study. The error due to that method probably does not alter the conclusion since non-adiabatic heating or cooling in the region is slow compared with adiabatic heating or cooling.

A comparison between Oort's result and the energy cycle in the troposphere clearly shows that the following particular chain of energy conversions in the lower stratosphere is exactly opposite to its counterpart in the troposphere.

Eddy Kinetic Energy → Eddy Available Potential Energy →
Zonal Available Potential Energy → Energy of the Environment

In the middle of this chain is the energy conversion from eddy available potential energy into zonal available potential energy which, as pointed out above, may be interpreted in terms of up-gradient eddy heat transport. Since the loss of zonal available potential energy to the environ-

ment is an effect rather than a cause of this chain, the cause of the up-gradient heat transport must then be closely related to the conversion from eddy kinetic energy into eddy available potential energy. Furthermore, since the conversion from kinetic energy into eddy available potential energy is a criterion of the passivity of the lower stratosphere, the up-gradient eddy heat transport must then be fundamentally related to the passive nature of the lower stratosphere; so also must be the positive meridional temperature gradient in the lower stratosphere if it is maintained by the up-gradient eddy heat transport. According to quasi-geostrophic theory of atmospheric motions the passivity of the lower stratosphere most likely depends upon two factors: one is the ratio of the static stability of the lower stratosphere to the static stability of the troposphere, the other is the ratio of the horizontal differential heating in the lower stratosphere to the horizontal differential heating in the troposphere. Therefore, using numerical experimentation, this study will first test whether the positive meridional temperature gradient in the lower stratosphere can be explained by the quasi-geostrophic theory under the existing vertical distributions of static stability and horizontal differential heating. Second, it will investigate how the overall positive meridional temperature gradient in the lower stratosphere depends upon the ratio of the horizontal differential heating in the lower stratosphere to the horizontal differential heating in the troposphere if the values of the

static stability in both layers are fixed. In addition, attention will be paid to the role of eddy heat transport, the relation between the eddy heat transport and the production of eddy kinetic energy, and the interactions between layers.

2. CONSTRUCTION OF THE MODEL

I. Governing equations

Large-scale motions in the atmosphere, except near the equator, are quasi-geostrophic in charactor. The quasi-geostrophic theory has been used with considerable success to explain the observed general circulation as a result of the prescribed distribution of heat sources and sinks (e. g., Phillips, 1956, and Charney, 1959). The quasi-geostrophic system of equations, with non-adiabatic heat and friction included, may be written in (x, y, p) coordinate system as follows.

$$\frac{\partial}{\partial t}\nabla^2\psi + J(\psi, \nabla^2\psi) + \beta_0 \frac{\partial \psi}{\partial x} - f_0 \frac{\partial \omega}{\partial p} = A\nabla^4\psi - g\vec{k}\cdot\nabla\times\frac{\partial \vec{\tau}}{\partial p} \tag{1}$$

$$\frac{\partial \theta}{\partial t} + J(\psi, \theta) - \sigma\omega = \frac{1}{c_p}\left(\frac{p}{p_0}\right)^{\kappa} Q \tag{2}$$

$$\nabla^2\theta = \frac{f_0}{\kappa c_p}\frac{p_0^{\kappa}}{p^{\kappa-1}}\frac{\partial}{\partial p}\nabla^2\psi \tag{3}$$

here x = eastward distance

y = northward distance

p = pressure (the vertical coordinate)

t = time

ψ = stream function for non-divergent part of velocity

ω = $\frac{dp}{dt}$

f_0 = Coriolis parameter at a fixed representative latitude

β_0 = (df/dy) the derivative of Coriolis parameter at the same latitude.

$A(p)$ = laternal kinematic eddy-viscosity coefficient (function of p)

g = acceleration of gravity

$\vec{k}$ = vertical unit vector

τ = small-scale frictional stress

θ = potential temperature

σ = standard value of $(-\partial\theta/\partial p)$

C_p, C_v = specific heats of air at constant pressure and volume

R = $C_p - C_v$

κ = R/C_p

Q = non-adiabatic rate of heating per unit mass

∇ = horizontal gradient operator on an isobaric surface

J = Jacobian operator

A natural extension of the above system of equations to cover a large latitudinal domain is to allow the variability of the Coriolis parameter and its derivative. Such an energetically consistant system may be written as follows.

$$\frac{\partial}{\partial t}\nabla^2\psi + J(\psi, \nabla^2\psi + f) - \nabla\cdot f\nabla\frac{\partial X}{\partial p} = A(p)\nabla^4\psi - g\vec{k}\cdot\nabla\times\frac{\partial\vec{\tau}}{\partial p} \qquad (4)$$

$$\frac{\partial}{\partial t}\theta + J(\psi, \theta) - \sigma \nabla^2 X = \frac{1}{c_p}\left(\frac{p_0}{p}\right)^{\kappa} Q \tag{5}$$

$$\frac{c_p}{p_0^{\kappa}} \nabla^2 \theta = -\nabla \cdot \frac{\partial}{\partial (p^{\kappa})} (f \nabla \psi) \tag{6}$$

here $X \equiv \int_0^p \chi \, dp$, χ is the velocity potential of the divergent part of wind, i.e., $\vec{v}_{div} = -\nabla \chi$. Noticing $\nabla^2 X = \omega$.

In the above two systems σ is taken as a function of p only. Here we neglect the detailed horizontal variation and time dependence of σ (Gates, 1961; Lorenz, 1960).

We shall take the latter system as the physical basis for the construction of our model.

II. Vertical approximations

In order to apply equations (4) - (6) to our problems, our first step is to follow the conventional method and divide our model atmosphere into several levels and to replace the vertical derivatives by the corresponding quotients of finite differences. Figure 1 shows the vertical resolution used in the model and the designation of dependent variables, which seem to be the simplest method suitable for the purpose of exposing the vertical difference of thermal structure and the

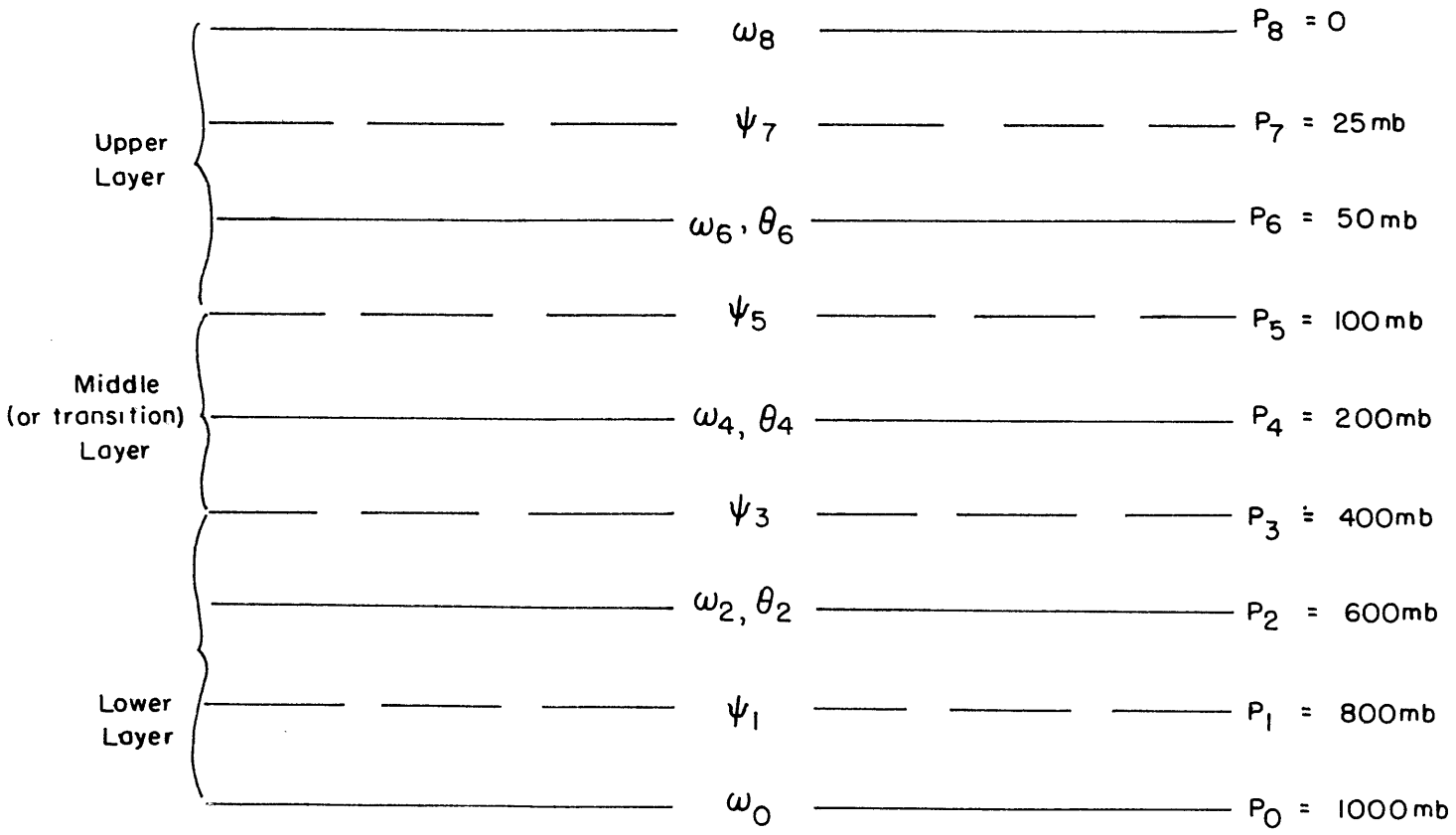

Figure 1. Vertical finite resolution.

energetic inter-dependence of the layers. The atmosphere is divided into unequal intervals of p so that physical processes taking place in the upper minor portion of the atmosphere can be detected. Stream functions are specified at isobaric surface p_j for odd j ; ω and potential temperatures are specified at p_j for even j .

After replacing the p-derivatives by their corresponding finite quotients, Eqs. (4) - (6) may be written in the following compact form.

$$\frac{\partial}{\partial t}\nabla^2\psi_j = -J(\psi_j, \nabla^2\psi_j + f) + \frac{1}{p_{j-1} - p_{j+1}} \nabla \cdot f \nabla (X_{j-1} - X_{j+1}) + A_j \nabla^4 \psi_j - g\vec{k} \cdot \nabla \times \frac{\vec{\tau}_{j-1} - \vec{\tau}_{j+1}}{p_{j-1} - p_{j+1}} \quad , j = 1, 3, 5, 7 \tag{7}$$

$$\frac{\partial}{\partial t}\theta_j = -J(\psi_j, \theta_j) + \sigma_j \omega_j + \frac{1}{c_p}\left(\frac{p_0}{p}\right)^{\kappa} Q_j \quad , j = 2, 4, 6 \tag{8}$$

$$\frac{c_p}{p_0^{\kappa}} \nabla^2 \theta_j = -\frac{1}{p_{j-1}^{\kappa} - p_{j+1}^{\kappa}} \nabla \cdot f \nabla (\psi_{j-1} - \psi_{j+1}), \quad j = 2, 4, 6 \tag{9}$$

where linear p-dependence of ψ is assumed, i..e.,

$$\psi_2 = \frac{1}{2}(\psi_1 + \psi_3) \tag{10}$$

$$\psi_j = \frac{1}{3}(2\psi_{j+1} + \psi_{j-1}) \quad , \quad j = 4, 6 \tag{11}$$

The boundary conditions at the top and the bottom of the atmosphere are

$$\omega_g = 0 \qquad \text{at } j = g \quad \text{or } p = 0 \tag{12}$$

and

$$\omega_0 = \omega_s \qquad \text{at } j = 0 \quad \text{or } p = p_0 = 1000 \text{ mb} \tag{13}$$

which will be specified later.

III. Parametric representations of energy sources and sinks

In the real atmosphere the distribution of energy sources and sinks is very complicated; it depends upon the motion and the state of the atmosphere, and the dependence is non-linear and largely unknown to us. In fact, the non-adiabatic heating and cooling in Eq. (8) includes long and short wave radiations, the release of latent heat, the vertical transport of heat by small-scale as well as large-scale eddies, and the lateral eddy diffusion on a scale smaller than that of the large-scale eddies. The two dissipation terms on the right hand of Eq. (7) consist respectively of lateral diffusions and horizontal eddy stresses on all scales smaller than those of the large-scale eddies. Each component of the forcing and dissipation is quite complex. With the crude vertical resolution in our model we, therefore, have no intention of describing the forcing and the dissipation terms in any detail but must resort to simple parameterization.

For the thermal forcing we postulate that the non-adiabatic heating and cooling would impose a certain distribution of potential temperature, θ_j^*,

upon each level in the atmosphere if large-scale motions were absent. The rate at which the potential temperature at each level is increased by non-adiabatic heating is then assumed to be proportional to the difference between the imposed potential temperature, θ_j^*, and the ambient potential temperature, θ_j, at that level. Thus,

$$\frac{1}{c_p}\left(\frac{p_0}{p}\right)^{\kappa} Q_j = h_j(\theta_j^* - \theta_j) \quad , \quad j = 2, 4, 6 \tag{14}$$

where h_j is assumed to be a function of p only. Although this parameterization is very crude and highly hypothetical, it depicts the dependence of thermal forcing on the instantaneous thermal state of the atmosphere.

For the kinetic dissipation we assume the eddy-viscosity coefficient to be independent of height and we follow Charney's postulation for surface friction and vertical eddy stress (Charney 1959). Thus, we put

$$A_j = A = \text{constant for} \quad j = 1, 3, 5, 7 \tag{15}$$

and

$$\frac{g}{p_0 - p_2}\vec{k}\cdot\nabla\times\vec{\tau}_0 = k_1\nabla^2\psi_1 \tag{16}$$

to represent the effect of surface friction. Since

$$\vec{\tau}_2 = \mu_2\left(\frac{\partial\vec{v}}{\partial z}\right)_2 \simeq \frac{-\mu_2 g}{\alpha_2}\left(\frac{\partial\vec{v}}{\partial p}\right)_2 \simeq -\frac{\mu_2 g p_2}{RT_2}\,\frac{\vec{v}_1 - \vec{v}_3}{p_1 - p_3}$$

we write

$$\tau_2 = k_1' \frac{p_0 - p_2}{g} (\vec{v_3} - \vec{v_1}) \tag{17}$$

$$= k_3 \frac{p_2 - p_4}{g} (\vec{v_3} - \vec{v_1}) \tag{18}$$

where

$$k_1' = \frac{\mu_2 g^2 p_2}{R T_2 (p_0 - p_2)(p_1 - p_3)} \quad = \text{constant} \tag{19}$$

$$k_3 = \frac{p_0 - p_2}{p_2 - p_4} k_1' \tag{20}$$

$\vec{v_1}, \vec{v_3}$ = velocity at p_1 and p_3 respectively

μ_2 = Austausch coefficient at p_2

α_2 = specific volume at p_2

and T_2 = normal temperature of the atmosphere at p_2.

Similarly

$$\vec{\tau_4} = k_5 \frac{p_4 - p_6}{g} (\vec{v_5} - \vec{v_3}) \tag{21}$$

$$= k_3' \frac{p_2 - p_4}{g} (\vec{v_5} - \vec{v_3}) \tag{22}$$

$$\vec{\tau_6} = k_5' \frac{p_4 - p_6}{g} (\vec{v_7} - \vec{v_5}) \tag{23}$$

$$= k_7' \frac{p_6 - p_8}{g} (\vec{v_7} - \vec{v_5}) \tag{24}$$

where

$$k_3' = \frac{\mu_4 g^2 \rho_4}{R T_4 (p_2 - p_4)(p_3 - p_5)} = \text{constant} \tag{25}$$

$$k_5 = \frac{p_2 - p_4}{p_4 - p_6} k_3' \tag{26}$$

$$k_5' = \frac{\mu_6 g^2 \rho_6}{R T_6 (p_4 - p_6)(p_5 - p_7)} = \text{constant} \tag{27}$$

$$k_7 = \frac{p_4 - p_6}{p_6 - p_8} k_5' \tag{28}$$

$\vec{v}_5, \vec{v}_7$ = velocity at p_5 and p_7 respectively ,

μ_4, μ_6 = Austausch coefficients at p_4 and p_6 respectively,

and T_4, T_6 = normal temperature at p_4 and p_6 respectively.

Finally,

$$\vec{\tau}_8 = 0 \tag{29}$$

Making use of (15) - (18), (21) - (24), and (29), we may write Eqs. (7) and (8) as follows:

$$\frac{\partial}{\partial t} \nabla^2 \psi_j = -J(\psi_j, \nabla^2 \psi_j + f) + \frac{1}{p_{j-1} - p_{j+1}} \nabla f \nabla (X_{j-1} - X_{j+1}) \tag{7a}$$

$$+ A \nabla^4 \psi_j - k_j \nabla^2 (\psi_j - \psi_{j-2}) - k_j' \nabla^2 (\psi_j - \psi_{j+2}),$$

$$j = 1, 3, 5, 7$$

and

$$\frac{\partial}{\partial t}\theta_j = -J(\psi_j, \theta_j) + \sigma_j \nabla^2 \chi_j + h_j(\theta_j^* - \theta_j), \qquad j = 2, 4, 6 \tag{8a}$$

Here ψ_0, ψ_{-1} and h_1' are identically zero.

IV. Spectral equations

In seeking time dependent solutions of the simultaneous non-linear partial differential equations (7a), (8a) and (9) we have to represent the dependent variables by numerical fields. The manner in which the variables are represented will determine the strategy of the subsequent mathematical procedures. In general, we may choose between two alternatives: (1) the variables may be represented as discrete functions on a mesh which covers the physical space, or (2) they may be represented by the coefficients of an expansion in orthogonal functions. Both methods have been used in the past, and each has certain advantages over the other. The appropriate choice depends upon the character of the problem which we deal with. In the present study we choose the second method, or spectral representation, on the ground of simplicity and potentiality of highly truncated spectral representations demonstrated by Lorenz (1962, 1963b), Bryan (1959) and Stackpole (1964).

A suitable set of orthogonal functions for the spectral expansion of $\nabla^2\psi_j$, θ_j and $\nabla^2\chi_j$, in equations (7a), (8a) and (9) is the complete set of surface spherical harmonics. (See Appendix for general properties of surface spherical harmonics).

$$\left\{ Y^m_{|m|+\ell} \;\middle|\; m = 0, \pm 1, \cdots ;\ \ell = 0, 1, \cdots \right\}$$

$Y^m_{|m|+\ell}$ will be referred as of wave m mode ℓ.

This set has the following advantages: a, the variation of the Coriolis parameter can be easily handled, b, no distortion of mass distribution, and c, no artificial lateral boundary conditions are necessary. However, we shall consider only the case that flow is symmetric about the equator so that no singularity is implied by the thermal wind relation. Thus

$$\left\{ Y^m_{|m|+\ell} \;\middle|\; m = 0, \pm 1, \cdots ;\ \ell = 0 \text{ , or positive even integral} \right\} \tag{30}$$

is only for the expansions of θ_j and $\nabla^2\chi_j$, while

$$\left\{ Y^m_{|m|+\ell} \;\middle|\; m = 0, \pm 1, \cdots ;\ \ell = 0 \text{ , or positive odd integral} \right\} \tag{31}$$

is only for the expansions of $\nabla^2\psi_j$.

When $\nabla^2\psi_j$, θ_j and $\nabla^2\chi_j$, expanded in surface spherical harmonics Y^m_n, are substituted into (7a), (8a) and (9) and coefficient of like harmonics are equated, a complete set of spectral equations

are obtained. However, in order to feasibly solve the spectral equations it is necessary to truncate the spectral expansions such that only a finite number of terms are retained. In fact, we shall choose the smallest subset of the set (30) and (31) which we think is still capable of representing the features of our major concern. To do that, we resort to our experience in atmospheric motions. In the real atmosphere, large-scale flow patterns can be thought of as consisting of a number of large-scale waves and a basic zonal flow. The large-scale waves generally fall into two categories, i.e., moving waves of intermediate wavelength; quasi-stationary waves, usually of very long wavelength and dominating the stratospheric flow patterns. In each category waves generally have tilting axes so that they are able to transport momentum and heat in meridional direction and hence to convert energy barotropically and baroclinically. The eddy transport of momentum and heat together with the external forcing usually gives rise to a three-cell meridional circulation, and largely determines the thermal structure of the atmosphere. In the present study our major concern is the meridional thermal structure of the lower stratosphere in connection with the energy flow in the atmosphere, a subset of the harmonics suitable for our purpose then should at least include m = 2 and 6, corresponding to planetary long wave and imtermediate wave, and two

values of ℓ , necessary for the meridional tilt of wave axes. Also, it is best to include Y_6^0 which is capable of representing a three-cell meridional circulation. Hence we chose the following subset.

$$\left\{ Y_1^0, Y_3^0, Y_5^0; \; Y_3^2, Y_3^{-2}, Y_5^2, Y_5^{-2}; \; Y_7^6, Y_7^{-6}, Y_9^6, Y_9^{-6} \right\} \tag{32}$$

for $\nabla^2 \psi_j$, and

$$\left\{ Y_2^0, Y_4^0, Y_6^0; \; Y_2^2, Y_2^{-2}, Y_4^2, Y_4^{-2}; \; Y_6^6, Y_6^{-6}, Y_8^6, Y_8^{-6} \right\} \tag{33}$$

for $\nabla^2 X_j$ and θ_j . It will be noticed that the chosen modes start from the lowest one, and that the omission of Y_0^0 , a constant, is allowed by the continuity equation and the assumption of constant σ_j . Assuming σ_j constant permits available potential energy to replace potential energy in energy considerations so that isobaric mean temperature is irrelevent to our study (Lorenz, 1960).

Now we introduce the expansions

$$\nabla^2 \psi_j = \zeta_{1j}^0 Y_1^0 + \zeta_{3j}^0 Y_3^0 + \zeta_{5j}^0 Y_5^0$$

$$+ \sum_{m=2,6} \left\{ \zeta_{m+1\,j}^{m} Y_{m+1}^{m} + \zeta_{m+1\,j}^{-m} Y_{m+1}^{-m} + \zeta_{m+3\,j}^{m} Y_{m+3}^{m} + \zeta_{m+3\,j}^{-m} Y_{m+3}^{-m} \right\}$$

$$j = 1, 3, 5, 7 \tag{34}$$

$$\nabla^2 X_j = \omega^0_{2j} Y^0_2 + \omega^0_{4j} Y^0_4 + \omega^0_{6j} Y^0_6$$

$$+ \sum_{m=2,6} \left\{ \omega^m_{mj} Y^m_m + \omega^{-m}_{mj} Y^{-m}_m + \omega^m_{m+2j} Y^m_{m+2} + \omega^{-m}_{m+2j} Y^{-m}_{m+2} \right\}$$

$$j = 2,\ 4,\ 6 \tag{35}$$

$$\theta_j = \theta^0_{2j} Y^0_2 + \theta^0_{4j} Y^0_4 + \theta^0_{6j} Y^0_6$$

$$+ \sum_{m=2,6} \left\{ \theta^m_{mj} Y^m_m + \theta^{-m}_{mj} Y^{-m}_m + \theta^m_{m+2j} Y^m_{m+2} + \theta^{-m}_{m+2j} Y^{-m}_{m+2} \right\}$$

$$j = 2.\ 4.\ 6 \tag{36}$$

Here the coefficients are all complex for $m \neq 0$.

We set

$$\zeta^{-m}_{nj} = (-1)^m \overline{\zeta^m_{nj}} \tag{37}$$

$$\omega^{-m}_{nj} = (-1)^m \overline{\omega^m_{nj}} \tag{38}$$

and

$$\theta_{nj}^{-m} = (-1)^m \overline{\theta_{nj}^{m}} \quad , \tag{39}$$

where a bar indicates the conjugate of a complex number or variable, so that the expansions (34) - (36) are real-valued, and substitute (34) - (36) into (7a), (8a) and (9). It should be pointed out here that spectral representations expanded in any non-trivial finite set of orthogonal functions can never exactly satisfy a non-linear equation or a system of non-linear equations, and particularly that spectral representations expanded in any finite set of surface spherical harmonics can never exactly satisfy (7a) and (9) even if the non-linear terms are completely neglected. In the former case non-linear interaction always disperse the spectra; in the latter case the terrestrial local vorticity always disperses the spectra. The new harmonics produced outside the prescribed finite spectra must be neglected in order to make the system of the spectral equations closed and energetically self-consistent. In so doing and making use of the general properties of spherical harmonics given in the Appendix, we find spectral equation as follows.

$$\frac{d}{dt}\zeta^{\circ}_{1j} = a^{\circ}_{12j}\left(\omega^{\circ}_{2j-1} - \omega^{\circ}_{2j+1}\right) - D^{\circ}_{1j}\zeta^{\circ}_{1j}$$

$$-k_j\left(\zeta^{\circ}_{1j} - \zeta^{\circ}_{1j-2}\right) - k'_j\left(\zeta^{\circ}_{1j} - \zeta^{\circ}_{1j+2}\right) \qquad (40)$$

$$j = 1, 3, 5, 7$$

$$\frac{d}{dt}\zeta^{\circ}_{3j} = a^{\circ}_{32j}\left(\omega^{\circ}_{2j-1} - \omega^{\circ}_{2j+1}\right) + a^{\circ}_{34j}\left(\omega^{\circ}_{4j-1} - \omega^{\circ}_{4j+1}\right)$$

$$-k_j\left(\zeta^{\circ}_{3j} - \zeta^{\circ}_{3j-2}\right) - k'_j\left(\zeta^{\circ}_{3j} - \zeta^{\circ}_{3j+2}\right) - D^{\circ}_{3j}\zeta^{\circ}_{3j} \qquad (41)$$

$$+ i\sum_{m=2,6} I^{\circ,m,-m}_{3,m+1,m+3}\left(\zeta^{m}_{m+1j}\zeta^{-m}_{m+3j} - \zeta^{m}_{m+3j}\zeta^{-m}_{m+1j}\right)$$

$$j = 1, 3, 5, 7$$

$$\frac{d}{dt}\zeta^{\circ}_{5j} = a^{\circ}_{54j}\left(\omega^{\circ}_{4j-1}-\omega^{\circ}_{4j+1}\right) + a^{\circ}_{56j}\left(\omega^{\circ}_{6j-1}-\omega^{\circ}_{6j+1}\right)$$

$$-k_j\left(\zeta^{\circ}_{5j}-\zeta^{\circ}_{5j-2}\right) - k_j'\left(\zeta^{\circ}_{5j}-\zeta^{\circ}_{5j+2}\right) - D^{\circ}_{5j}\zeta^{\circ}_{5j}$$

$$+ i\sum_{m=2,6} I^{\circ,m,-m}_{5,m+1,m+3}\left(\zeta^{m}_{m+1j}\zeta^{-m}_{m+3j}-\zeta^{m}_{m+3j}\zeta^{-m}_{m+1j}\right),$$

$$j = 1,3,5,7. \qquad (42)$$

$$\frac{d}{dt}\zeta^{m}_{m+1j} = a^{m}_{10j}\left(\omega^{m}_{mj-1}-\omega^{m}_{mj+1}\right) + a^{m}_{12j}\left(\omega^{\circ}_{m+2j-1}-\omega^{\circ}_{m+2j+1}\right)$$

$$-k_j\left(\zeta^{m}_{m+1j}-\zeta^{m}_{m+1j-2}\right) - k_j'\left(\zeta^{m}_{m+1j}-\zeta^{m}_{m+1j+2}\right) - D^{m}_{1j}\zeta^{m}_{m+1j} \qquad (43)$$

$$+ i\sum_{l=1,3,5}\sum_{n=1,3} I^{m,\circ,m}_{m+1,l,m+n}\zeta^{\circ}_{lj}\zeta^{m}_{m+nj} + i B_1\zeta^{m}_{m+1j},$$

$$m = 2,6 \;; \quad j = 1,3,5,7.$$

$$\frac{d}{dt}\zeta^{m}_{m+3j} = a^{m}_{32j}\left(\omega^{m}_{m+2j-1} - \omega^{m}_{m+2j+1}\right) - D^{m}_{3j}\zeta^{m}_{m+3j}$$

$$- k_j\left(\zeta^{m}_{m+3j} - \zeta^{m}_{m+3j-2}\right) - k'_j\left(\zeta^{m}_{m+3j} - \zeta^{m}_{m+3j+2}\right)$$

$$+ i\sum_{\ell=1,3,5}\sum_{n=1,3} I^{m,0,m}_{m+3,\ell,m+n}\,\zeta^{0}_{\ell j}\,\zeta^{m}_{m+nj} + iB^{m}_{3}\zeta^{m}_{m+3j}$$

$$m = 2, 6\,; \quad j = 1, 3, 5, 7 \tag{44}$$

$$\frac{d}{dt}\theta^{0}_{2j} = \sigma_j\,\omega^{0}_{2j}$$

$$+ i\sum_{m=2,6}\sum_{n=1,3}\sum_{\ell=0,2} A^{0,m,-m}_{2,m+n,m+\ell}\left(\zeta^{m}_{m+nj}\,\theta^{-m}_{m+\ell j} - \theta^{m}_{m+\ell j}\,\zeta^{-m}_{m+nj}\right) \tag{45}$$

$$+ h_j\left(\theta^{*0}_{2j} - \theta^{0}_{2j}\right)$$

$$j = 2, 4, 6$$

$$\frac{d}{dt}\theta^{\circ}_{4j} = \nabla_j \omega^{\circ}_{4j}$$

$$+ i \sum_{m=2,6} \sum_{n=1,3} \sum_{l=0,2} A^{0,m,-m}_{4,m+n,m+l} \left(\zeta^{m}_{m+nj} \theta^{-m}_{m+lj} - \zeta^{-m}_{m+nj} \theta^{m}_{m+lj} \right)$$

$$+ h_j \left(\theta^{*\circ}_{4j} - \theta^{\circ}_{4j} \right)$$

$$j = 2, 4, 6 \qquad (46)$$

$$\frac{d}{dt}\theta^{\circ}_{6j} = \nabla_j \omega^{\circ}_{6j}$$

$$+ i \sum_{m=2,6} \sum_{n=1,3} \sum_{l=0,2} A^{0,m,-m}_{6,m+n,m+l} \left(\zeta^{m}_{m+nj} \theta^{-m}_{m+lj} - \zeta^{-m}_{m+nj} \theta^{m}_{m+lj} \right) \qquad (47)$$

$$+ h_j \left(\theta^{*\circ}_{6j} - \theta^{\circ}_{6j} \right)$$

$$j = 2, 4, 6$$

$$\frac{d}{dt}\theta^{m}_{mj} = \nabla_j \omega^{m}_{mj} + h_j\left(\theta^{*m}_{mj} - \theta^{m}_{mj}\right)$$

$$+ i \sum_{\ell=1,3,5} \sum_{n=0,2} A^{m,0,m}_{m,\ell,m+n}\, \zeta^{0}_{\ell j}\, \theta^{m}_{m+n\,j}$$

$$+ i \sum_{\ell=1,3} \sum_{n=2,4,6} A^{m,m,0}_{m,m+\ell,n}\, \zeta^{m}_{m+\ell j}\, \theta^{0}_{nj} \,,$$

$$m = 2,6 \;;\; j = 2,4,6. \qquad (48)$$

$$\frac{d}{dt}\theta^{m}_{m+2\,j} = \nabla_j \omega^{m}_{m+2\,j} + h_j\left(\theta^{*m}_{m+2\,j} - \theta^{m}_{m+2\,j}\right)$$

$$+ i \sum_{\ell=1,3,5} \sum_{n=0,2} A^{m,0,m}_{m+2,\ell,m+n}\, \zeta^{0}_{\ell j}\, \theta^{m}_{m+n\,j}$$

$$+ i \sum_{\ell=1,3} \sum_{n=2,4,6} A^{m,m,0}_{m+2,m+\ell,n}\, \zeta^{m}_{m+\ell j}\, \theta^{0}_{nj} \,, \qquad (49)$$

$$m = 2,6 \;;\; j = 2,4,6.$$

$$\theta^{\circ}_{2j} = C^{\circ}_{21j}\left(\zeta^{\circ}_{1j-1} - \zeta^{\circ}_{1j+1}\right) + C^{\circ}_{23j}\left(\zeta^{\circ}_{3j-1} - \zeta^{\circ}_{3j+1}\right) \qquad (50)$$

$$j = 2, 4, 6.$$

$$\theta^{\circ}_{4j} = C^{\circ}_{43j}\left(\zeta^{\circ}_{3j-1} - \zeta^{\circ}_{3j+1}\right) + C^{\circ}_{45j}\left(\zeta^{\circ}_{5j-1} - \zeta^{\circ}_{5j+1}\right) \qquad (51)$$

$$j = 2, 4, 6.$$

$$\theta^{\circ}_{6j} = C^{\circ}_{65j}\left(\zeta^{\circ}_{5j-1} - \zeta^{\circ}_{5j+1}\right), \qquad j = 2, 4, 6. \qquad (52)$$

$$\theta^{m}_{mj} = C^{m}_{01j}\left(\zeta^{m}_{m+1j-1} - \zeta^{m}_{m+1j+1}\right), \qquad m = 2, 6; \qquad (53)$$

$$j = 2, 4, 6.$$

$$\theta^{m}_{m+2j} = C^{m}_{21j}\left(\zeta^{m}_{m+1j-1} - \zeta^{m}_{m+1j+1}\right) + C^{m}_{23j}\left(\zeta^{m}_{m+3j-1} - \zeta^{m}_{m+3j+1}\right) \qquad (54)$$

$$m = 2, 6; \quad j = 2, 4, 6.$$

where

$$\omega^{m}_{n8} = 0 \qquad \text{for all } m \text{ and } n \qquad (55)$$

$$\zeta^{m}_{n-1} = 0 \qquad \text{for all } m \text{ and } n \qquad (56)$$

$$\zeta^{m}_{n9} = 0 \qquad \text{for all } m \text{ and } n \qquad (57)$$

$$\zeta^{m}_{nj} = \frac{1}{2}\left(\zeta^{m}_{n1} + \zeta^{m}_{n3}\right) \qquad \text{for } j = 2 \qquad (58)$$

$$\zeta^{m}_{nj} = \frac{1}{3}\left(2\zeta^{m}_{nj+1} + \zeta^{m}_{nj-1}\right) \qquad \text{for } j = 4, 6. \tag{59}$$

$$I^{m_1,m_2,m_3}_{n_1,n_2,n_3} = \left\{ \frac{1}{n_2(n_2+1)} - \frac{1}{n_3(n_3+1)} \right\} L^{m_1,m_2,m_3}_{n_1,n_2,n_3} \tag{60}$$

$$L^{m_1,m_2,m_3}_{n_1,n_2,n_3} = \int_{-1}^{1} P^{m_1}_{n_1}(\mu)\left\{ m_2 P^{m_2}_{n_2}(\mu) \frac{dP^{m_3}_{n_3}(\mu)}{d\mu} - m_3 P^{m_3}_{n_3}(\mu) \frac{dP^{m_2}_{n_2}(\mu)}{d\mu} \right\} d\mu \tag{61}$$

$$A^{m_1,m_2,m_3}_{n_1,n_2,n_3} = \frac{1}{n_2(n_2+1)} L^{m_1,m_2,m_3}_{n_1,n_2,n_3} \tag{62}$$

$$B^{m}_{n} = \frac{2\Omega m}{(m+n)(m+n+1)} \tag{63}$$

$$a^{m}_{n\,n-1\,j} = \frac{m+n+1}{m+n}\left[\frac{n\,(n+2m)}{(2m+2n+1)(2m+2n-1)}\right]^{\frac{1}{2}}\frac{2\Omega}{p_{j-1}-p_{j+1}} \tag{64}$$

$$a^{m}_{n\,n+1\,j} = \frac{m+n}{m+n+1}\left[\frac{(n+1)(n+2m+1)}{(2m+2n+1)(2m+2n-1)}\right]^{\frac{1}{2}}\frac{2\Omega}{p_{j-1}-p_{j+1}} \tag{65}$$

$$C^{m}_{n\,n-1\,j} = \frac{1}{(m+n)^2}\left\{\frac{n(n+2m)}{(2m+2n+1)(2m+2n-1)}\right\}^{\frac{1}{2}}\frac{2\Omega a^2 p_0^{\kappa}}{c_p\left(p_{j-1}^{\kappa}-p_{j+1}^{\kappa}\right)} \tag{66}$$

$$C^{m}_{n\,n+1\,j} = \frac{1}{(m+n+1)^2}\left\{\frac{(n+1)(n+2m+1)}{(2m+2n+1)(2m+2n-1)}\right\}^{\frac{1}{2}}\frac{2\Omega a^2 p_0^{\kappa}}{c_p\left(p_{j-1}^{\kappa}-p_{j+1}^{\kappa}\right)} \tag{67}$$

$$D^{m}_{n\,j} = \frac{(m+n)(m+n+1)}{a^2}A \tag{68}$$

V. Numerical values for the parameters

The parameters involved in the equations of our model will be assigned values derived from our knowledge of the real atmosphere.

a) The static stability at j = 2, 4 and 6 are estimated from the observed mean temperature distribution

σ_2 = .055 ^{o}K - mb^{-1}

σ_4 = .232 ^{o}K - mb^{-1}

σ_6 = 2.17 ^{o}K - mb^{-1}

b) The lateral eddy coefficient is presumably independent of height

A = 10^5 m^2 - sec^{-1}

c) The dissipation coefficient due to ground friction is

k_1 = 2 x 10^{-6} sec^{-1}

d) In determining vertical eddy coefficient we take

μ_2 = 150 gm - cm^{-1} sec^{-1}

and assume that the variation of μ with height is inversely proportional to the static stability, i.e.,

$$\mu_2 : \mu_4 : \mu_6 = \sigma_2^{-1} : \sigma_4^{-1} : \sigma_6^{-1}$$

this gives

μ_4 = 35.6 gm - cm^{-1} - sec^{-1}

μ_6 = 3.8 gm - cm^{-1} - sec^{-1}

Estimating T_j from the observed mean temperature distribution in

the atmosphere we have, from equations (19), (20) and (25) - (28),

$$k_1' = .48 \times 10^{-6} \text{ sec}^{-1} = k_3$$

$$k_3' = .48 \times 10^{-7} \text{ sec}^{-1}$$

$$k_5 = 1.28 \times 10^{-7} \text{ sec}^{-1}$$

$$k_5' = .11 \times 10^{-7} \text{ sec}^{-1}$$

$$k_7 = .33 \times 10^{-7} \text{ sec}^{-1}$$

e) The parameters in the non-adiabatic heating term are estimated in the following way: The mean meridional distribution of the annual net radiative heating and cooling in the troposphere estimated by Houghton (1954) is normalized to represent the distribution of mean heating at 600 mb, or Q_2 . The mean temperature distribution at 600 mb is obtained from Peixoto (1960). Since both distributions may be well-represented by Y_2^0 , or P_2^0 , we substitute them into

$$\left(\frac{d\theta_{22}^0}{dt} \right)_{diabatic} = h_2 (\theta_{22}^{*0} - \theta_{22}^0) \tag{69}$$

to determine h_2 and θ_{22}^{*0} , and let

$$\theta_{42}^{*0} = 0$$

$$\theta_{62}^{*0} = 0$$

Another condition needed to determine h_2 and θ_{22}^{*0} may be obtained from Manabe et al (1961). At 600 mb the annual mean difference between the radiative equilibrium temperature at the equator and at the

pole estimated from Manabe's computation is about 62°C. We take this difference to be the maximum variation of θ_{22}^{*0}, i.e.,

$$\theta_{22}^{*0}\left\{P_2^0(1)-P_2^0(0)\right\}=-62\left(\frac{p_0}{p_2}\right)^{\kappa} \tag{70}$$

this gives

$$\theta_{22}^{*0} = -30\ ^{\circ}K$$

and from (69) we have approximately

$$h_2 = .45 \times 10^{-6}\ \text{sec}^{-1}$$

We next assume that radiation and other processes which are not dynamically included in the model would give rise to an inclination of the tropopause from the equator to the pole with a total difference in height about 7 km. In view of the difference in lapse rate between the stratosphere and the troposphere predicated by atmospheric radiative theory, the inclination of the tropopause implies that the equator-to-pole temperature difference (approximately in radiative equilibrium) at a level thoroughly above the tropopause would be about 50 degrees less than that at a level thoroughly below the tropopause. Based on this simple argument, we assume the imposed equator-to-pole temperature difference to be 10°C at 50 mb and 30°C at 200 mb. Further assuming that the distributions of the imposed temperature at 50 mb and at 200 mb can be fairly represented by Y_2^0 we have

$$\theta^{*0}_{24} = -20^{\circ}K$$

$$\theta^{*0}_{26} = -10^{\circ}K$$

and that

$$\theta^{*0}_{44} = \theta^{*0}_{64} = \theta^{*0}_{46} = \theta^{*0}_{66} = 0$$

The constant parameter λ_4 and λ_6 are chosen such that if observed annual potential temperature distributions at 200 mb and 50 mb are substituted for θ_4 and θ_6 respectively in the non-adiabatic heating term it will give a magnitude of heating rate comparable to the annual heating and cooling at the corresponding level estimated by Manabe et al (1961) and Ohring (1958).

$$\lambda_4 = .40 \times 10^{-6} \text{ sec}^{-1}$$

$$\lambda_6 = .20 \times 10^{-6} \text{ sec}^{-1}$$

For the asymmetric part of non-adiabatic heating in equations (49) and (48), we notice that (a) the non-adiabatic eddy heating is important to planetary long waves only, its effect on unstable intermediate waves is negligible, (b) the major eddy non-adiabatic heating is due to the land-sea contrast. There is qualitative evidence that ozone distribution is correlated with the quasi-stationary long waves in the atmosphere, but its dynamical significance is still in a speculation stage. Hence we put

$$\theta^{*6}_{nj} = 0 \qquad \text{for all } n \text{ and } j$$

in our model. The imposed eddy potential temperature assumes the following ideal distribution at $j = 2$,

in our model. The imposed p

following ideal distribution

$$\theta^*_{Eddy,2} = 3.9 \left(P_2^2 + 3 P_4^2 \right) \sin 2\lambda \,, \tag{71}$$

here λ = longitude ,

or

$$\theta^{*2}_{22} = -1.95 \; i \; (^{o}K)$$

$$\theta^{*2}_{42} = -5.85 \; i \; (^{o}K)$$

The magnitude is chosen such that the maximum gradient of asymmetric heating is about half the maximum gradient of symmetric heating. The distribution of the imposed heating, $h_j \theta^*_{Eddy,2}$, has its maximum magnitude at 50^{o} latitude and is quite similar to Clapp's estimates for a layer below 500 mb. (Clapp, 1961). The magnitude is smaller than one half of Clapp's value.

For upper levels we simply assume

$$\theta^{*2}_{24} = \frac{1}{10} \theta^{*2}_{22}$$

$$\theta^{*2}_{44} = \frac{1}{10} \theta^{*2}_{42}$$

and

$$\theta_{26}^{*2} = \theta_{46}^{*2} = 0$$

f) For the lower boundary mechanical forcing term $\nabla \cdot f \nabla \chi_0$, we also assume that its effect on the intermediate unstable wave is negligible. The effect of the topography of the earth's surface on the planetary long wave has long been recognized by Charney and Eliassen (1949) and others. In our simple model the lower boundary term $\nabla \cdot f \nabla \chi_0$ will be approximately given by

$$f_0 \rho_s g J(\psi_1/2, H P_3^2 \sin 2\lambda)$$

where f_0 = $2\Omega \sin 35^\circ$

ρ_s = standard air density at the ground

H = 1 km

and $-H P_3^2 \sin 2\lambda$ represents the idealized topography of the ground surface. Noticing that no net kinetic energy flux across the lower boundary is allowed and that the imposed asymmetric potential temperature distribution and the ground topography are 180° out of phase. The truncated expansion of $\nabla \cdot f \nabla \chi_0$ is given by

$$\nabla \cdot f \nabla \chi_0 = \frac{f_0 \rho_s g H}{2} \sum_{n=1,3,5} \left(\sum_{\ell=1,3} L^{0,2,-2}_{n,3,2+\ell} \frac{S^2_{2+\ell,1} + S^{-2}_{2+\ell,1}}{2(2+\ell)(3+\ell)} \right) Y^0_n$$

$$+ \frac{f_0 \rho_s g H}{2} \sum_{\ell=1,3} \left(\sum_{n=1,3,5} L^{-2,2,0}_{2+\ell,3,n} \frac{S^0_{n,1}}{2n(n+1)} \right) \left(Y^2_{2+\ell} + Y^{-2}_{2+\ell} \right) \quad (72)$$

The lower boundary terms in Eqs. (40)-(44) will be replaced by the corresponding harmonic components on the right hand of the above equation.

3. EQUATIONS FOR ENERGY TRANSFORMATIONS

It has been mentioned in Section 2.1 that our system of equations is energetically consistent. In this section we shall now derive the energy equations and show that if the non-adiabatic heating and frictional dissipation are set equal to zero the sum of kinetic energy and available potential energy will be conserved in our system.

In the following, we define

$$\overline{(\ )} = \frac{1}{2\pi}\int_0^{2\pi} (\ )\, d\lambda$$

$$(\ )' = (\ ) - \overline{(\ )}$$

$$\{(\ )\} = \frac{1}{2}\int_{-\pi/2}^{\pi/2} (\ )\cos\phi\, d\phi$$

where λ and ϕ are longitude and latitude respectively. Then, in our model the available potential energy per unit area may be defined as

$$A = \frac{c_p}{2g\,p_0^{\kappa}} \sum_{j=2,4,6} (p_{j-1}^{\kappa} - p_{j+1}^{\kappa})\, \sigma_j^{-1} \{\overline{\theta_j^2}\}$$

since $\{\bar{\theta}\}$ is set equal to zero for all j's. Or we may write

$$A = \sum_{j=2,4,6} (\bar{A}_j + A_j') \tag{73}$$

where

$$\bar{A}_j = \frac{c_p}{2g\sigma_j} \frac{p_{j-1}^{\kappa} - p_{j+1}^{\kappa}}{p_0^{\kappa}} \{\bar{\theta}_j^2\}$$

$$= \frac{c_p}{4g\sigma_j} \frac{p_{j-1}^{\kappa} - p_{j+1}^{\kappa}}{p_0^{\kappa}} \left[(\theta_{2j}^{o})^2 + (\theta_{4j}^{o})^2 + (\theta_{6j}^{o})^2 \right] \tag{74}$$

is the zonal available potential energy per unit area in the layer from p_{j-1} to p_{j+1}, and

$$A_j' = \frac{c_p}{2g\sigma_j} \frac{p_{j-1}^{\kappa} - p_{j+1}^{\kappa}}{p_0^{\kappa}} \left\{ \overline{\theta_j'^2} \right\}$$

$$= \frac{c_p}{2g\sigma_j} \frac{p_{j-1}^{\kappa} - p_{j+1}^{\kappa}}{p_0^{\kappa}} \sum_{m=2,6} \left(|\theta_{mj}^{m}|^2 + |\theta_{m+2j}^{m}|^2 \right) \tag{75}$$

is the eddy available potential energy per unit area in the layer from p_{j-1} to p_{j+1}.

The kinetic energy per unit area in our model may be defined as

$$K = -\frac{1}{2g} \sum_{j=1,3,5,7} (p_{j-1} - p_{j+1}) \left\{ \overline{\psi_j \nabla^2 \psi_j} \right\}$$

or, we may write

$$K = \sum_{j=1,3,5,7} (\bar{K}_j + K_j') \tag{76}$$

where

$$\bar{K}_j = -\frac{1}{2g}(p_{j-1}-p_{j+1})\left\{\bar{\psi}_j \nabla^2 \bar{\psi}_j\right\}$$

$$= \frac{a^2}{4g}(p_{j-1}-p_{j+1})\left(\frac{\zeta^0_{1j}\zeta^0_{1j}}{2} + \frac{\zeta^0_{3j}\zeta^0_{3j}}{12} + \frac{\zeta^0_{5j}\zeta^0_{5j}}{30}\right) \tag{77}$$

is the zonal kinetic energy per unit area in the layer from p_{j-1} to p_{j+1}, and

$$K'_j = -\frac{1}{2g}(p_{j-1}-p_{j+1})\left\{\overline{\psi'_j \nabla^2 \psi'_j}\right\}$$

$$= \frac{a^2}{2g}(p_{j-1}-p_{j+1})\sum_{m=2,6}\left[\frac{|\zeta^m_{m+1j}|^2}{(m+1)(m+2)} + \frac{|\zeta^m_{m+3j}|^2}{(m+3)(m+4)}\right] \tag{78}$$

is the eddy kinetic energy per unit area in the layer from p_{j-1} to p_{j+1}, $|\ |$ indicates the absolute value of a complex number and a is the radius of the earth.

Then the rate of change of available potential energy is given by

$$\frac{d}{dt}A = \sum_{j=2,4,6}\left(\frac{d}{dt}\bar{A}_j + \frac{dA'_j}{dt}\right) \tag{79}$$

where

$$\frac{d\bar{A}_j}{dt} = \frac{c_p}{g\sigma_j}\frac{p_{j-1}^{\kappa} - p_{j+1}^{\kappa}}{p_0^{\kappa}}\left\{\bar{\theta}_j\frac{\partial\bar{\theta}_j}{\partial t}\right\} \qquad j = 2,4,6$$

and

$$\frac{dA'_j}{dt} = \frac{c_p}{g\sigma_j}\frac{p_{j-1}^{\kappa} - p_{j+1}^{\kappa}}{p_0^{\kappa}}\left\{\overline{\theta'_j\frac{\partial\theta'_j}{\partial t}}\right\} \qquad j = 2,4,6$$

Making use of (8a), or, (34) - (39) and (45) - (49), we have

$$\frac{d\bar{A}_j}{dt} = -\left[\bar{A}_j\cdot\bar{A}'_j\right] - \left[\bar{A}_j\cdot\bar{K}_j\right] + \left[\bar{Q}_j\cdot\bar{A}_j\right] \qquad (80)$$

and $j = 2,4,6$

$$\frac{dA'_j}{dt} = \left[\bar{A}_j\cdot A'_j\right] - \left[A'_j\cdot K'_j\right] + \left[Q'_j\cdot A'_j\right] \qquad (81)$$

where $j = 2,4,6$

$$\left[\bar{A}_j\cdot A'_j\right] = \frac{c_p}{g\sigma_j}\frac{p_{j-1}^{\kappa} - p_{j+1}^{\kappa}}{p_0^{\kappa}}\left\{\bar{\theta}_j\,\overline{J(\psi'_j,\theta'_j)}\right\}$$

$$= \frac{c_p}{2g\sigma_j}\frac{p_{j-1}^{\kappa} - p_{j+1}^{\kappa}}{p_0^{\kappa}}\sum_{m=2,6}\sum_{k=2,4,6}\sum_{n=1,3}\sum_{l=0,2}\theta^{0}_{kj}\,A^{0,m,-m}_{k,m+n,m+l}$$

$$\times\, Im\left(\zeta^{m}_{m+nj}\,\theta^{-m}_{m+lj} - \theta^{m}_{m+lj}\,\zeta^{-m}_{m+nj}\right) \qquad (82)$$

is the conversion from zonal available potential energy to eddy available potential energy per unit area within the layer $p_{j-1} \to p_{j+1}$, j = 2, 4, 6. (Im indicates the imaginary part of a complex number).

$$[\bar{A}_j \cdot \bar{K}_j] = -\frac{c_p}{g} \frac{p_{j-1}^{\kappa} - p_{j+1}^{\kappa}}{p_0^{\kappa}} \{\bar{\theta}_j \bar{\omega}_j\}$$

$$= -\frac{c_p}{2g} \frac{p_{j-1}^{\kappa} - p_{j+1}^{\kappa}}{p_0^{\kappa}} \left(\theta_{2j}^{\circ} \omega_{2j}^{\circ} + \theta_{4j}^{\circ} \omega_{4j}^{\circ} + \theta_{6j}^{\circ} \omega_{6j}^{\circ}\right) \tag{83}$$

is the conversion from zonal available potential energy to zonal kinetic energy per unit area in the layer $p_{j-1} \to p_{j+1}$, j = 2, 4, 6 ,

$$[A_j' \cdot K_j'] = -\frac{c_p}{g} \frac{p_{j-1}^{\kappa} - p_{j+1}^{\kappa}}{p_0^{\kappa}} \{\overline{\theta_j' \omega_j'}\}$$

$$= -\frac{c_p}{g} \frac{p_{j-1}^{\kappa} - p_{j+1}^{\kappa}}{p_0^{\kappa}} \sum_{m=2,6} Rl\left(\theta_{mj}^{m} \omega_{mj}^{-m} + \theta_{m+2j}^{m} \omega_{m+2j}^{-m}\right) \tag{84}$$

is the conversion from eddy available potential energy to eddy kinetic energy per unit area in the layer $p_{j-1} \to p_{j+1}$, j = 2, 4, 6 . (Rl indicates the real part of a complex number).

$$\left[\bar{Q}_j \cdot \bar{A}_j\right] = \frac{c_p}{g\sigma_j} \frac{p_{j-1}^{\kappa} - p_{j+1}^{\kappa}}{p_0^{\kappa}} h_j \left\{\bar{\theta}_j \left(\bar{\theta}_j^{*} - \bar{\theta}_j\right)\right\}$$

$$= \frac{c_p}{2g\sigma_j} \frac{p_{j-1}^{\kappa} - p_{j+1}^{\kappa}}{p_0^{\kappa}} h_j \sum_{n=2,4,6} \theta_{nj}^{o} \left(\theta_{nj}^{*o} - \theta_{nj}^{o}\right) \tag{85}$$

is the generation of zonal available potential energy by zonal non-adiabatic heating per unit area in the layer $p_{j-1} \rightarrow p_{j+1}$, $j = 2, 4, 6$,

$$\left[Q_j' \cdot A_j'\right] = \frac{c_p}{g\sigma_j} h_j \frac{p_{j-1}^{\kappa} - p_{j+1}^{\kappa}}{p_0^{\kappa}} \left\{\theta_j' \left(\theta_j^{*\prime} - \theta_j'\right)\right\}$$

$$= \frac{c_p h_j}{g\sigma_j} \frac{p_{j-1}^{\kappa} - p_{j+1}^{\kappa}}{p_0^{\kappa}} \sum_{m=2,6} \sum_{l=0,2} Rl\left[\theta_{m+l\,j}^{-m} \left(\theta_{m+l\,j}^{*m} - \theta_{m+l\,j}^{m}\right)\right] \tag{86}$$

is the generation of eddy available potential energy by asymmetric non-adiabatic heating per unit area in the layer $p_{j-1} \rightarrow p_{j+1}$, $j = 2, 4, 6$.

The rate of change of kinetic energy is given by

$$\frac{dK}{dt} = \frac{d\bar{K}}{dt} + \frac{dK'}{dt}$$

where

$$\frac{d\bar{K}}{dt} = -\frac{1}{g}\sum_{j=1,3,5,7}(p_{j-1}-p_{j+1})\left\{\bar{\psi}_j\,\nabla^2\frac{\partial\bar{\psi}_j}{\partial t}\right\}$$

and

$$\frac{dK'}{dt} = -\frac{1}{g}\sum_{j=1,3,5,7}(p_{j-1}-p_{j+1})\left\{\overline{\psi_j'\,\nabla^2\frac{\partial\psi_j'}{\partial t}}\right\}.$$

Making use of equations (7a), (8a) and (9), we have

$$\frac{d\bar{K}}{dt} = \frac{1}{g}\sum_{j=1,3}^{5,7}(p_{j-1}-p_{j+1})\left\{\bar{\psi}_j\,\overline{J(\psi_j',\nabla^2\psi_j')}\right\}$$

$$-\frac{1}{g}\left\{\bar{\psi}_1\,\nabla\cdot f\nabla\bar{X}_0\right\} - \frac{c_p}{g p_0^*}\sum_{j=2}^{4,6}(p_{j-1}^*-p_{j+1}^*)\left\{\bar{\theta}_j\,\bar{\omega}_j\right\}$$

$$-\frac{A}{g}\sum_{j=1,3,5,7}(p_{j-1}-p_{j+1})\left\{\bar{\psi}_j\,\nabla^4\bar{\psi}_j\right\}$$

$$+\frac{p_0-p_2}{g}k_1\left\{\bar{\psi}_1\,\nabla^2\bar{\psi}_1\right\} + \sum_{j=2}^{4,6}\frac{p_{j-2}-p_j}{g}k_{j-1}'\left\{(\bar{\psi}_{j+1}-\bar{\psi}_{j-1})\nabla^2(\bar{\psi}_{j+1}-\bar{\psi}_{j-1})\right\} \tag{87}$$

and

$$\frac{dK'}{dt} = -\frac{1}{g}\sum_{j=1,3}^{5,7}(p_{j-1}-p_{j+1})\left\{\bar{\psi}_j\,\overline{J(\psi_j', \nabla^2\psi_j')}\right\}$$

$$-\frac{1}{g}\left\{\psi_1'\nabla\cdot f\nabla X_0'\right\} - \frac{c_p}{g p_0^{\kappa}}\sum_{j=2}^{4,6}(p_{j-1}^{\kappa}-p_{j+1}^{\kappa})\left\{\overline{\theta_j'\omega_j'}\right\}$$

$$-\frac{A}{g}\sum_{j=1,3}^{5,7}(p_{j-1}-p_{j+1})\left\{\overline{\psi_j'\nabla^2\psi_j'}\right\}$$

$$+\frac{p_0-p_2}{g}k_1\left\{\overline{\psi_1'\nabla^2\psi_1'}\right\} + \sum_{j=2}^{4,6}k_{j-1}'\frac{p_{j-2}-p_j}{g}\left\{\overline{(\psi_{j+1}'-\psi_{j-1}')\nabla^2(\psi_{j+1}'-\psi_{j-1}')}\right\} \tag{88}$$

It is readily seen that if we set the non-adiabatic heating, the dissipation, and the lower boundary forcing equal to zero, the sum of kinetic energy and available potential energy will be conserved.

For the purpose of examining the stratosphere-troposphere interaction it is desirable to separate the rate of change of kinetic energy of the upper two levels from that of the lower two levels and to regard the 200 mb level as a time-and-space mean position of the tropopause. Thus, the equations of the kinetic energy of the stratosphere (above 200 mb) may be approximately written as

$$\frac{d\bar{K}_5}{dt} = \frac{1}{g}\sum_{j=5,7}(p_{j-1}-p_{j+1})\left\{\bar{\psi}_j\, J(\overline{\psi_j', \nabla^2\psi_j'})\right\}$$

$$-\frac{1}{g}\left\{\bar{\psi}_5\,\nabla\cdot f\nabla\bar{X}_4\right\} + \frac{1}{g}\left\{(\bar{\psi}_5-\bar{\psi}_7)\,\nabla\cdot f\nabla\bar{X}_6\right\}$$

$$+\frac{p_2-p_4}{2g}k_3'\left\{(\bar{\psi}_5-\bar{\psi}_3)\nabla^2(\bar{\psi}_5+\bar{\psi}_3)\right\} + \frac{p_4-p_6}{2g}k_5\left\{(\bar{\psi}_5-\bar{\psi}_3)\nabla^2(\bar{\psi}_5-\bar{\psi}_3)\right\}$$

$$+\frac{p_4-p_6}{g}k_5'\left\{(\bar{\psi}_7-\bar{\psi}_5)\nabla^2(\bar{\psi}_7-\bar{\psi}_5)\right\} - \frac{A}{g}\sum_{j=5,7}(p_{j-1}-p_{j+1})\left\{\bar{\psi}_j\nabla^4\bar{\psi}_j\right\}$$

$$\frac{d\bar{K}_5'}{dt} = -\frac{1}{g}\sum_{j=5,7}(p_{j-1}-p_{j+1})\left\{\bar{\psi}_j\, J(\overline{\psi_j', \nabla^2\psi_j'})\right\}$$

$$-\frac{1}{g}\left\{\overline{\psi_5'\nabla\cdot f\nabla X_4'}\right\} + \frac{1}{g}\left\{\overline{(\psi_5'-\psi_7')\nabla\cdot f\nabla X_6'}\right\}$$

$$+\frac{p_2-p_4}{2g}k_3'\left\{\overline{(\psi_5'-\psi_3')\nabla^2(\psi_5'+\psi_3')}\right\} + \frac{p_4-p_6}{2g}k_5\left\{\overline{(\psi_5'-\psi_3')\nabla^2(\psi_5'-\psi_3')}\right\}$$

$$+\frac{p_4-p_6}{g}k_5'\left\{\overline{(\psi_7'-\psi_5')\nabla^2(\psi_7'-\psi_5')}\right\} - \frac{A}{g}\sum_{j=5,7}(p_{j-1}-p_{j+1})\left\{\overline{\psi_j'\nabla^4\psi_j'}\right\}$$

Similarly, the equations of the kinetic energy of the troposphere (below 200 mb) may be approximately written as

$$\frac{d\bar{K}_T}{dt} = \frac{1}{g}\sum_{j=1,3}(p_{j-1}-p_{j+1})\left\{\bar{\psi}_j\, J(\overline{\psi_j', \nabla^2\psi_j'})\right\} - \frac{1}{g}\left\{\bar{\psi}_1\nabla\cdot f\nabla\bar{X}_0\right\}$$

$$+\frac{1}{g}\left\{(\bar{\psi}_1-\bar{\psi}_3)\nabla\cdot f\nabla\bar{X}_2\right\} + \frac{1}{g}\left\{\bar{\psi}_3\nabla\cdot f\nabla\bar{X}_4\right\} + \frac{p_0-p_2}{2}k_1\left\{\bar{\psi}_1\nabla^2\bar{\psi}_1\right\}$$

$$-\frac{p_2-p_4}{2g}k_3'\left\{(\bar{\psi}_5-\bar{\psi}_3)\nabla^2(\bar{\psi}_5+\bar{\psi}_3)\right\} + \frac{p_2-p_4}{2g}k_3'\left\{(\bar{\psi}_5-\bar{\psi}_3)\nabla^2(\bar{\psi}_5-\bar{\psi}_3)\right\}$$

$$+\frac{p_2-p_4}{g}k_3\left\{(\bar{\psi}_3-\bar{\psi}_1)\nabla^2(\bar{\psi}_3-\bar{\psi}_1)\right\} - \frac{A}{g}\sum_{j=1,3}(p_{j-1}-p_{j+1})\left\{\bar{\psi}_j\nabla^4\bar{\psi}_j\right\}$$

$$\frac{dK_T'}{dt} = -\frac{1}{g}\sum_{j=1,3}(p_{j-1}-p_{j+1})\{\bar{\psi}_j' J(\overline{\psi_j'}, \nabla^2\psi_j')\} - \frac{1}{g}\{\overline{\psi_1'\nabla\cdot f\nabla X_0'}\}$$

$$+ \frac{1}{g}\{\overline{(\psi_1'-\psi_3')\nabla\cdot f\nabla X_2'}\} + \frac{1}{g}\{\overline{\psi_3'\nabla\cdot f\nabla X_4'}\} + \frac{p_0-p_2}{g}k_1\{\overline{\psi_1'\nabla^2\psi_1'}\}$$

$$- \frac{p_2-p_4}{2g}k_3'\{\overline{(\psi_5'-\psi_3')\nabla^2(\psi_5'+\psi_3')}\} + \frac{p_2-p_4}{2g}k_3'\{\overline{(\psi_5'-\psi_3')\nabla^2(\psi_5'-\psi_3')}\}$$

$$+ \frac{p_2-p_4}{g}k_3\{\overline{(\psi_3'-\psi_1')\nabla^2(\psi_3'-\psi_1')}\} - \frac{A}{g}\sum_{j=1,3}(p_{j-1}-p_{j+1})\{\overline{\psi_j'\nabla^4\psi_j'}\}$$

In the above equations the terms $\frac{1}{g}\{\bar{\psi}_3\nabla\cdot f\nabla\bar{X}_4\}$ and $-\frac{1}{g}\{\bar{\psi}_5\nabla\cdot f\nabla\bar{X}_4\}$ form a pair and the terms $\frac{1}{g}\{\overline{\psi_3'\nabla\cdot f\nabla X_4'}\}$ and $-\frac{1}{g}\{\overline{\psi_5'\nabla\cdot f\nabla X_4'}\}$ form another. They measure the direct effect of interaction between the stratosphere and the troposphere. They not only contain the direct vertical transport of (kinetic) energy across the interface due to large scale motions but also include baroclinic energy conversions immediately above and below the interface, which are closely related to the vertical velocity at the 200 mb level because of the finite difference resolution. For example, making use of (6) we have approximately

$$\frac{1}{g}\{\overline{\psi_3'\nabla\cdot f\nabla X_4'}\} = -\frac{2}{3}\frac{c_p}{g}\frac{p_3^\kappa-p_5^\kappa}{p_0^\kappa}\{\overline{\theta_4'\omega_4'}\} + \frac{1}{g}\{\overline{\psi_4'\nabla\cdot f\nabla X_4'}\}$$

$$-\frac{1}{g}\{\overline{\psi_5'\nabla\cdot f\nabla X_4'}\} = -\frac{1}{3}\frac{c_p}{g}\frac{p_3^\kappa-p_5^\kappa}{p_0^\kappa}\{\overline{\theta_4'\omega_4'}\} - \frac{1}{g}\{\overline{\psi_4'\nabla\cdot f\nabla X_4'}\}$$

Clearly the last terms on the right hand side of the above equations, which have the same magnitude but with opposite sign may be interpreted as vertical energy transport across the 200 mb level, while the first terms on the right hand side of the equations may be interpreted as energy conversions between eddy available potential and eddy kinetic energy immediately above and below the 200 mb level. Although the agreement of sign and the proportionality of the energy conversions directly above and below 200 mb level are due to the vertical finite difference resolution, it can nevertheless be interpreted as a result of changing of position of the tropopause in the real atmosphere. As we know, the tropopause is not an isobaric surface. It is above the 200 mb level in the lower latitudes and below the 200 mb level in the high latitudes. If we take its position in middle latitudes as its spatial mean position, it still shifts up and down with time. The entire range in position of the tropopause is in fact between 400 mb and 100 mb. The energy conversion in the vicinity of 200 mb hence may take place either within the stratosphere or within the troposphere. Since in the above energy partitioning we are not dealing with the energetics of the exact stratosphere and the exact troposphere but dealing with the energetics of the two portions of the atmosphere separated by the 200 mb level, it is then natural that the energy conversion around the 200 mb level is dis-

tributed above and below proportional to the mass distribution. Hence the equation governing the kinetic energy of the stratosphere may be approximately rewritten as the following.

$$\frac{d}{dt}\bar{K}_s = \left[K_s' \cdot \bar{K}_s\right] + \left[\bar{A}_s \cdot \bar{K}_s\right] + \left[\bar{K}_T \cdot \bar{K}_s\right]_A + \left[\bar{K}_T \cdot \bar{K}_s\right]_B - \left[k \cdot \bar{K}_s\right], \tag{89}$$

$$\frac{d}{dt}K_s' = -\left[K_s' \cdot \bar{K}_s\right] + \left[A_s' \cdot K_s'\right] + \left[K_T' \cdot K_s'\right]_A + \left[K_T' \cdot K_s'\right]_B - \left[k \cdot K_s'\right]. \tag{90}$$

And similarly

$$\frac{d}{dt}\bar{K}_T = \left[K_T' \cdot \bar{K}_T\right] + \left[\bar{A}_T \cdot \bar{K}_T\right] - \left[\bar{K}_T \cdot \bar{K}_s\right]_A - \left[\bar{K}_T \cdot \bar{K}_s\right]_B - \left[k \cdot \bar{K}_T\right] + \left[K_T' \cdot \bar{K}_T\right]_G \tag{91}$$

$$\frac{d}{dt}K_T' = -\left[K_T' \cdot \bar{K}_T\right] + \left[A_T' \cdot K_T'\right] - \left[K_T' \cdot K_s'\right]_A - \left[K_T' \cdot K_s'\right]_B - \left[k \cdot K_T'\right] - \left[K_T' \cdot \bar{K}_T\right]_G \tag{92}$$

Where

$$\left[K_S' \cdot \bar{K}_S\right] = \frac{1}{g} \sum_{j=5,7} (p_{j-1} - p_{j+1}) \left\{ \bar{\psi}_j \, J(\overline{\psi_j', \nabla^2 \psi_j'}) \right\}$$

or, making use of (34) - (39),

$$\left[K_S' \cdot \bar{K}_S\right] = -\frac{a^2}{2g} \sum_{j=5,7} (p_{j-1} - p_{j+1}) \sum_{m=2,6} \sum_{k=3,5} \frac{\overset{o}{\zeta}_{kj}}{k(k+1)} I^{o,m,-m}_{k,m+1,m+3}$$

$$\times \, Im \left(\zeta^{m}_{m+1,j} \, \zeta^{-m}_{m+3,j} - \zeta^{m}_{m+3,j} \, \zeta^{-m}_{m+1,j} \right) \tag{93}$$

is the energy conversion from eddy kinetic energy to zonal kinetic energy per unit area above 200 mb,

$$\left[K_T' \cdot \bar{K}_T\right] = -\frac{a^2}{2g} \sum_{j=1,3} (p_{j-1} - p_{j+1}) \sum_{m=2,6} \sum_{k=3,5} \frac{\overset{o}{\zeta}_{kj}}{k(k+1)} I^{o,m,-m}_{k,m+1,m+3}$$

$$\times \, Im \left(\zeta^{m}_{m+1,j} \, \zeta^{-m}_{m+3,j} - \zeta^{m}_{m+3,j} \, \zeta^{-m}_{m+1,j} \right) \tag{94}$$

is the conversion from eddy kinetic energy to zonal kinetic energy per unit area below 200 mb,

$$\left[\bar{A}_S \cdot \bar{K}_S\right] = \left[\bar{A}_6 \cdot \bar{K}_6\right] + \frac{1}{3}\left[\bar{A}_4 \cdot \bar{K}_4\right] \tag{95}$$

and

$$\left[\bar{A}_T \cdot \bar{K}_T\right] = \left[\bar{A}_2 \cdot \bar{K}_2\right] + \frac{2}{3}\left[\bar{A}_4 \cdot \bar{K}_4\right] \tag{96}$$

are the conversions from zonal available potential energy to zonal kinetic energy per unit area above and below 200 mb respectively,

$$\left[A_S' \cdot K_S'\right] = \left[A_6' \cdot K_6'\right] + \frac{1}{3}\left[A_4' \cdot K_4'\right] \tag{97}$$

and

$$\left[A_T' \cdot K_T'\right] = \left[A_2' \cdot K_2'\right] + \frac{2}{3}\left[A_4' \cdot K_4'\right] \tag{98}$$

are the conversions from eddy available potential energy to eddy kinetic energy per unit area above and below 200 mb respectively,

$$\left[\bar{K}_T \cdot \bar{K}_S\right]_A = -\frac{1}{g}\left\{\bar{\Psi}_4 \nabla \cdot f \nabla \overline{\chi_4}\right\}$$

or,

$$\left[\bar{K}_T \cdot \bar{K}_S\right]_A = \frac{a^2}{2g}(p_2 - p_4)\left[\frac{a^\circ_{123}\omega^\circ_{24}\zeta^\circ_{14}}{2} + \frac{a^\circ_{323}\omega^\circ_{24} + a^\circ_{343}\omega^\circ_{44}}{12}\zeta^\circ_{34} + \frac{a^\circ_{543}\omega^\circ_{44} + a^\circ_{563}\omega^\circ_{64}}{30}\zeta^\circ_{54}\right] \tag{99}$$

is the upward vertical transport of zonal kinetic energy per unit area across the 200 mb level due to the large-scale eddies,

$$\left[K_T' \cdot K_S'\right]_A = -\frac{1}{g}\left\{\overline{\Psi_4' \nabla \cdot f \nabla \chi_4'}\right\}$$

or

$$\left[K_T' \cdot K_S'\right]_A = \frac{a^2}{g}(p_2-p_4)\sum_{m=2,6} Rl\left(\frac{a^m_{323}\,\omega^m_{m+2\,4}\,\zeta^{-m}_{m+3\,4}}{(m+3)(m+4)} + \frac{a^m_{103}\,\omega^m_{m\,4} + a^m_{123}\,\omega^m_{m+2\,4}}{(m+1)(m+2)}\,\zeta^{-m}_{m+1\,4}\right) \tag{100}$$

is the upward vertical transport of eddy kinetic energy per unit area across the 200 mb level due to large-scale eddies,

$$\left[\bar{K}_T \cdot \bar{K}_S\right]_B = \frac{p_2-p_4}{2g} k_3' \left\{(\bar{\psi}_5 - \bar{\psi}_3)\nabla^2(\bar{\psi}_5+\bar{\psi}_3)\right\}$$

or,

$$\left[\bar{K}_T \cdot \bar{K}_S\right]_B = -a^2\frac{p_2-p_4}{4g} k_3' \sum_{n=1,3,5} \frac{(\zeta^o_{n5})^2 - (\zeta^o_{n3})^2}{n(n+1)} \tag{101}$$

is the upward vertical transport of zonal kinetic energy per unit area across the 200 mb level due to shear drag,

$$\left[K_T' \cdot K_S'\right]_B = -a^2\frac{p_2-p_4}{2g} k_3' \sum_{m=2,6}\sum_{l=1,3} \frac{|\zeta^m_{m+l\,5}|^2 - |\zeta^m_{m+l\,3}|^2}{(m+l)(m+l+1)} \tag{102}$$

is the upward vertical transport of eddy kinetic energy per unit area across the 200 mb level due to shear drag,

$$\left[k\cdot\bar{K}_S\right] = \frac{a^2 k_5}{4g}(p_4-p_6)\sum_{n=1,3,5}\frac{(\zeta^0_{n5}-\zeta^0_{n3})^2}{n(n+1)} + \frac{a^2 k_5'}{2g}(p_4-p_6)\sum_{n=1,3,5}\frac{(\zeta^0_{n7}-\zeta^0_{n5})^2}{n(n+1)} + \frac{A}{2g}\sum_{j=5,7}(p_{j-1}-p_{j+1})\sum_{n=1,3,5}(\zeta^0_{nj})^2 \tag{103}$$

and

$$\left[k\cdot\bar{K}_T\right] = \frac{a^2 k_3'}{4g}(p_2-p_4)\sum_{n=1,3,5}\frac{(\zeta^0_{n5}-\zeta^0_{n3})^2}{n(n+1)} + \frac{a^2 k_3}{2g}(p_2-p_4)\sum_{n=1,3,5}\frac{(\zeta^0_{n3}-\zeta^0_{n1})^2}{n(n+1)} + \frac{p_0-p_2}{2g}a^2 k_1\sum_{n=1,3,5}\frac{(\zeta^0_{n1})^2}{n(n+1)} + \frac{A}{2g}\sum_{j=1,3}(p_{j-1}-p_{j+1})\sum_{n=1,3,5}(\zeta^0_{nj})^2 \tag{104}$$

are the frictional dissipation of zonal kinetic energy per unit area above and below 200 mb respectively

$$\left[k\cdot K_S'\right] = \frac{a^2}{g}(p_4-p_6)\sum_{m=2,6}\sum_{l=1,3}\left[k_5\frac{\left|\zeta^m_{m+l5}-\zeta^m_{m+l3}\right|^2}{2(m+l)(m+l+1)} + k_5'\frac{\left|\zeta^m_{m+l7}-\zeta^m_{m+l5}\right|^2}{(m+l)(m+l+1)}\right] + \frac{A}{g}\sum_{j=5,7}\sum_{l=1,3}\sum_{m=2,6}(p_{j-1}-p_{j+1})\left|\zeta^m_{m+l}\right|^2 \tag{105}$$

and

$$\left[k\cdot K_T'\right] = \frac{a^2}{g}(p_2-p_4)\sum_{m=2,6}\sum_{\ell=1,3}\frac{\frac{k_3'}{2}\left|\zeta^m_{m+\ell 5}-\zeta^m_{m+\ell 3}\right|^2+k_3\left|\zeta^m_{m+\ell 3}-\zeta^m_{m+\ell 1}\right|^2}{(m+\ell)(m+\ell+1)}$$

$$+\frac{A}{g}\sum_{m=2,6}\sum_{j=1,3}\sum_{\ell=1,3}(p_{j-1}-p_{j+1})\left|\zeta^m_{m+\ell j}\right|^2+\frac{p_0-p_2}{g}a^2k_1\sum_{\substack{m=2,6\\ \ell=1,3}}\sum\frac{\left|\zeta^m_{m+\ell 1}\right|^2}{(m+\ell)(m+\ell+1)} \tag{106}$$

are the frictional dissipation of eddy kinetic energy per unit area above and below 200 mb respectively, and, by equation (72),

$$\left[K_T'\cdot\bar{K}_T\right]_G = \frac{f_0\rho_s H a^2}{2}\sum_{n=1,3,5}\sum_{\ell=1,3}\frac{\zeta^0_{n1}\,RL\,\zeta^2_{2+\ell 1}}{n(n+1)(\ell+2)(\ell+3)}L^{0\ 2\ -2}_{n\ 3\ \ell+2} \tag{107}$$

is the conversion from K_T' into $\bar{K}_T$ due to the topography of the earth's surface.

4. STEADY SYMMETRIC SOLUTION

For symmetric flow the system of equations (37) - (54) reduces to the following,

$$\frac{d}{dt}\zeta^{\circ}_{1j} = a^{\circ}_{12j}\left(\omega^{\circ}_{2j-1} - \omega^{\circ}_{2j+1}\right) - D^{\circ}_{1j}\,\zeta^{\circ}_{1j} - k_j\left(\zeta^{\circ}_{1j} - \zeta^{\circ}_{1j-2}\right)$$

$$- k_j'\left(\zeta^{\circ}_{1j} - \zeta^{\circ}_{1j+2}\right), \qquad j = 1, 3, 5, 7.$$

$$\frac{d}{dt}\zeta^{\circ}_{3j} = a^{\circ}_{32j}\left(\omega^{\circ}_{2j-1} - \omega^{\circ}_{2j+1}\right) + a^{\circ}_{34j}\left(\omega^{\circ}_{4j-1} - \omega^{\circ}_{4j+1}\right)$$

$$- D^{\circ}_{3j}\,\zeta^{\circ}_{3j} - k_j\left(\zeta^{\circ}_{3j} - \zeta^{\circ}_{3j-2}\right) - k_j'\left(\zeta^{\circ}_{3j} - \zeta^{\circ}_{3j+2}\right),$$

$$j = 1, 3, 5, 7.$$

$$\frac{d}{dt}\zeta^{\circ}_{5j} = a^{\circ}_{54j}\left(\omega^{\circ}_{4j-1} - \omega^{\circ}_{4j+1}\right) + a^{\circ}_{56j}\left(\omega^{\circ}_{6j-1} - \omega^{\circ}_{6j+1}\right)$$

$$- D^{\circ}_{5j}\,\zeta^{\circ}_{5j} - k_j\left(\zeta^{\circ}_{5j} - \zeta^{\circ}_{5j-2}\right) - k_j'\left(\zeta^{\circ}_{5j} - \zeta^{\circ}_{5j+2}\right),$$

$$j = 1, 3, 5, 7.$$

$$\frac{d}{dt}\theta^{\circ}_{nj} = \sigma_j\,\omega^{\circ}_{nj} + k_j\left(\theta^{*\circ}_{nj} - \theta^{\circ}_{nj}\right), \qquad n = 2, 4, 6;\ j = 2, 4, 6,$$

$$\theta^{\circ}_{2j} = C_{21j}\left(\zeta^{\circ}_{1j-1} - \zeta^{\circ}_{1j+1}\right) + C_{23j}\left(\zeta^{\circ}_{3j-1} - \zeta^{\circ}_{3j+1}\right), \qquad j = 2, 4, 6,$$

$$\theta^{\circ}_{4j} = C_{43j}\left(\zeta^{\circ}_{3j-1} - \zeta^{\circ}_{3j+1}\right) + C_{45j}\left(\zeta^{\circ}_{5j-1} - \zeta^{\circ}_{5j+1}\right), \qquad j = 2, 4, 6,$$

and

$$\theta^{\circ}_{6j} = C_{65j}\left(\zeta^{\circ}_{5j-1} - \zeta^{\circ}_{5j+1}\right), \qquad j = 2, 4, 6$$

where $\omega^{\circ}_{n0} = \omega^{\circ}_{n8} = 0$ for all n.

A steady-state solution is obtained by simple matrix inversion. The analytic form of the solution is cumbersome and the dependence of the solution on the parameters can hardly be seen. For the values of the parameters given in Section 2, V, the solution is given below.

Table 1 gives the distribution of the zonal velocity of the steady state solution. It shows that zonal winds increase with increasing height to the uppermost level. Maximum velocity is about 43 m - sec^{-1} located near 40^{o} latitude. The concentration of the zonal velocity is likely due to the fact that only one single lowest harmonic is chosen to represent the non-adiabatic heating.

Table 2 shows a single meridional cell in which southward motion is concentrated in the lower troposphere while northward motions prevail elsewhere. The center of the cell is located at about 25^{o} latitude below the 400 mb level.

The distribution of potential temperature, given in Table 3 shows a monotonic decreasing of temperature with increasing latitude. In the middle troposphere the total potential temperature difference between the equator and the pole is $62^{o}K$. The total potential temperature difference decreases with increasing height. The value at 50 mb is about $24^{o}K$.

Table 1

Zonal Velocity Distribution of the Steady Symmetric Solution: Units: $m\text{-}sec^{-1}$

Latitude	0^o	10^o	20^o	30^o	40^o	50^o	60^o	70^o	80^o	90^o
25 mb	25.7	28.3	34.2	40.4	42.9	40.0	32.4	21.8	10.9	0
100 mb	15.4	19.2	28.2	37.0	40.4	36.4	27.0	15.8	7.0	0
400 mb	5.5	7.8	13.1	18.4	20.5	18.3	13.1	7.2	3.0	0
800 mb	.3	.2	-.1	-.3	-.4	-.3	0	.1	.1	0

Table 2

Meridional Velocity Distribution of the Steady Symmetric Solution: Units: $cm\ sec^{-1}$

Latitude	0^o	10^o	20^o	30^o	40^o	50^o	60^o	70^o	80^o	90^o
25 mb	0	.2	.5	.8	.9	.7	.4	0	0	0
100 mb	0	3.1	4.8	4.6	3.3	2.0	1.4	1.1	.7	0
400 mb	0	10.1	15.1	13.8	9.1	5.3	4.2	4.1	3.0	0
800 mb	0	-11.3	-17.0	-15.6	-10.4	-6.1	-4.8	-4.6	-3.3	0

Table 3

Potential Temperature Distribution of the Steady Symmetric Solution:* Units: deg^oK

Latitude	0^o	10^o	20^o	30^o	40^o	50^o	60^o	70^o	80^o	90^o
50 mb	6.1	5.2	3.2	1.2	-.5	-2.6	-6.3	-11.3	-16.0	-17.9
200 mb	12.6	12.0	9.8	5.2	-2.0	-10.6	-18.9	-25.2	-28.9	-30.1
600 mb	18.2	17.6	15.0	8.4	-2.6	-16.3	-28.9	-37.8	-42.7	-44.0

*values in the table are the potential temperature departures from isobaric mean

5. METHOD OF NUMERICAL SOLUTION

I. Solution of simultaneous equation

The system of spectral equations in Section 2, IV is a system of 110 simultaneous complex ordinary differential equations in 110 dependent complex variables. The 110 equations can be reduced to 77 equations by eliminating the ω's . The resulting system of 77 complex ordinary differential equations can be written in the form of a complex matrix equation

$$A\dot{Z} = F(Z)$$

where A is an 77 x 77 constant real matrix, $\dot{Z}$ is a column matrix whose 77 elements are time derivatives either $\zeta^m_{m+\ell j}$, $\theta^m_{m+\ell j}$ or their conjugates, and F is a column matrix whose 77 elements are generally non-linear complex functions of $\zeta^m_{m+\ell j}$ and $\theta^m_{m+\ell j}$.

By simply multiplying the coefficient matrix A we have

$$\dot{Z} = A^{-1}F(Z).$$

Then by separation of the real and imaginary parts of this equation we obtain 77 real ordinary differential equations which may be represented by a real matrix equation.

$$\dot{X} = G(X)$$

where both $\dot{X}$ and G are 77 x 1 matrices.

II. Finite difference scheme for time integration

The finite difference scheme for the time integration of the system of equation

$$\dot{X} = G(X)$$

is the double approximation procedure used by Lorenz (1963). Let Δt be the time increment and let variables with subscript n represent the values of the variables at time $n\Delta t$. Introducing the auxiliary definitions

$$Y_{n+1} = X_n + G(X_n)\Delta t$$

$$Y_{n+2} = X_{n+1} + G(Y_{n+1})\Delta t$$

The double approximation is defined by the relation

$$X_{n+1} = X_n + \frac{1}{2}\left[G(Y_{n+1}) + G(X_n)\right]\Delta t$$

or $$X_{n+1} = \frac{1}{2}(X_n + Y_{n+2})$$

It has been shown by Lorenz (1963) that if this double approximation procedure is applied to a non-conservative system of equations and if a sufficiently small Δt is used the solution will not blow up

and the effect of computational instability will be small and equivalent to a slight reduction of the dissipation rate in the system.

III. Preliminary integration - initial flow for wave regime

The ideal form of a numerical experiment of the atmospheric general circulation is to start with an atmosphere at rest, except for disturbances of small amplitudes, and simply make a numerical forecast for a long time. However, since the numerical integration of a system of equations for non-symmetric flow takes much more time than that for symmetric flow and since disturbances with small amplitudes will presumably die out and have no significant influence on the basic symmetric flow before the basic flow reaches critical baroclinicity, the conventional procedure of a numerical experiment of the general circulation is to develop a symmetric zonal flow, without introducing disturbances, up to the critical point of baroclinicity, then put in disturbances of small amplitudes and carry on. We shall follow this procedure.

Without going into a linear perturbation analysis a good guess for the critical total temperature difference for baroclinic instability in our model atmosphere would be around $50^{\circ}C$. It would take integration time of the order of two months to set up such a temperature

gradient in the model. To save computation time, therefore, a preliminary integration of the equations for 50 days was first made before disturbances were put in. This preliminary integration started with the atmosphere at rest. The distributions of zonal velocity, potential temperature, and ω on the 50th day are shown in Tables (4) - (6) respectively.

It is seen in Table 4 that weak east winds appear everywhere in the lower troposphere with a maximum speed about 2.5 m - sec^{-1}. Winds shift west in the upper troposphere, and continue to increase with increasing height as a consequence of the monotonic decreasing of potential temperature from the equator to the pole both at 600 mb and 200 mb shown in Table 5. The total temperature difference is about $45^{o}C$ at 600 mb and $19^{o}C$ at 200 mb. At 50 mb the temperature pattern changes; temperature decreases slowly with increasing latitude in the high latitudes but increases with increasing latitude in the lower latitudes; the magnitude of temperature difference is about $4^{o}C$ between the equator and 50^{o} latitude and about $2^{o}C$ between 50^{o} latitude and the pole; the temperature at the pole is $2^{o}C$ higher than that at the equator. Consequently west winds increase slightly with increasing height in the belt between 50^{o} latitude and the pole, decrease slightly with increasing height in the belt between 50^{o} latitude and the equator,

Table 4

Zonal Velocity Distribution
of the Preliminary Flow: Unit: m sec^{-1}

Latitude	0°	10°	20°	30°	40°	50°	60°	70°	80°	90°
25 mb	.7	3.5	10.4	18.5	24.2	25.4	22.2	15.7	8.1	0
100 mb	4.0	7.5	16.0	25.0	29.3	27.5	20.9	12.4	5.6	0
400 mb	3.6	5.3	9.4	13.5	15.2	13.6	9.8	5.4	2.2	0
800 mb	-.2	-.6	-1.3	-2.2	-2.5	-2.3	-1.6	-.9	-.4	0

Table 5

The Distribution of Potential Temperature*
of the Preliminary Flow: Unit:deg°K

Latitude	0°	10°	20°	30°	40°	50°	60°	70°	80°	90°
50 mb	-4.5	-4.2	-3.0	- .5	2.8	5.3	5.3	3.3	.5	- .8
200 mb	7.8	7.7	7.0	4.5	- .3	-6.8	-13.5	-18.7	-21.9	-23.0
600 mb	15.2	14.8	12.7	7.3	-2.1	-13.6	-24.4	-32.0	-36.1	-37.2

*values in the table are the potential temperature departures from the isobaric mean

Table 6

The Distribution of $\bar{\omega}$ of the
Preliminary Flow: Unit: 10^{-5} mb-sec^{-1}

Latitude	0°	10°	20°	30°	40°	50°	60°	70°	80°	90°
50 mb	- .1	- .1	0	0	0	.1	.1	.1	.1	.1
200 mb	- .8	- .6	- .2	.2	.4	.4	.4	.4	.4	.5
600 mb	-4.9	-3.5	- .5	2.0	2.6	1.7	1.0	1.4	2.7	3.3

and has an overall decrease with increasing height. A maximum wind of 30 m - sec^{-1} is at 40^{o} near 100 mb. A single direct meridional cell with its center at about 25^{o} latitude is clearly shown in Table 6. The kinetic energy of the flow is of course derived from the direct meridional overturning. The wind and temperature distributions in the upper layer, if one does not doubt its reality, might leave one with the impression that the mechanism there would support Brewer's postulation if large-scale eddies were permanently excluded from the atmosphere. However, one should always keep in mind that this stage of the model atmosphere, if not completely fictitious, is necessarily transient. Comparing the temperature and wind patterns in the upper layer with those of the steady symmetric solution, one immediately realizes the differences between them. The upper temperature pattern here can be explained by taking a simple inspection of the thermodynamic equation. Considering equation (44), for instance, in the case of symmetric flow equation (44) becomes

$$\frac{d}{dt}\theta_{26}^{o} = \sigma_6 \omega_{26}^{o} + \gamma_6 (\theta_{26}^{*o} - \theta_{26}^{o})$$

for $j = 6$. The change of the overall temperature pattern is determined by two opposite processes. In a single direct cell ω_{26}^{o} is positive, i.e., transport heat poleward, tending to increase θ_{26}^{o} .

Since meridional circulation is the only meridional transport mechanism and is tending to increase θ°_{26} so that $\theta^{*\circ}_{26} - \theta^{\circ}_{26}$ is kept negative. In the stage while the whole atmosphere is being accelerated the upper layer is being accelerated both by the thermal forced overturning within itself and by the lower layer where the major acceleration force lies. Hence ω°_{26} is larger than is needed to balance $\lambda_6(\theta^{*\circ}_{26} - \theta^{\circ}_{26})$, and θ°_{26} is actually increasing. If the acceleration of the lower layer is strong and long enough, θ°_{26} may become significantly positive. However, as the model atmosphere approaches the steady state, a positive θ°_{26} may or may not be maintained depending upon the vertical distribution of thermal forcing, static stability, and dissipation. In our case the steady solution shows the negative answer.

6. RESULTS AND DISCUSSION

I. General description.

The initial condition consists of the symmetric flow described in Section 5, IV and a slight perturbation of the type $P_7^6(\sin\phi)\cos 6\lambda$ which is independent of pressure and has a wave kinetic energy of $.49 \times 10^5$ ergs - cm^{-2}. No perturbation of zonal wave number 2 was initially put in. Such a perturbation was immediately set up by the surface topography. The initial zonal flow is baroclinically unstable with respect to the shorter wave -- the perturbation of wave number six. After the dispersion stage in the very beginning, the shorter wave begins to grow. It takes about 20 days for the shorter wave to attain an amplitude of about forty times of the initial value which is comparable to the normal intensity of the observed intermediate waves in the middle atmosphere. During its growing stage the shorter wave grows as a whole, but the conversion from the eddy available potential energy into eddy kinetic energy in the shorter wave, $[A' \cdot K']_6$, has opposite signs in the upper and the lower layers; positive in the lower layer, negative in the upper layer. A direct or indirect vertical transport of kinetic energy of the shorter wave is then implied. The amplitude of the shorter wave has its maximum value at the 400 mb level, and becomes insignificant at the 25 mb level -- the uppermost

level in the model. The upward decrease of the intensity of the shorter wave agrees with our synoptic experience; the downward decrease is partly due to the surface skin friction -- the major dissipative mechanism in the system.

With respect to the longer wave and the perturbation set up by the lower boundary, the initial zonal flow would be of no baroclinic instability according to linear perturbation theory. That is to say, the longer wave in the system can not be self-excited. However, that does not necessarily exclude a energy conversion from the available potential energy of the longer wave to the kinetic energy of the longer wave, $[A' \cdot K']_2$. In the present system the divergence and the temperature fields of the longer wave are continuously and directly influenced by the external forcing. The divergence field forced by boundary topography and temperature field forced by land-sea contrast could influence the total dynamics of the longer wave such that the energy conversion $[A' \cdot K']_2$ changes its sign from time to time and from level to level. As a matter of fact, during the first 20 days the conversion $[A' \cdot K']_2$ is positive in the lower layer but negative in the upper layer, and later on the directions of the conversion are occasionally reversed. On the average, the baroclinic source of the kinetic energy of the longer wave is in the lower layer and the baroclinic sink of the kinetic energy of the longer wave is in the upper layer.

Despite this distribution of the source and sink the longer wave of the present system has its maximum amplitude in the upper layer. Therefore, a large amount of kinetic energy of the longer wave has to be transported upward. A discussion of energy flow and vertical transport mechanism will be given in a later section.

During the period when the amplitudes of the waves are still small, especially the first 10 days, eddy effects are unimportant, the meridional distribution of zonal wind and temperature and the pattern of meridional circulation are generally just the continuations of the case of symmetric flow. A single direct cell dominates the pattern of meridional circulation. The west wind generally increases with time at upper levels while the east wind still appears at the lowest level. Since the meridional circulation is not effective enough in transporting heat poleward to cancel the strong differential heating at 600 mb and 200 mb the meridional temperature differences at these levels are still increasing. Later on as the waves attain almost normal intensity, their role in the transport of heat and momentum become important. The west wind then begins to appear in the middle latitudes at the lowest level. Meridional temperature gradients at the lower levels no longer monotonically increase with time. A three-cell pattern of meridional circulation then takes place. The meridional distributions

of zonal wind, temperature and ω on the 10th day and the 30th day are given in Tables 7 - 12 respectively.

After the 30th day oscillatory characters are apparently present in the model atmosphere. The mean distributions of zonal wind, temperature, heat and momentum convergence due to the eddies, and the mean meridional circulation will be given in later sections. Generally speaking, oscillations in the lower layer become less and less frequent and are damping as time goes on. Oscillations in the upper layer are in general less frequent than those in the lower layers. This is actually expected because the assigned time constants for both heating and shear friction decrease with increasing height. The numerical integration of the wave regime was performed on the IBM 7094. It was carried out up to 3600 time steps which corresponds to 90 days. Although variables show remarkable oscillatory characteristics as just mentioned, no simultaneous approximate repetition of the variables was observed during the total time span. That is to say, there exists no well-defined cycle in the 90 days. For a hydrodynamic system having so many degree of freedom such as the present one it is not easy to even intuitively convince ourselves that there would exist any well-defined cycle. In the real atmosphere the existence of cycles shorter than the annual cycle has been questioned (Ward and Shipiro, 1961).

Table 7

Zonal Velocity Distribution
on the 10th day. Unit: $m\text{-}sec^{-1}$

Latitude	0°	10°	20°	30°	40°	50°	60°	70°	80°	90°
25 mb	1.1	4.3	12.1	21.1	27.3	28.6	24.8	17.4	9.0	0
100 mb	4.8	8.8	18.0	27.9	32.6	30.6	23.3	13.8	6.2	0
400 mb	3.9	5.9	10.6	15.4	17.4	15.8	11.7	6.6	2.9	0
800 mb	-.4	-.6	-.8	-1.0	-1.0	-.7	-.3	0.1	.1	0

Table 8

The Distribution of Potential Temperature*
on the 10th day. Unit: deg°K

Latitude	0°	10°	20°	30°	40°	50°	60°	70°	80°	90°
50 mb	-4.5	-4.3	-3.0	- .4	3.0	5.5	5.6	3.3	.2	-1.1
200 mb	8.4	8.3	7.5	4.7	- .5	-7.4	-14.4	-19.9	-23.2	-24.2
600 mb	15.9	15.5	13.2	7.5	-2.2	-14.2	-25.4	-33.4	-37.7	-38.9

*values in the table are the zonally averaged potential temperature departures from the isobaric mean

Table 9

The Distribution of $\bar{\omega}$ on the 10th day.
Unit: 10^{-5} $mb\text{-}sec^{-1}$

Latitude	0°	10°	20°	30°	40°	50°	60°	70°	80°	90°
50 mb	- .1	- .1	0	0	+ .1	.1	0.1	0	0	0
200 mb	-1.0	- .8	- .1	.5	.6	.4	.2	.1	.2	.3
600 mb	-5.6	-4.0	- .4	2.5	3.0	1.8	.8	1.4	2.9	3.6

Table 10

Zonal Velocity Distribution on the 30-th Day

Units: $m\text{-}sec^{-1}$

Latitude	0^o	10^o	20^o	30^o	40^o	50^o	60^o	70^o	80^o	90^o
25 mb	1.9	5.4	13.9	23.6	29.9	30.6	26.0	17.8	9.0	0
100 mb	2.6	6.9	17.2	28.4	34.9	34.1	27.3	17.3	8.3	0
400 mb	4.6	6.2	10.2	14.8	17.8	18.0	15.5	10.9	5.6	0
800 mb	-4.9	-3.2	.7	4.3	5.2	3.1	-.3	-2.8	-2.3	0

Table 11

The Distribution of Potential Temperature* on the 30-th Day

Units: deg^oK

Latitude	0^o	10^o	20^o	30^o	40^o	50^o	60^o	70^o	80^o	90^o
50 mb	-3.9	-3.8	-3.2	-1.5	1.3	4.2	6.0	6.3	5.7	5.4
200 mb	8.8	8.8	8.1	5.2	-.5	-8.2	-15.6	-20.9	-23.8	-24.6
600 mb	13.9	13.1	10.8	6.8	.5	-8.9	-21.0	-33.9	-44.1	-47.9

*departure from the isobaric mean

Table 12

The Distribution of $\bar{\omega}$ on the 30th Day

Units: 10^{-5} $mb\text{-}sec^{-1}$

Latitude	0^o	10^o	20^o	30^o	40^o	50^o	60^o	70^o	80^o	90^o
50 mb	.3	.2	0	-.1	-.1	0	0	-.2	-.4	-.5
200 mb	-3.1	-1.0	3.1	4.3	.9	-4.2	-5.6	-1.2	5.6	8.8
600 mb	-17.9	-8.7	9.4	17.3	6.6	-11.6	-17.0	-.9	24.4	36.4

II. The latitudinal temperature profile in the upper layer.

In this section we shall first consider the time sequence of the latitudinal temperature profiles and the mean latitudinal temperature profile, then examine the possible mechanisms which may be responsible for the temperature distribution and look into why that is so.

a) Time sequence of the latitudinal temperature profiles

The time sequence of the latitudinal temperature profiles at the 50 mb level is given in Figure 2. It clearly shows the oscillatory character of the zonally averaged temperature field. Before the 30th day the temperature field oscillates only slightly, and the equator-to-pole temperature difference is slightly positive. After that, rather strong oscillation takes place in the temperature field as the waves, especially the longer waves, are intensified. The positive equator-to-pole temperature difference increases continuously from the 30th day to the 58th day and reaches a maximum of $38.5^{\circ}C$, then decreases continuously and attains a minimum of about $9^{\circ}C$ on the 66th day. From then it again increases continuously to a maximum of $41^{\circ}C$ on the 78th day and then decreases continuously to $2.5^{\circ}C$ on the 90th day. The oscillation is remarkable.

b) The mean meridional temperature profile

The temperatures at 50 mb are averaged over a period from

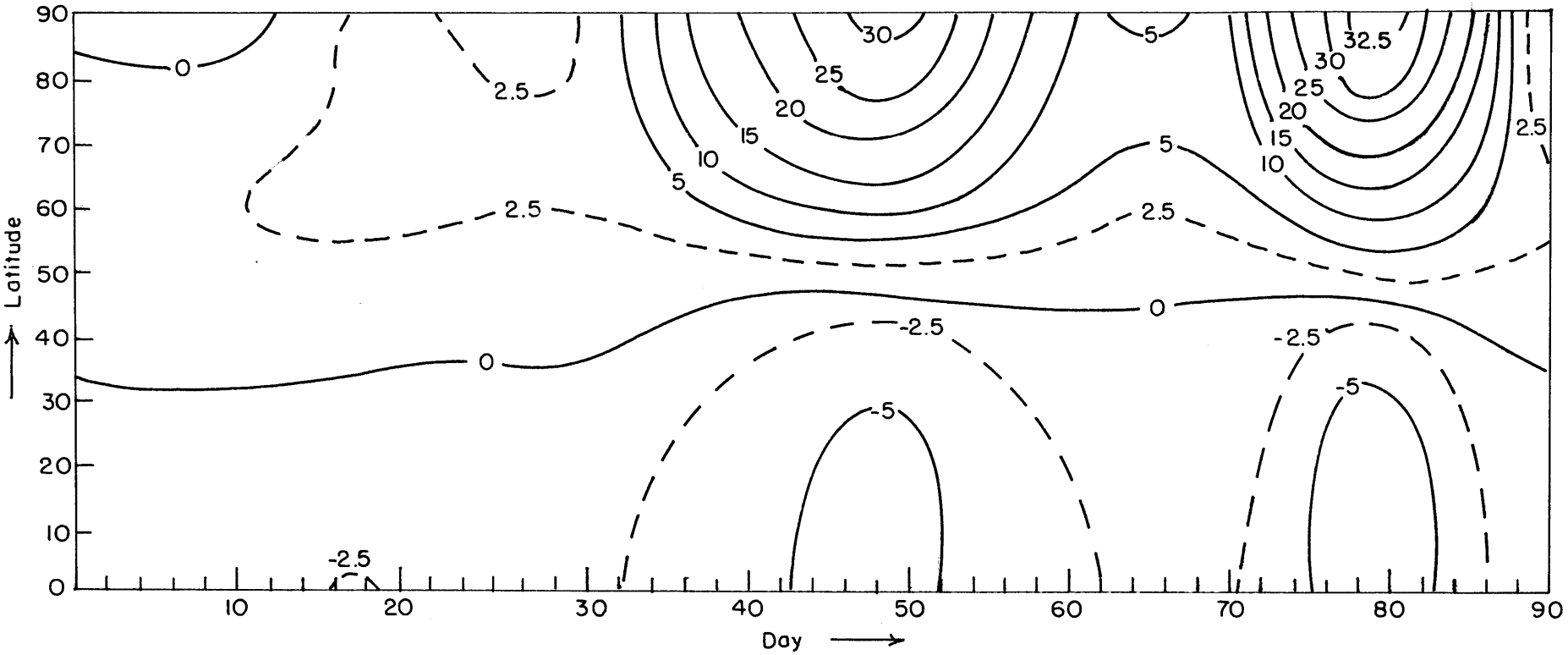

Figure 2. Time sequence of latitudinal temperature profile at 50 mb. Units: degrees C.

the 30th to the 90th day in which the meridional distribution displays two remarkable oscillations. The mean latitudinal potential temperature profile is given in Figure 3 in which the imposed potential temperature at 50 mb is also given for comparison. Although the imposed potential temperature monotonically decreases from the equator to the pole, the mean potential temperature increases monotonically from the equator to the pole. The total increase is as much as 48.7°K, corresponding to total temperature difference of 20.6 °C. It is also noticed that the gradient of the mean potential temperature generally increases from the equator to the pole; the potential temperature difference is only about 8°K between the equator and 45° latitude while it is 40°K between 45° and the pole.

c) Responsible mechanisms

We shall now examine the mechanisms which may be responsible for the potential temperature distribution described above. From equation (8a) it is readily seen that three thermal processes included in our model would affect the meridional distribution of zonally averaged temperature, namely, eddy transport, meridional circulation and non-adiabatic heating or cooling. The first term on the right hand side of equation (8a) is positive where eddy transport converges and is negative where eddy transport diverges. The second term is positive where

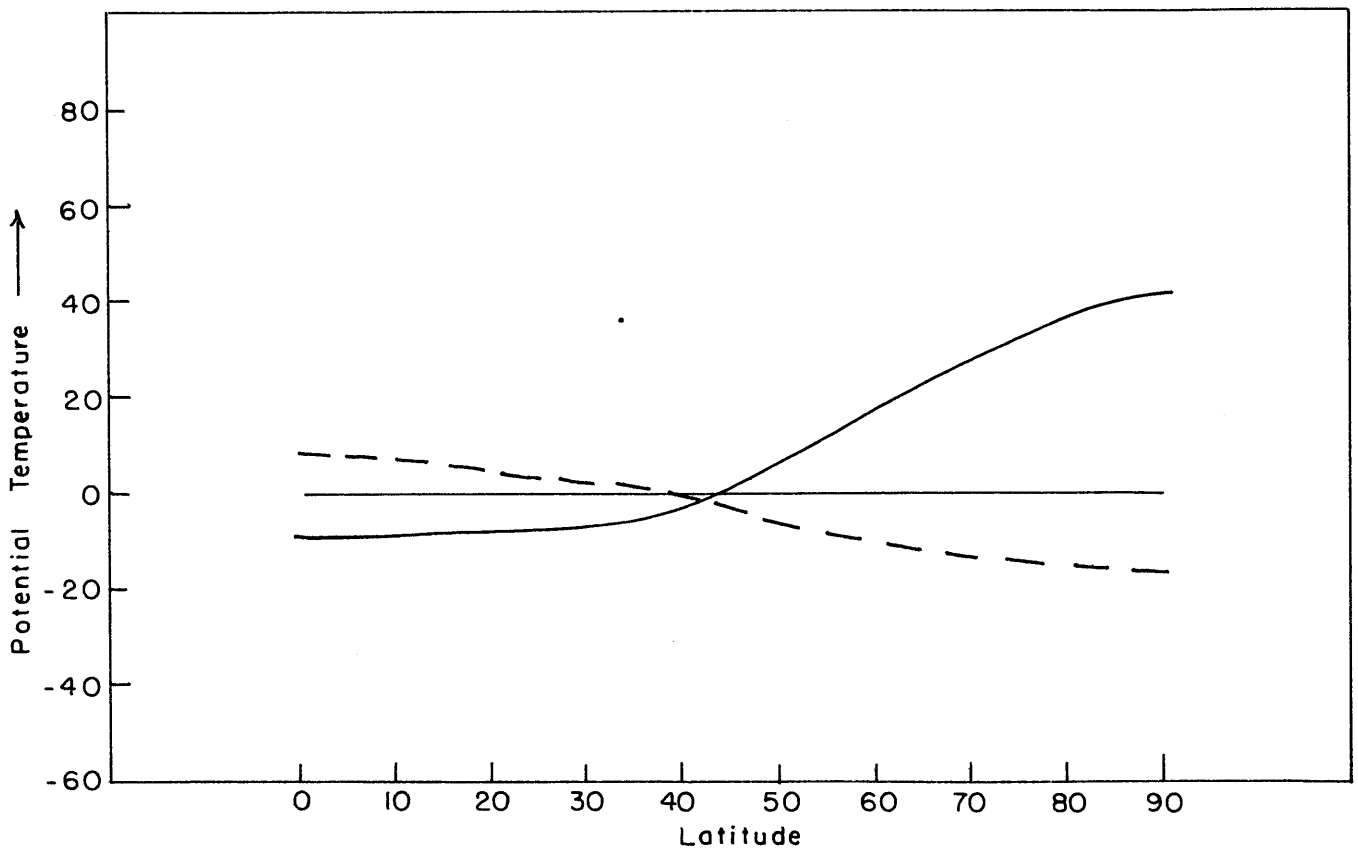

Figure 3. Mean potential temperature profile (30th - 90th day, solid) and the imposed potential temperature profile (dashed line) at 50 mb. Units: degrees K.

meridional circulation is downward and is negative where meridional circulation is upward. The third term is positive where the actual temperature is colder than the imposed temperature and is negative where the actual temperature is warmer than the imposed temperature. In this section we shall determine which one of these is most responsible for the distribution of the zonally averaged temperature at the 50 mb level. Shown in Figure 4 are the distributions of the 60-day mean rate of change of potential temperature at 50 mb due to each of those three processes. Also shown is the rate of actual overall change. The small value of the overall actual change indicates that the mean potential temperature distribution in Figure 3 is almost in statistical equilibrium. A comparison between Figure 3 and Figure 4 clearly shows that eddy thermal advection is primarily responsible for the latitudinal temperature profile except in the tropical region where the effect of mean meridional circulation is more important. In order to find out the dominant process in various phases of the oscillation of the temperature distribution the rate of change of potential temperature at 500 mb due to each of the three processes is averaged over every 10 day period. The values are given in Table 13. A glance at Table 13 immediately gives us the impression that during various stages of the oscillation the rate of change of potential temperature due to the convergence of eddy heat

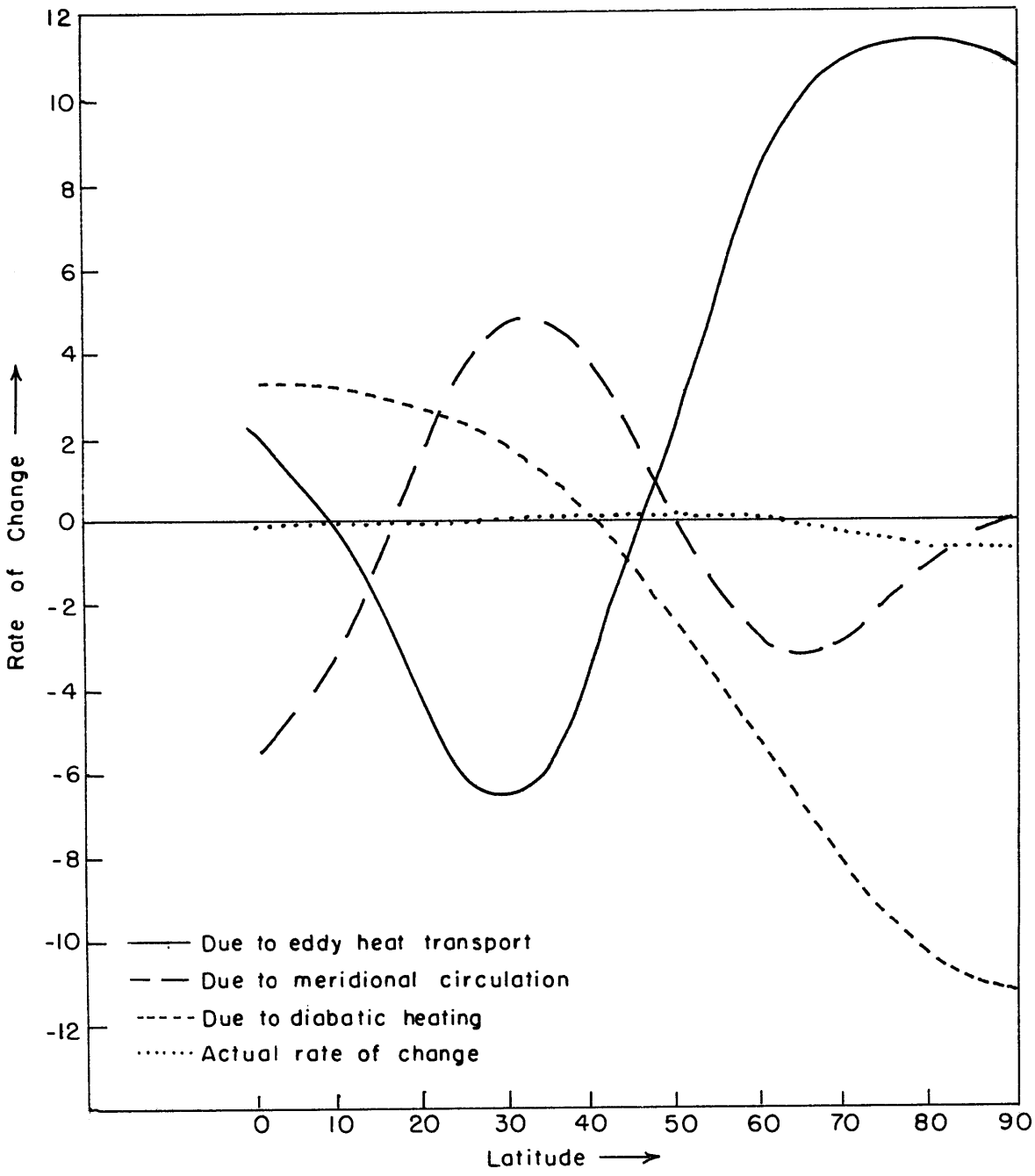

Figure 4. Mean rate of potential temperature change at 50 mb (30th - 90th day). Units: 10^{-6} deg^{o}K sec^{-1}.

Table 13

The Mean Rate of Change of Zonally Averaged Potential Temperature at 50 mb Due to Various Processes

Units: 10^{-6} deg $^{o}K\text{-sec}^{-1}$

Latitude	0^{o}	10^{o}	20^{o}	30^{o}	40^{o}	50^{o}	60^{o}	70^{o}	80^{o}	90^{o}
				30th day-40th day						
eddy	15.6	5.4	-16.5	-31.6	-26.0	-.5	32.0	58.4	73.0	77.2
meridional circulation	-25.1	-14.6	8.0	23.9	21.4	3.0	-15.3	-22.9	-20.9	-18.6
diabatic heating	2.7	2.6	2.1	1.2	-.1	-1.9	-4.0	-6.0	-7.5	-8.1
				40th day-50th day						
eddy	6.8	0	-13.8	-21.0	-13.0	6.7	26.4	37.2	39.2	38.8
meridional circulation	-13.5	-6.8	6.9	15.1	10.4	-2.7	-12.9	-13.4	-7.3	-3.7
diabatic heating	3.9	3.8	3.3	2.5	.8	-2.2	-6.6	-11.5	-15.3	-17.2
				50th day-60th day						
eddy	-13.4	-5.1	12.7	24.6	19.9	-.2	-24.6	-42.8	-51.6	-53.8
meridional circulation	17.0	9.0	-7.9	-18.8	-14.7	0.6	14.9	19.6	16.4	13.9
diabatic heating	3.3	3.2	2.7	1.7	-.1	-2.4	-5.2	-7.8	-9.7	-10.4
				60th day-70th day						
eddy	8.1	4.2	-4.6	-11.6	-11.4	-3.1	9.2	20.6	28.0	30.6
meridional circulation	-11.3	-7.1	2.5	10.1	10.5	4.0	-4.8	-11.4	-14.3	-14.9
diabatic heating	2.6	2.4	1.9	1.1	1.0	-1.9	-3.7	-5.4	-6.6	-7.0
				70th day-80th day						
eddy	15.3	1.6	-26.2	-40.6	-25.0	13.3	50.0	67.8	68.4	66.0
meridional circulation	-27.9	-14.7	12.5	28.7	19.7	-5.2	-23.4	-21.2	-6.1	2.2
diabatic heating	3.9	3.8	3.3	2.4	.7	-2.3	-6.5	-11.2	-15.0	-16.5
				80th day-90th day						
eddy	-19.3	-5.9	22.6	41.4	32.2	-2.4	-44.0	-75.2	-90.2	-94.0
meridional circulation	27.9	14.8	-12.9	-30.8	-24.0	1.2	24.5	31.6	25.9	21.5
diabatic heating	3.0	2.9	2.5	1.5	.8	-2.5	-4.8	-6.7	-7.9	-8.4

transport is always in the sense opposite to the effect of mean meridional circulation, and that the rate of change of the potential temperature due to non-adiabatic heating or cooling is always the smallest of the three in every 10- day period.

In the period from the 30th day to the 40th day the eddy transport term dominates the zonally averaged temperature changes in the region from the pole down to 20^{o} latitude. Strong convergence of eddy heat transport takes place between 50^{o} latitude and the pole, slight convergence takes place from the equator to 12^{o} latitude, and divergence takes place in between. This implies that from the region around 30^{o} latitude a large amount of heat is transported to the polar region and a small amount of heat is transported toward the equator since no meridional eddy heat transport across the equator is allowed in the model. The effect of meridional circulation on the temperature change is in the opposite sense and is smaller than the effect of eddy heat transport except in the lower tropical region. Since the effect of non-adiabatic heating or cooling is much smaller than the other two, the rate of change of potential temperature is negative and small in the lower latitudes but is positive and large in the high latitudes.

From the 40th to the 50th day the temperature change due to each of the three processes remains in the same sense as in the previous

period. The effects of eddy heat transport and meridional circulation decrease in intensity. The effect of non-adiabatic heating increases in intensity as a result of the increase of the meridional temperature gradient in the previous period, but it is still the smallest. Hence, the net change of the temperature distribution is still in the same sense as the previous period but its magnitude is smaller.

In the period from the 50th day to the 60th day only the effect of non-adiabatic heating or cooling remains nearly the same as before. Each of the other two alters a great deal and reverses the sign. More specific, the eddy heat transport now converges between 15^{o} latitude and 50^{o} latitude but diverges elsewhere; the mean meridional circulation now tends to decrease the potential temperature between 15^{o} and 50^{o} latitudes but to increase the potential temperature elsewhere. It is very interesting to notice that the effect of eddy heat transport still dominates the potential temperature change except below 20^{o} latitude so that the net rate of change of potential temperature is in the sense almost exactly opposite to what is before.

From the 60th day to the 70th day the mean rate of change of potential temperature due to each of the two major mechanisms reverses its sign again, and one is about the same magnitude of the other. Hence the net mean rate of change of potential temperature is everywhere

small in this period. Thereafter, the rate of change of potential temperature repeats the same kind of oscillation described above only with some changes in period and in intensity, and the actual meridional temperature profile oscillates accordingly as already shown in Figure 2. Thus, we have seen that during the various phrases of the oscillation of the latitudinal temperature profile in the upper layer the effect of eddy heat transport is almost always the dominant one except in the region near the equator or when all three are small.

From Figure 4 we infer that, the eddies, on the average, transport heat from the tropical region toward the pole up the mean meridional temperature gradient. As we have mentioned in the introduction, from the energy point of view, eddy heat transports up the mean temperature gradient imply conversions from eddy available potential energy to zonal available potential energy, i.e., $[A' \cdot \bar{A}] > 0$. An alternative way to appreciate the importance of eddy transport process in the change of the latitudinal temperature profile is to compare the actual change of the equator-to-pole temperature difference with the conversion $[A' \cdot \bar{A}]$. In Figure 5 such a comparison is made. The instant value of the equator-to-pole difference of the zonally averaged potential temperature at the 50 mb level is plotted with the energy conversion $[A' \cdot \bar{A}]$ at the same level. The close relation between them is

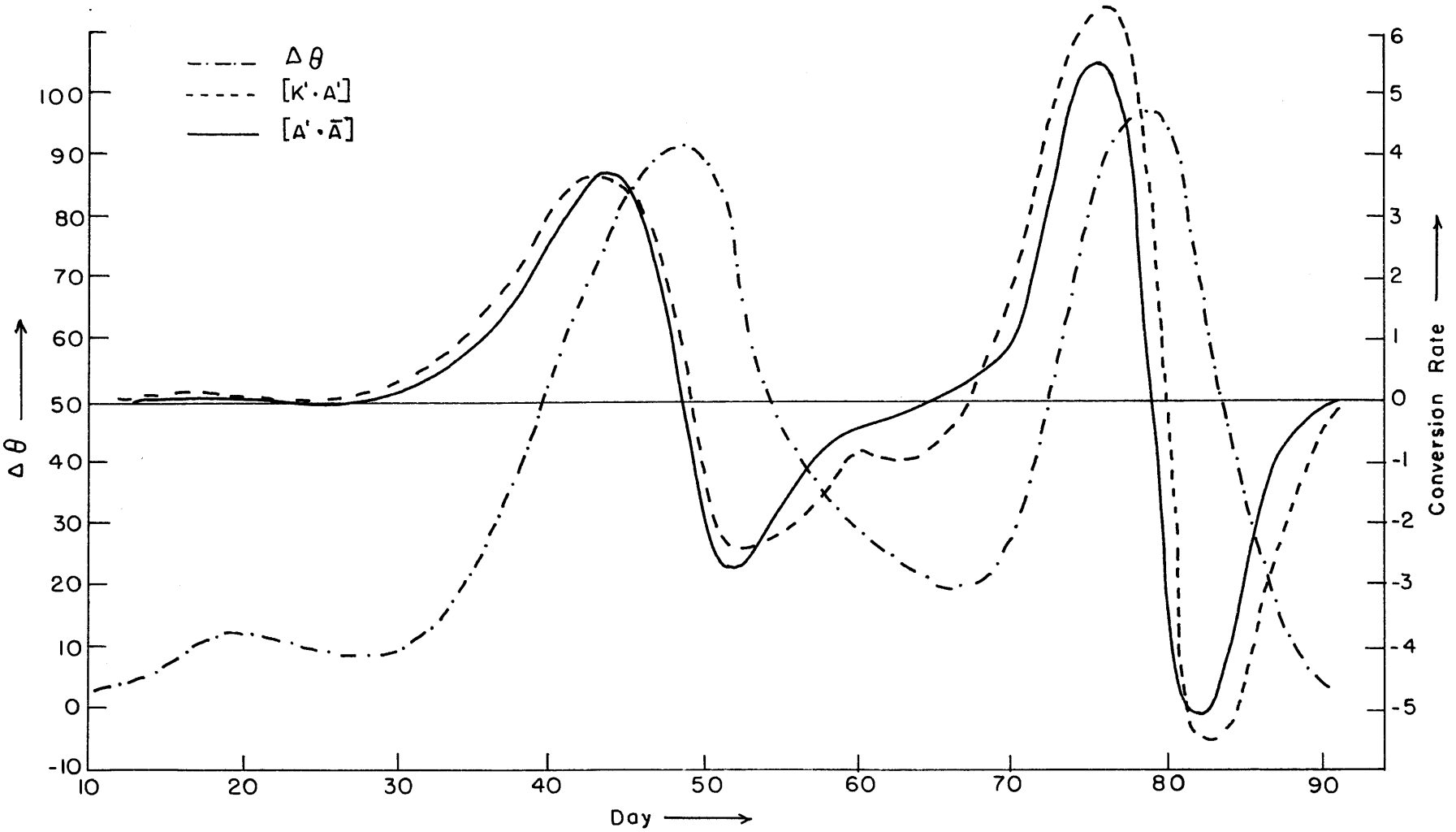

Figure 5. Relationship among the equator-to-pole potential temperature increase and energy conversions $[A' \cdot \bar{A}]$ and $[K' \cdot A']$ in the upper layer. Units: $\Delta\theta$, degrees K. Conversion rate, $.866 \times 10^2$ ergs cm^{-2} sec^{-1}.

clearly shown. The potential temperature difference increases as the conversion is positive and decreases as the conversion is negative. This is another evidence of the eddy heat transport being a controlling process of the latitudinal temperature profile.

e) The dominance of the longer wave in eddy heat transport

In the above we have just shown that the meridional temperature profile is controlled by the convergence of eddy heat transport. Since the intensity of the shorter wave decreases with increasing height while the intensity of the longer wave increases with increasing height, we expect that the eddy heat transport is mainly carried out by the longer wave. This is actually the case. The ratio of the convergence of eddy heat transport due to the longer wave only to the convergence of eddy heat transport due to all the eddies is given in Table 14. It is apparent that the longer wave controls the eddy heat transport and hence the latitudinal temperature profile in the upper layer.

Table 14. Ratio of the horizontal heat convergence due to the wave 2 to the horizontal heat convergence due to all waves.

period (days)	30th - 40th	40th - 50th	50th - 60th	60th - 70th	70th - 80th	80th - 90th
ratio	1.05	.80	1.11	1.25	.88	1.02

f) The relation between the meridional heat transport and the baroclinic production of eddy kinetic energy.

Let us now return to the question of why the eddy transport of heat is, on the average, up-gradient in the lower stratosphere. In the introduction we briefly discussed the question and realized that the up-gradient heat transport in the stratosphere must be tied up with the passive nature of the lower stratosphere. As we know, because of the quasi-geostrophic constraint, any baroclinic production or consumption of kinetic energy must be accompanied by a distortion of temperature field by horizontal motions (Kuo, 1956; Eady, 1949; Fjortoft, 1960). In some simple cases it has been shown theoretically that a baroclinic production of eddy kinetic energy is accompanied by a down-gradient eddy heat transport (e. g., Kuo, 1952, Thompson, 1961). For an atmosphere with layer structure, especially

for a single layer such as the lower stratosphere, no analytical approach can be made because of the complexity of the problem. However, one may intuitively expect that the above statement is still generally true and that a baroclinic consumption of eddy kinetic energy is generally accompanied by an up-gradient eddy heat transport. These statements are proven to be true in our study. In Figure 5 the energy conversion $[A' \cdot \bar{A}]$ and $[K' \cdot A']$ in the upper layer are plotted. They are almost always exactly in phase.

III. Energy distribution and energy transformation

a) Available potential energy

The available potential energy and the related energy transformations in the lower, middle, and upper layers, calculated from equations (80) - (86), are given in Table (15) - (17) respectively. The total available potential energy, as one expects, decreases rapidly with increasing height as a consequence of the rapid increase of static stability with increasing height. The mean zonal potential energy in the upper layer falls off to 1.2 per cent of the value of the lower layer; the available potential energy of the shorter wave in the upper layer is even less than one per cent of the value in the lower layer. However, the available potential energy of the longer wave in the upper layer is about the same

Table 15. Available Potential Energy and the Related Energy Transformations in the Lower Layer.
Units: .866 x 10^7 ergs cm^{-2} or .866 ergs cm^{-2} sec^{-1}

Day	$\bar{A}$	A'	$[\bar{A}\cdot A']$	$[\bar{A}\cdot\bar{K}]$	$[A'\cdot K']$	$[\bar{a}\cdot\bar{A}]$	$[a'A']$
2	502.0	.3	24.6	520.6	-1.0	1209.0	24.1
4	512.9	1.3	26.8	578.4	4.5	1173.0	40.0
6	521.7	3.3	116.2	542.9	27.7	1144.0	39.1
8	529.1	5.6	211.1	564.7	60.2	1119.0	27.0
10	535.0	8.5	189.6	566.6	85.5	1099.0	9.8
12	539.7	11.1	287.1	538.1	123.4	1083.0	-21.6
14	544.9	12.4	223.4	558.8	132.9	1066.0	-49.1
16	550.3	12.7	112.0	539.4	123.4	1046.0	-74.2
18	557.4	10.7	60.0	536.9	118.1	1020.0	-85.5
20	565.6	7.4	.3	517.2	137.3	988.4	-75.8
22	572.0	4.6	269.0	450.5	324.6	962.7	-57.8
24	571.3	4.2	1025.1	337.5	900.9	960.7	-37.0
26	556.3	7.9	2293.0	101.6	1918.2	1005.0	-25.4
28	521.1	16.0	3946.0	-76.0	3174.9	1102.0	-27.6
30	460.7	29.2	5370.9	-19.1	4164.2	1225.0	-60.2
32	404.0	40.4	3411.3	63.2	3273.9	1263.0	-94.4
34	387.9	40.4	907.8	175.8	827.4	1263.0	-79.2
36	404.9	39.9	-839.0	451.8	-740.9	1287.0	-118.8
38	437.8	37.2	-971.2	409.5	-661.2	1271.0	-166.3
40	460.3	31.1	351.3	240.6	602.8	1234.0	-210.5
42	459.2	25.5	1672.7	281.0	1584.2	1235.0	-284.9
44	439.1	24.7	2326.2	333.7	1909.5	1270.0	-362.2
46	419.3	24.9	2013.6	43.9	1848.9	1280.0	-351.5
48	410.7	22.0	1765.0	-64.8	1484.8	1269.0	-217.4
50	401.3	29.8	1381.2	326.7	579.3	1284.0	-129.9
52	405.2	39.6	96.6	271.8	-112.9	1301.0	-114.8
54	428.7	38.4	-366.2	97.8	32.2	1270.0	-56.8
56	450.2	31.2	160.4	249.7	590.9	1210.0	21.6
58	456.1	28.5	693.1	485.2	765.7	1186.0	34.8
60	455.2	30.1	493.8	343.4	781.6	1186.0	9.4
62	455.2	32.2	1105.6	102.1	965.2	1187.0	-12.0
64	452.0	34.3	1544.8	61.0	1381.2	1198.0	-40.7
66	447.1	37.0	1725.9	263.7	1478.7	1228.0	-105.1
68	430.1	37.8	1284.5	377.8	1163.9	1257.0	-189.0
70	428.2	33.4	731.2	385.7	860.8	1258.0	-256.5
72	432.5	25.3	625.1	340.1	846.8	1243.0	-298.1
74	435.5	17.6	980.2	222.9	1018.9	1232.0	-300.2
76	433.5	15.1	1390.5	134.8	998.3	1239.0	-239.7
78	426.2	21.8	1615.5	119.6	839.6	1264.0	-161.2
80	420.7	32.2	1279.7	61.8	692.9	1288.0	-106.2
82	426.2	35.8	549.5	56.6	616.4	1278.0	-38.1
84	440.7	30.3	63.3	295.6	630.8	1227.0	42.2
86	452.6	24.0	136.3	567.6	551.1	1179.0	59.9
88	458.1	23.0	397.3	545.0	456.2	1162.0	22.9
90	461.8	24.6	590.6	346.7	496.3	1158.0	-62.6
Mean (Day 21-90)	448.8	27.7	1158.9	239.6	1035.6	1213.2	-114.7

Table 16. Available Potential Energy and the Related Energy and Transformations in the Transition Layer.
Units: 1.298×10^7 ergs cm^{-2} or 1.298 ergs cm^{-2} sec^{-1}

Day	$\bar{A}$	A'	$[\bar{A}\cdot\bar{A}']$	$[\bar{A}\cdot\bar{K}]$	$[A'\cdot K']$	$[\bar{q}\cdot\bar{A}]$	$-[q'\cdot A']$
2	31.3	0	.5	58.5	0	122.0	0
4	32.3	0	1.2	65.7	-.7	120.0	-.2
6	32.2	0	11.1	57.9	3.0	118.1	-.1
8	33.9	.2	23.8	57.2	9.7	116.6	.5
10	34.4	.5	43.2	51.9	32.9	115.7	1.8
12	34.7	.7	62.0	43.8	41.6	115.3	3.3
14	34.8	.8	60.8	46.9	46.4	115.2	4.6
16	35.0	1.0	51.6	50.3	37.5	115.2	6.0
18	35.3	1.1	31.3	56.8	18.6	114.7	7.5
20	36.0	1.2	-6.9	59.3	-9.6	113.3	9.1
22	37.1	1.3	-17.2	55.1	-30.6	110.8	10.9
24	38.4	1.3	+.2	39.0	-19.2	107.5	12.9
26	39.4	1.5	+69.7	-6.7	42.1	104.6	15.0
28	39.7	2.2	+214.4	-103.5	117.4	103.3	20.5
30	39.0	4.2	+421.1	-236.5	189.1	104.1	35.0
32	36.8	6.5	+443.5	-179.6	223.2	107.9	50.6
34	34.7	7.6	+55.2	105.1	18.1	114.0	56.4
36	35.5	7.9	-135.2	146.6	-176.4	114.3	56.0
38	36.5	7.6	+14.8	102.2	-12.5	112.6	52.9
40	35.7	7.0	+145.4	59.2	148.9	115.7	47.9
42	34.1	5.9	+211.6	-35.0	213.9	119.5	42.7
44	34.0	5.6	+227.2	-129.1	186.4	118.9	42.3
46	33.9	5.0	+276.8	-115.5	281.1	118.1	40.6
48	33.6	3.6	+63.9	-11.3	134.3	118.3	30.9
50	36.7	2.7	-202.0	71.7	-190.0	111.1	21.9
52	40.0	2.5	-163.7	143.4	-194.8	102.3	18.6
54	41.2	2.6	-60.5	127.4	-81.6	100.3	17.4
56	42.4	2.7	-98.3	65.2	-132.5	97.8	18.3
58	45.4	3.1	-98.0	5.1	-134.8	88.5	23.9
60	47.5	3.0	-79.8	-54.9	45.1	80.9	26.3
62	47.4	3.5	+221.1	-71.8	82.2	80.2	31.4
64	45.2	5.9	+314.5	-51.7	45.3	86.3	47.7
66	41.5	10.1	+320.2	15.9	-9.8	97.8	75.0
68	37.4	13.6	+283.7	51.9	54.7	109.6	98.0
70	34.4	14.8	+138.4	78.7	21.3	116.0	107.2
72	33.6	13.8	76.2	59.6	93.4	117.6	103.6
74	33.8	11.1	+56.5	19.3	133.1	117.6	89.1
76	34.8	8.6	+118.5	-59.7	175.4	115.6	74.3
78	35.2	6.2	+280.6	-145.0	361.6	114.2	55.7
80	33.8	4.5	+376.1	-125.1	364.8	116.4	38.6
82	31.4	5.7	+246.0	-24.0	45.1	121.2	42.4
84	31.4	9.0	-95.6	102.8	-332.1	121.9	63.5
86	34.9	10.7	-291.5	158.1	-386.7	115.0	76.1
88	39.0	9.9	-259.6	147.8	-244.2	104.8	75.0
90	42.2	7.5	-141.5	77.0	-29.5	96.2	61.6
Mean (Day 21-90)	37.6	6.2	90.2	8.0	28.6	108.0	48.0

Table 17. Available Potential Energy and the Related Energy Transformations in the Upper Layer.
Units: .866 x 10^6 ergs cm^{-2} or .866 ergs cm^{-2} sec^{-1}

Day	$\bar{A}$	A'	$[\bar{A}\cdot\bar{A}]$	$[\bar{A}\cdot\bar{K}]$	$[A'\cdot K']$	$-[\bar{Q}\cdot\bar{A}]$	$-[Q'\cdot A']$
2	4.5	0	0	-4.6	0	4.7	0
4	4.5	0	-.1	-5.0	-1.0	4.7	0
6	4.5	.3	-.5	-4.4	-2.0	4.7	.1
8	4.6	.5	-.7	-4.5	-1.6	4.6	.2
10	4.7	.9	-1.1	-4.9	-4.7	4.9	.4
12	5.0	1.8	-1.7	-5.7	-10.3	5.2	.7
14	5.5	2.9	-3.2	-6.4	-13.1	5.7	1.2
16	6.4	4.1	-6.5	-5.8	-18.3	6.5	1.6
18	7.4	5.4	-7.8	-4.8	-17.4	7.2	2.1
20	7.9	5.8	-4.2	-4.1	-8.6	7.6	2.3
22	7.7	6.0	-.6	-3.9	-8.3	7.5	2.5
24	7.0	7.4	.7	-3.0	-8.6	6.9	3.0
26	6.2	8.4	-.3	-1.0	-7.3	6.3	3.4
28	5.3	9.7	-3.7	2.7	-19.0	5.7	3.9
30	4.7	12.3	-11.2	7.3	-31.3	5.3	4.9
32	5.5	14.3	-26.7	8.3	-44.1	5.9	5.7
34	9.4	15.9	-63.2	22.4	-88.7	8.5	6.4
36	16.9	20.9	-110.4	40.8	-146.5	13.0	8.4
38	29.8	27.0	-160.6	43.7	-203.1	20.1	10.8
40	51.5	36.7	-230.1	44.5	-291.4	31.2	14.7
42	81.2	52.2	-326.7	103.7	-365.3	45.6	20.9
44	109.2	64.7	-374.5	167.8	-355.9	58.7	25.9
46	134.8	72.1	-300.9	81.5	-317.4	70.6	28.9
48	154.0	84.8	-76.6	-34.0	-178.2	79.4	33.9
50	136.2	100.8	197.7	-52.1	103.8	71.3	40.3
52	94.0	106.7	274.4	-90.8	247.1	52.0	42.7
54	61.1	103.2	200.5	-93.6	221.8	36.4	41.3
56	41.3	89.6	115.5	-46.9	193.7	26.5	35.9
58	28.0	69.3	58.6	-21.2	123.7	19.4	27.7
60	20.8	55.5	32.8	-16.7	73.4	15.4	22.2
62	16.4	40.1	15.3	-7.9	101.2	12.8	16.0
64	13.3	22.5	7.3	-.9	81.4	10.9	9.0
66	10.7	11.5	-3.3	4.7	31.5	9.3	4.6
68	10.5	8.0	-40.4	18.5	-43.4	9.2	3.2
70	17.0	13.8	-124.5	40.2	-178.7	13.1	5.6
72	38.7	31.0	-298.8	85.6	-385.9	24.7	12.4
74	81.8	60.8	-513.7	171.4	-581.6	45.8	24.3
76	134.3	89.0	-546.2	184.1	-645.8	70.4	35.6
78	175.3	113.8	-283.1	41.9	-514.4	89.3	45.5
80	174.3	136.7	207.3	-111.3	13.9	89.0	54.7
82	117.9	138.7	517.7	-171.2	542.0	63.3	55.5
84	55.0	117.0	377.8	-132.5	512.6	33.4	46.8
86	22.0	89.3	170.1	-64.5	301.3	16.2	35.7
88	8.3	59.5	50.7	-15.8	177.4	7.9	23.8
90	5.1	42.5	1.9	-4.1	40.1	5.4	17.0
Mean (Day 21-90)	53.9	55.2	-36.2	5.6	-47.1	27.4	22.1

magnitude of its value in the lower layer, so that the available potential energy of the longer wave becomes a major portion of the total available potential energy in the upper layer.

As we pointed out earlier, the change of available potential energy is very closely related to the meridional temperature profile, and the difference of the flow of available potential energy in the upper and the lower layers would indicate the interdependence of these layers. It is therefore of great interest to examine the similarities and the differences between energy transformations in the upper layer and those in the lower layer.

In the lower layer, or around 600 mb level, zonal non-adiabatic heating or cooling has maximum intensity. It generates zonal available potential energy at a mean rate of 1050.6 ergs cm^{-2} sec^{-1} during the period from the 20th day to the 90th. The meridional circulation in this layer converts zonal available potential energy into zonal kinetic energy at most times and reverses the direction only when the energy conversion from eddy available potential energy into eddy kinetic energy is very large. On the average, the rate of the energy conversion from zonal available potential energy into zonal kinetic energy, $\left(\bar{A}\cdot\bar{K}\right)$, is 207.5 ergs cm^{-2} sec^{-1}, which is much too small to balance the generation of zonal available energy by non-adiabatic

heating or cooling. The major sink of zonal available potential energy is the loss of zonal available potential energy to the eddies which almost always extract available potential energy from the zonal flow. On the average, zonal flow loses available potential energy to the eddies at a rate of 1003.6 ergs cm^{-2} sec^{-1}. Although eddy available potential energy has a diabatic source in this layer, namely the generation of eddy available potential energy through diabatic heating or cooling caused by the land-sea thermal contrast, the lower layer loses more A' to the space than it gains from the bottom. The net rate of the diabatic loss of eddy available potential energy averaged over the period is 99.3 ergs cm^{-2} sec^{-1}. The most of the available potential energy extracted by the eddies from the zonal flow is converted into eddy kinetic energy through the sinking of colder air and the rising of warmer air. In the beginning of the period the conversion of eddy available potential energy into eddy kinetic energy, $[A' \cdot K']$, oscillates strongly and even becomes negative in a few very short periods, then remains positive throughout. Its mean rate is 896.8 ergs cm^{-2} sec^{-1} which is the major kinetic energy source of the entire model atmosphere. A schematic representation of the energy flow is given in the lower half of Figure 6.

In the upper layer, or around 50 mb level, the flow of available potential energy is dramatically different. Here eddy kinetic

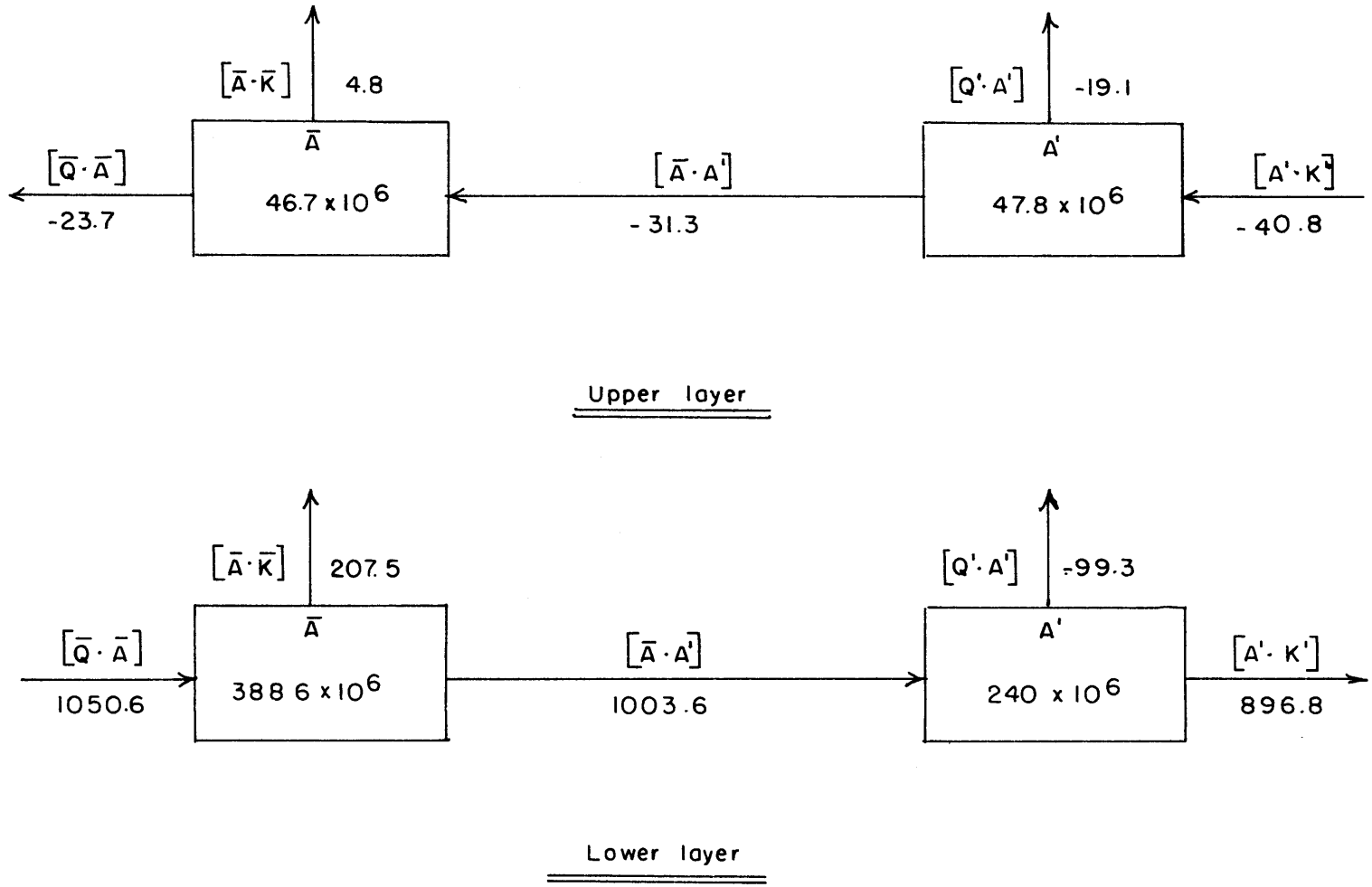

Figure 6. Flow chart of available potential energy. Units: Energy = ergs cm^{-2}, Conversion rate = ergs cm^{-2} sec^{-1}.
(See Table 16 for the transition layer).

energy is, on the average, converted by baroclinic process into eddy available potential energy at a mean rate of 40.8 ergs cm^{-2} sec^{-1}. That is, eddy available energy receives its supply from eddy kinetic energy instead of expending it. As in the lower layer diabatic eddy heating or cooling dissipates only a small portion of the available potential energy in this layer. The rate of dissipation is 19.1 ergs - cm^{-2} sec^{-1}. The major sink of the eddy available potential energy is the loss to the zonal available potential energy through eddy transport process. Although the instant value of the conversion $[\bar{A}\cdot\acute{A}]$ oscillates below and above zero, the mean value over the whole period gives a large negative value -31.3 ergs cm^{-2} sec^{-1}. The zonal available potential energy receives this amount to compensate its loss to space caused by non-adiabatic heating or cooling which on the average is -23.7 ergs cm^{-2} sec^{-1}, and to compensate the expenditure in the production of zonal kinetic energy through meridional overturning which is 4.8 ergs cm^{-2} sec^{-1}. The differences in energy transformation between the upper and the lower layer are indeed very striking. The directions of the biggest transformations in the two layers are unmistakably opposite to each other. Non-adiabatic heating, the only source of available potential energy in the lower layer, is the major sink of the upper layer. Eddy kinetic energy, the major sink of the

available potential energy in the lower layer becomes the major supplier of the available potential energy in the upper layer. A flow chart of the available potential energy in the upper layer is given in the upper part of Figure 6. Comparing the upper part and lower part of Figure 6, one immediately sees that in the lower layer imported heat flow creates kinetic energy while in the upper layer imported kinetic energy results in export of heat, in other words, the lower layer of the model works as a heat engine while the upper layer of the model works like a refrigerator. The reason for the passive nature of the upper layer is of course due to the vertical decrease of the inposed horizontal differential heating and the vertical increase of the hydrostatic stability.

It ought to be mentioned here that the transformations of eddy energy in the upper layer is mainly carried out by the longer wave while the reverse is true in the lower layer. The percentage of $[A' \cdot K']_2$ to $[A' \cdot K']_{total}$ is 98% in the upper layer but only 12% in the lower layer during the period from the 20th day to the 90th day.

b) Kinetic energy

Zonal kinetic energy per unit mass has its maximum around the level p = 100 mb (Figure 7). It decreases both upward and downward according to the different meridional temperature profiles above and below. The kinetic energy per unit mass in wave number six has its

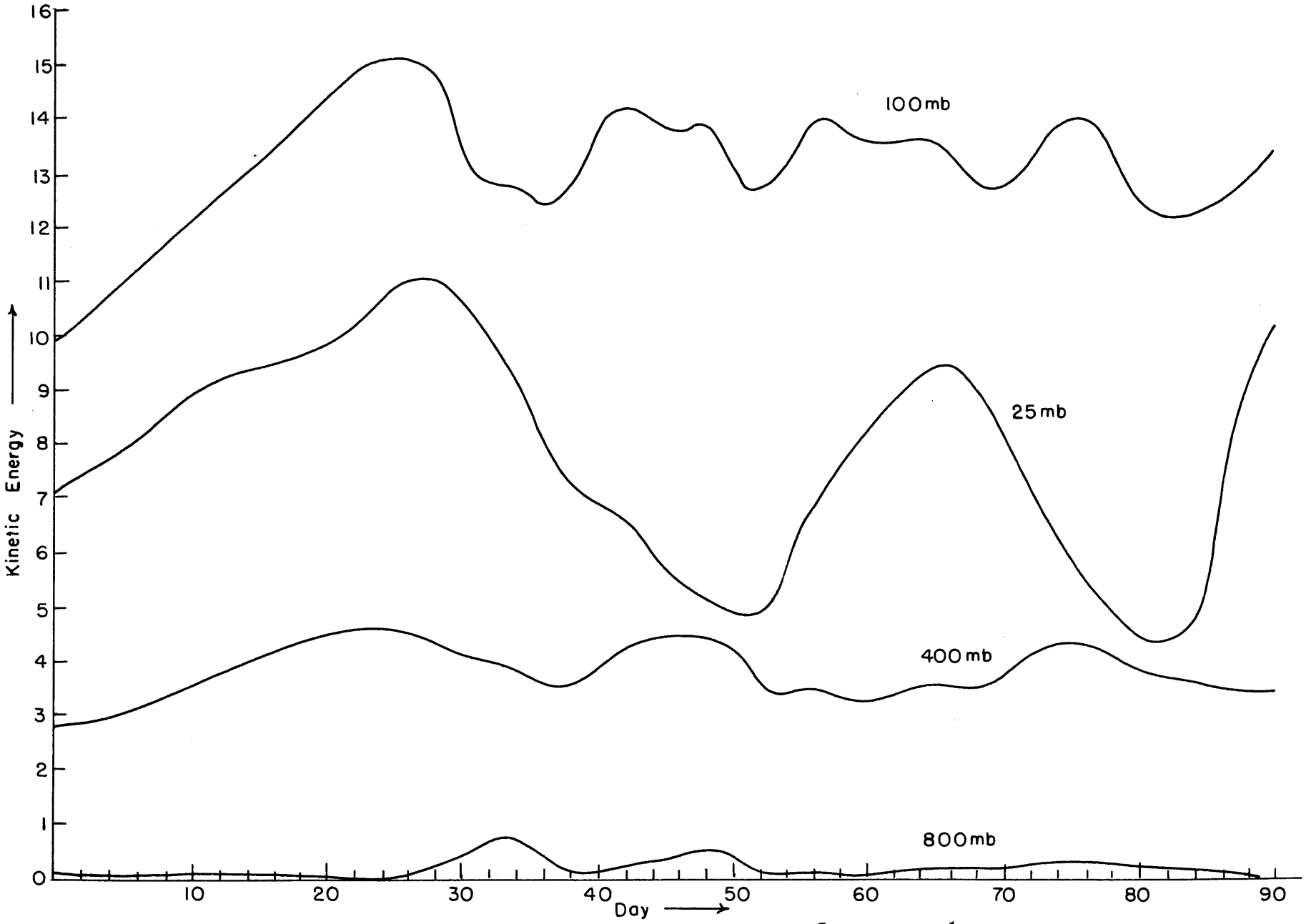

Figure 7. Time sequence of zonal kinetic energy. Units: 2.03×10^5 ergs gm^{-1}.

maximum around the level p = 400 mb. The kinetic energy per unit mass in wave number 2 has its maximum around p = 25 mb which is the highest level in the model. At the lower two levels the shorter wave dominates the eddy flow except in the very beginning of the experiment; the longer wave always dominates the eddy flow at the uppermost level (see Figure 8). Similar spectral distribution is found for the energy conversion between eddy kinetic energy and zonal kinetic energy. The conversion $[K' \cdot \bar{K}]$ generally oscillates about zero but it gives a positive mean value at all the levels. The mean dissipation of kinetic energy due to lateral eddy viscosity is about the same magnitude as the mean dissipation due to vertical shear. The mean dissipation due to the lower boundary skin friction and the mean dissipation due to vertical shear in the lower layer are about the same magnitude since both zonal flow and the eddies are very weak at the bottom and hence have strong shear in the lowest layer.

We have seen in the previous section III,a that the major kinetic energy source is in the lower layer, and that the upper layer baroclinically expends much more kinetic energy than what is generated within the layer. It is then necessary for the upper layer to get a kinetic energy supply from below. In order to see how the kinetic energy propagates from the lower layer into the upper layer in this

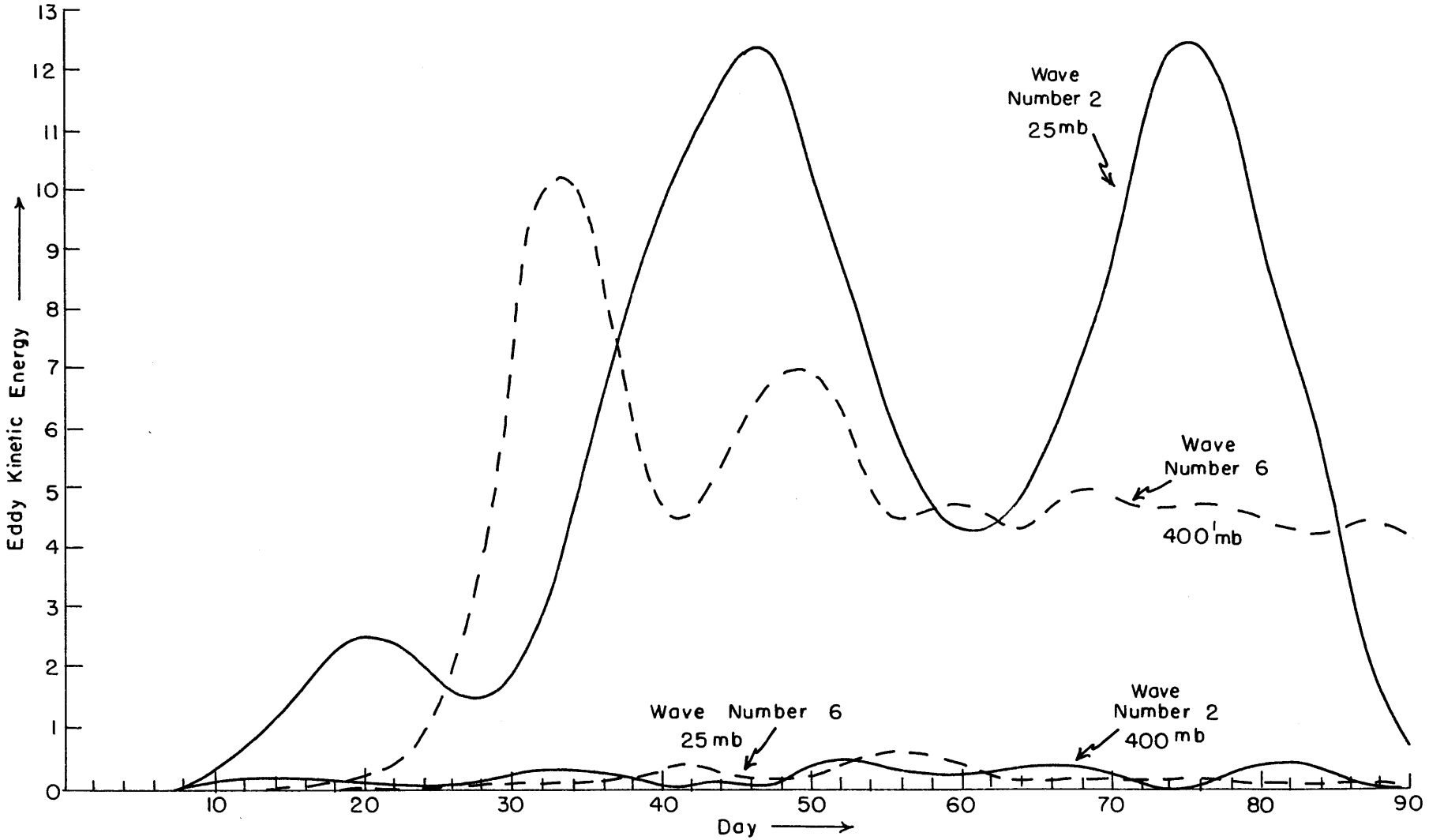

Figure 8. Time series of eddy kinetic energy. Units: 2.03×10^5 ergs gm $^{-1}$.

simple model we roughly regard the middle layer as a loose "internal boundary layer" and examine the upward flow of kinetic energy within it, i.e., the upward flow of kinetic energy across the isobaric surface p = 200 mb. The energy equation above and below 200 mb has been given by equations (89) - (107) in Chapter 3. The calculated energy transformations for the period from the 20th day to the 90th day are given in Table 18. Before the 20th day the entire model atmosphere is almost completely controlled by the symmetric flow.

One notices in Table 18 that the vertical transport of zonal kinetic energy across 200 mb due to shear drag is always negative because the zonal kinetic energy at 100 mb is always bigger than the value at 400 mb. The vertical transport of eddy kinetic energy across 200 mb due to shear drag is almost always positive because the dominant part of eddy kinetic energy, wave number six, is always bigger at 400 mb than at 100 mb. The vertical transport of kinetic energy due to large-scale motions is quite different in character. It generally oscillates around zero but stays longer at large positive values than at small negative values. The vertical transport due to mean meridional circulation oscillates more frequently and with smaller magnitude than the vertical transport due to large-scale eddies. Hence, on the average, the vertical transport due to mean meridional circulation is one

Table 18. Kinetic energy and energy transformation. Units: 10^6 ergs cm^{-2} or ergs cm^{-2} sec^{-1}.

DAY	Below 200 mb							
	$\bar{K}$	K'	$[K' \cdot \bar{K}]$	$[K' \cdot \bar{K}]_G$	$[\bar{A} \cdot \bar{K}]$	$[A' \cdot K']$	$[k \cdot \bar{K}]$	$[k \cdot K']$
22	378.9	42.3	27.0	9.0	437.8	254.6	363.1	85.3
24	382.3	100.2	95.6	5.0	326.0	763.6	361.4	183.6
26	381.5	223.9	230.4	-4.4	82.2	1697.6	355.8	384.9
28	379.1	430.8	182.0	-20.4	-155.4	2851.1	356.9	725.7
30	364.6	754.4	62.6	-35.6	-221.3	3770.0	385.3	1209.2
32	382.0	1006.2	416.4	-46.0	-100.8	3028.5	496.1	1415.2
34	391.2	985.0	217.3	-7.3	243.1	732.2	515.3	1297.4
36	326.4	806.3	-309.3	29.3	518.1	-794.4	365.6	1054.1
38	302.5	571.5	-10.3	33.0	443.1	-583.4	293.7	736.6
40	333.6	417.3	353.5	62.8	259.6	651.0	297.8	543.7
42	382.7	407.7	40.9	93.6	213.0	1557.2	334.3	574.7
44	386.6	525.1	-235.2	64.8	177.2	1815.0	351.9	752.4
46	398.4	629.8	415.4	13.2	-62.3	1844.6	386.9	848.4
48	421.3	641.2	400.8	-46.3	-66.3	1402.1	428.2	849.9
50	359.7	683.3	-334.0	-39.2	345.1	337.1	358.0	895.5
52	300.0	647.9	58.0	-10.3	359.3	-266.5	314.7	804.5
54	292.6	509.1	457.5	5.6	195.0	-42.8	289.2	629.9
56	303.6	421.5	125.1	16.0	272.7	397.0	284.6	557.9
58	288.3	444.8	-256.9	12.8	424.4	546.4	283.8	611.6
60	279.7	464.6	-47.2	4.7	249.5	715.9	291.8	617.1
62	289.2	438.5	194.3	-.4	26.1	907.0	292.3	633.7
64	305.8	428.3	314.1	-1.7	8.0	1235.3	296.1	578.9
66	311.2	477.9	-11.0	12.6	242.3	1272.1	303.0	679.1
68	314.0	517.1	-57.9	39.6	372.2	1055.3	314.7	737.1
70	330.3	496.7	10.3	72.2	402.1	763.9	325.9	704.4
72	356.9	460.8	117.5	96.9	346.1	814.2	339.1	654.6
74	385.5	451.3	188.1	79.8	209.8	997.6	359.7	640.5
76	388.9	460.5	10.6	5.8	65.2	1016.4	365.4	648.3
78	356.1	476.1	-145.6	-41.3	-21.6	1040.2	341.3	654.8
80	329.1	472.4	48.6	-34.2	-54.7	916.0	319.3	624.3
82	321.7	440.2	256.8	-10.8	28.2	572.9	305.6	574.8
84	318.6	420.1	142.1	21.3	344.6	258.7	298.4	587.1
86	302.8	437.8	-122.2	37.5	627.8	142.4	293.3	643.7
88	295.0	441.6	-70.9	31.8	599.9	183.6	298.4	631.3
90	300.1	412.9	82.8	21.5	366.7	404.2	301.6	559.6
Mean	341.5	501.3	81.3	13.5	214.3	921.6	339.1	695.1

Table 18 continued.

DAY	Across 200 mb			
	$[\bar{K}_T \cdot \bar{K}_S]_A$	$[\bar{K}_T \cdot \bar{K}_S]_B$	$[K'_T \cdot K'_S]_A$	$[K'_T \cdot K'_S]_B$
22	135.8	-40.5	-38.6	-1.4
24	96.2	-41.5	18.8	1.3
26	-10.5	-41.9	170.3	5.4
28	-240.9	-41.2	422.3	10.4
30	-510.0	-38.5	765.3	17.0
32	-388.3	-35.5	784.0	20.3
34	194.6	-35.2	-6.8	18.4
36	244.2	-35.3	-254.2	14.5
38	167.2	-36.6	5.8	9.8
40	114.2	-38.7	263.0	7.4
42	-101.8	-39.3	442.9	7.7
44	-291.4	-38.1	511.6	10.4
46	-226.8	-36.7	560.5	13.1
48	-10.8	-37.2	161.2	14.8
50	142.4	-36.5	-388.2	17.0
52	262.4	-36.4	-357.6	16.0
54	279.0	-39.2	-186.4	12.4
56	177.1	-41.2	-179.0	10.4
58	45.5	-41.6	-89.4	12.3
60	-60.6	-40.8	179.9	11.9
62	-112.7	-40.5	367.6	7.6
64	-103.5	-40.3	399.0	5.6
66	-8.1	-38.7	288.1	2.3
68	17.7	-36.5	281.2	-2.2
70	64.9	-35.6	205.0	-4.9
72	79.4	-36.4	184.8	-2.7
74	30.2	-37.9	192.1	3.4
76	-134.5	-38.8	265.6	10.4
78	-208.8	-37.3	483.8	11.7
80	-234.1	-34.5	477.1	5.8
82	6.5	-33.5	68.8	-3.1
84	304.5	-34.4	-443.3	-5.9
86	380.1	-35.8	-548.1	-2.3
88	293.1	-37.5	-318.1	.8
90	164.4	-39.4	-50.0	2.0
Mean	13.3	-38.0	132.6	7.4

Table 18 continued

DAY	Above 200 mb						
	$\bar{K}$	K'	$[\acute{K}\cdot\bar{K}]$	$[\bar{A}\cdot\bar{K}]$	$[A'\cdot\acute{K}]$	$[\bar{k}\cdot\bar{K}]$	$[\bar{k}\cdot\acute{K}]$
22	564.8	47.6	-12.5	20.5	-20.5	28.0	9.8
24	576.5	31.1	18.9	14.3	-13.6	28.8	10.2
26	583.5	37.3	104.0	-3.7	12.0	29.3	25.3
28	575.8	58.1	229.9	-42.4	34.5	29.4	28.3
30	549.0	102.8	411.8	-97.1	54.7	30.0	55.3
32	504.5	163.6	421.4	-70.5	68.7	28.7	87.8
34	493.9	229.3	-301.1	64.9	-68.8	28.5	93.7
36	472.7	223.5	-364.7	98.8	-203.7	26.6	72.7
38	473.0	203.3	-104.9	82.2	-181.1	26.5	57.3
40	496.4	189.8	51.6	64.1	-187.8	27.6	50.3
42	513.8	191.7	97.2	74.4	-223.6	29.7	52.3
44	497.7	211.1	125.0	89.4	-227.5	29.4	64.4
46	481.2	231.1	262.5	20.4	-153.2	31.4	76.0
48	486.6	219.0	86.5	-34.3	-96.2	32.5	77.2
50	458.1	196.8	-279.2	-14.0	7.8	30.1	69.6
52	443.3	188.2	-115.7	-16.7	129.6	29.2	61.5
54	471.1	151.7	31.7	-25.9	156.7	29.4	48.9
56	503.5	126.2	34.3	-12.4	110.6	30.6	42.4
58	511.8	101.6	32.2	-16.2	48.5	31.0	41.9
60	508.6	104.0	175.0	-38.3	83.1	31.0	46.7
62	515.0	121.1	287.8	-37.8	123.2	31.9	54.8
64	524.0	144.0	206.2	-23.2	90.1	32.3	61.4
66	512.8	201.4	-55.4	10.9	22.9	30.9	71.0
68	492.1	256.6	-91.7	38.5	-14.2	28.8	77.9
70	482.8	290.8	-74.9	68.9	-145.8	27.6	79.9
72	488.7	283.0	-55.7	100.0	-295.9	28.3	73.0
74	500.3	247.3	-66.5	156.4	-441.2	29.2	66.5
76	499.1	198.0	-20.1	133.5	-483.8	32.2	58.0
78	469.5	174.3	178.3	-26.4	-288.5	32.3	59.0
80	435.4	199.7	299.3	-150.5	170.1	30.8	69.8
82	423.0	249.7	235.2	-158.9	488.5	28.9	82.4
84	439.9	247.4	-25.2	-70.5	300.2	28.1	82.4
86	466.3	194.6	-172.2	12.5	93.4	28.2	70.2
88	495.4	149.6	-93.1	50.3	47.7	29.5	58.6
90	524.6	124.4	25.6	29.6	22.0	31.2	49.4
Mean	498.1	174.0	42.3	8.3	28.0	29.7	59.6

order of magnitude smaller than the value due to large-scale eddies.

The mean flow of kinetic energy above and below 200 mb can be schematically represented by the upper and lower part of Figure 9 respectively. It is noticed that the directions of energy flow above and below 200 mb are in the same sense except, 1. the conversion between eddy kinetic energy and eddy available potential energy, 2. of course, the interactions between the two layers.

IV. Mean zonal wind and the convergence of momentum due to eddies.

The mean zonal wind and the convergence of momentum due to eddies averaged over the period from the 30th day to the 90th day are given in Table 19 and Figure 10 respectively. The mean zonal wind is west almost everywhere from 800 mb up except in the tropical region at 800 mb. The west wind generally increases with increasing height from 800 mb up to about 100 mb then decreases with increasing height. There is only one maximum, 34 m sec^{-1}, located around 40^{o} latitude at the 100 mb level. The axis of the maximum zonal wind generally tilts with height toward the equator.

The mean convergence of momentum due to eddies at levels 800 mb, 200 mb and 100 mb is positive in the latitudinal belt from about 20^{o} to about 65^{o} latitude, and negative elsewhere. Since no

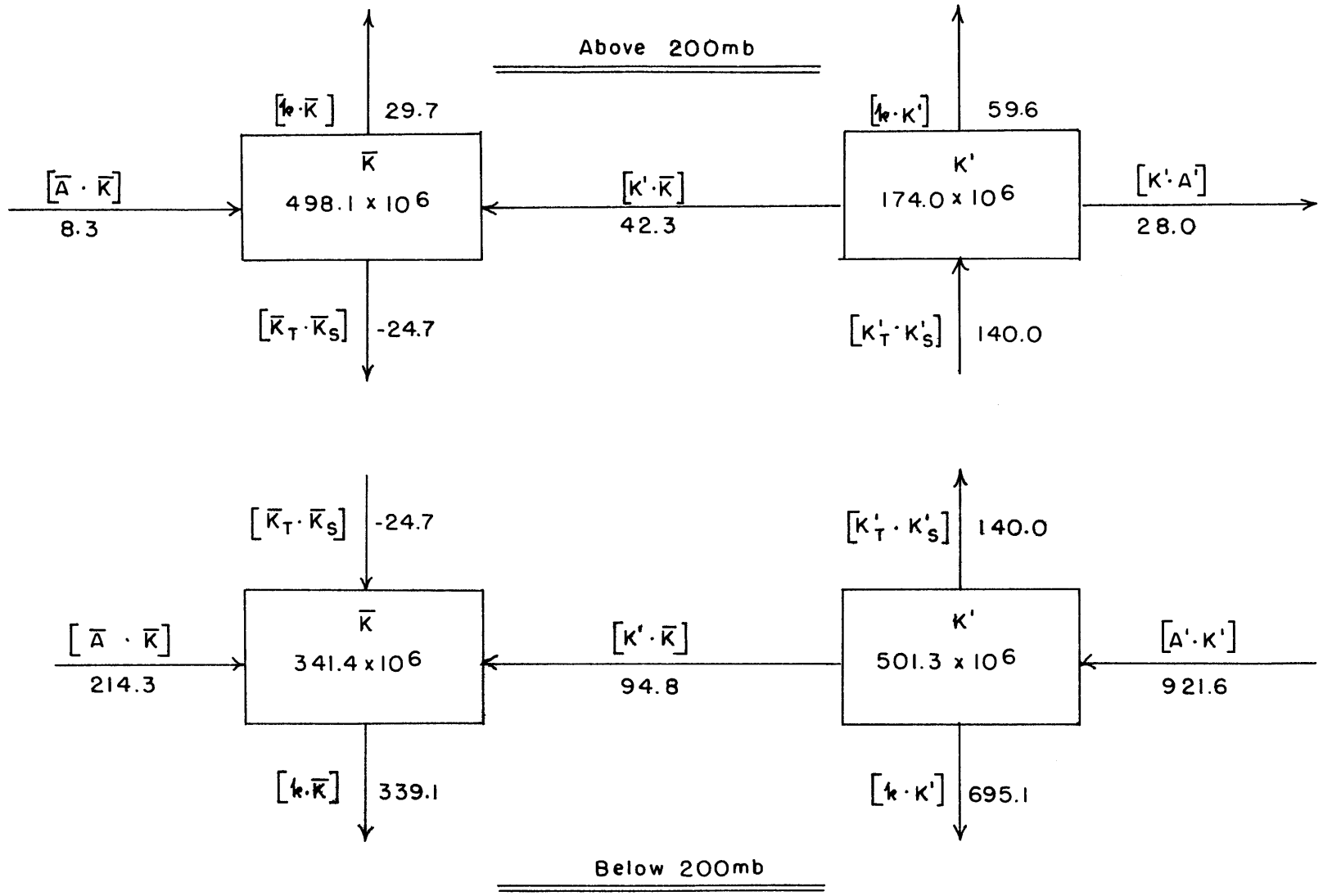

Figure 9. Kinetic energy flow above and below 200 mb. Units: Energy = ergs cm^{-2}, Conversion rate = ergs cm^{-2} sec^{-1}.

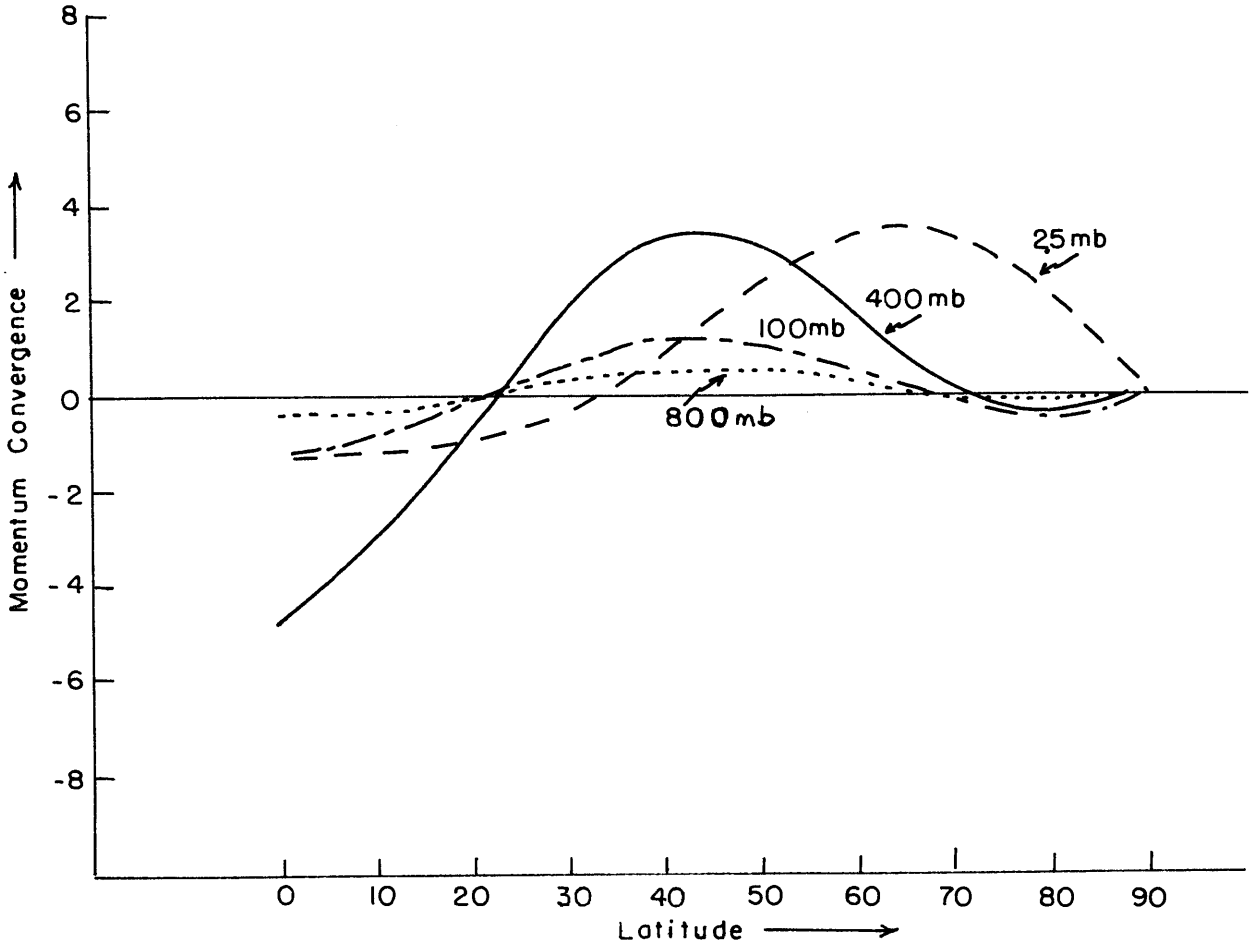

Figure 10. Mean momentum convergence due to eddies. Units: 10^{-6} m sec^{-2}.

Table 19. Zonal velocity averaged over the period from the 30th day to the 90th day. Unit m - sec^{-1}.

latitude	0^{o}	10	20	30	40	50	60	70	80	90
50 mb	4.0	7.4	15.3	22.8	25.1	20.9	13.0	5.0	1.2	0
100 mb	2.6	6.6	16.5	27.2	33.6	33.2	27.0	17.5	8.5	0
400 mb	5.4	6.1	8.0	11.2	15.0	18.1	18.9	15.9	9.1	0
800 mb	-3.5	-2.5	-.1	2.4	3.8	3.6	2.3	.9	.2	0

transport of momentum is allowed at the equator, the above distribution of momentum convergence implies momentum transports from the tropical region and from the polar region toward the middle latitudes. At the 25 mb level, the zone of the convergence of eddy transport of momentum shifts toward the poleside, and the maximum convergence located at 65^{o} latitude. From 35^{o} latitude down to the equator there is a divergence region. The eddy transport of momentum then tends to build up maximum zonal winds near 40^{o} latitude at the levels p = 800 mb, 400 mb and 100 mb, and a maximum zonal wind near 60^{o} latitude at the 25 mb level. However, no polar maximum zonal wind actually appears in the meridional profile of mean zonal wind at 25 mb because the convergence is not strong enough to overcome the effect of mean

meridional motion.

V. Mean meridional circulation.

The mean values of $\bar{\omega}$ in the period from the 30th day to the 90th day are given in Table 20. Upward mean motion prevails in the equatorial region and the region around 60° latitude while downward mean motion prevails near the pole and in the region around 30° latitude. A three-cell mean meridional pattern is clearly revealed.

The equation of continuity in our model may be written as

$$\omega_j = \nabla^2 X_j \quad , \qquad j = 2, 4, 6.$$

$$X_j = \nabla^{-2}\omega_j = -a^2\left(\frac{\omega^{\circ}_{2j}}{6}P^{\circ}_2 + \frac{\omega^{\circ}_{4j}}{20}P^{\circ}_4 + \frac{\omega^{\circ}_{6j}}{42}P^{\circ}_6\right), \qquad j = 2, 4, 6.$$

By definition we have for mean meridional velocity

$$\bar{v}_j = -\frac{\partial}{a\partial\phi}\,\frac{\bar{X}_{j-1} - \bar{X}_{j+1}}{\beta_{j-1} - \beta_{j+1}} \quad , \qquad j = 1, 3, 5, 7,$$

or,

$$\bar{v}_j = \frac{a}{\beta_{j-1} - \beta_{j+1}}\left\{\frac{\omega^{\circ}_{2j-1} - \omega^{\circ}_{2j+1}}{6}\frac{dP^{\circ}_2}{d\phi} + \frac{\omega^{\circ}_{4j-1} - \omega^{\circ}_{4j+1}}{20}\frac{dP^{\circ}_4}{d\phi}\right.$$

$$\left. + \frac{\omega^{\circ}_{6j-1} - \omega^{\circ}_{6j+1}}{42}\frac{dP^{\circ}_6}{d\phi}\right\} \qquad j = 1, 3, 5, 7,$$

where $\omega^{\circ}_{n8} = \omega^{\circ}_{n0} = 0$. The averaged value of the mean meridional velocity over the period from the 30th day to the 90th day are given in Table 21. A three-cell pattern appears in the lower layer but the

Table 20. Averaged $\bar{\omega}$ from the 30th day to the 90th day. Units: 10^{-6} mb sec^{-1}

Latitude	0	10	20	30	40	50	60	70	80	90
50 mb	-1.8	-1.0	.5	1.5	1.2	.1	-.9	-1.0	-.3	0
200 mb	-6.6	-4.3	.8	4.3	3.9	.8	-1.4	-.5	2.2	3.6
600 mb	-85.1	-48.1	26.5	66.6	36.8	-25.3	-47.4	4.4	89.7	131.0

Table 21. Mean meridional velocity from the 30th day to the 90th day. Units: cm sec^{-1}

Latitude	90	80	70	60	50	40	30	20	10	0
25 mb	0	-.2	-1.3	-2.7	-3.1	-1.2	2.0	4.2	3.4	0
100 mb	0	1.1	1.3	.8	.6	1.8	3.6	4.5	3.2	0
400 mb	0	14.8	16.3	4.8	-6.5	-4.5	10.0	22.2	18.7	0
600 mb	0	-15.2	-16.7	-4.8	6.6	3.9	-11.6	-24.5	-20.3	0

indirect cell is the weakest. A large cell appears in the upper layer covering thehigh and middle latitudes. Generally speaking, northward mean meridional motion prevails in the lower stratosphere from about 35^{o} down to the equator while southward mean meridional motion prevails in the high latitudes of the lower stratosphere. The dominant appearance of the direct cell in the lower layer is certainly responsible for the large value of $\{\bar{A}\cdot\bar{K}\}$ shown in the lower part of Figure 9.

VI. A brief note on truncation errors of integration scheme

No detailed analysis of the truncation error will be attempted in this study. However, some brief checks will be made in order to have an idea whether the error might be important to our conclusions. We computed the mean rate of the net change of eddy and zonal available potential energies in the upper and lower layers from Figure 6, also computed the mean rate of the net change of eddy and zonal kinetic energies for the layers above and below 200 mb from Figure 9. Both these values are shown in Table 22 with the actual net changes of the corresponding energies in the corresponding layers. In general errors are bigger in eddy energy than in zonal energy. This is probably due to the fact that the conversions of eddy energy are bigger and more oscillatory than those of zonal energy and that the mean values

Table 22. Truncation error in the rate of energy change.

Energy	Actual rate of change	Computed rate	Difference
$\bar{A}_6$	-.4	2.8	-3.2
A_6'	4.7	-9.6	14.3
$\bar{A}_2$	-150.7	-160.5	9.8
A_2'	27.0	7.5	19.5
$\bar{K}_s$	-2.6	-3.8	1.2
K_s'	9.9	10.1	-.2
$\bar{K}_T$	-12.0	-5.3	-6.7
K_T'	61.2	-8.3	69.5

are obtained from the data of every other day. Comparing the truncation errors with the magnitudes of the conversions and the mean values of the energies shown in Figure 6 and Figure 9, it is safe to say that those truncation errors will not change our conclusions.

VII. A comparison with observations in the real atmosphere.

Generally speaking, whenever a model is employed to study any accumulative phenomenon in a complicated dynamical system the capability of explaining such a phenomenon by the model does not necessarily imply the correctness of the model in describing the major responsible mechanism of the real phenomenon. In other words, the major mechanism which explains the phenomenon in the model is not necessarily the major mechanism responsible for the real phenomenon. One way to ascertain the validity of the explanation is to verify also the other phenomena which are known to be physically related to the one of major concern. In the following we shall therefore compare the features in our model with the corresponding observations in the real atmosphere.

a) Given in Figure 11 are the meridional temperature profiles at 50 mb in January - March and April - June, 1958, and our result. Although our meridional temperature profile at 50 mb does

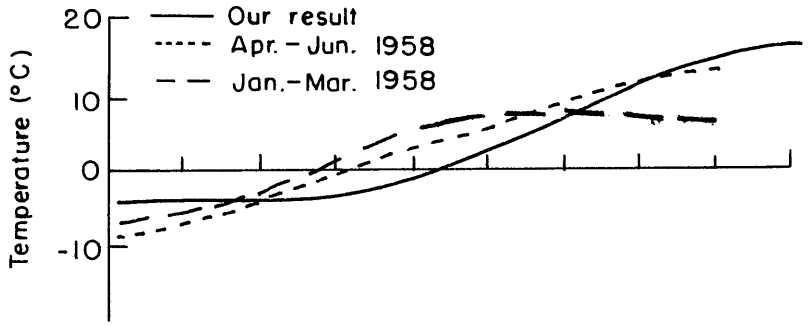

Figure 11. A comparison of temperature profile at 50 mb with observed data.

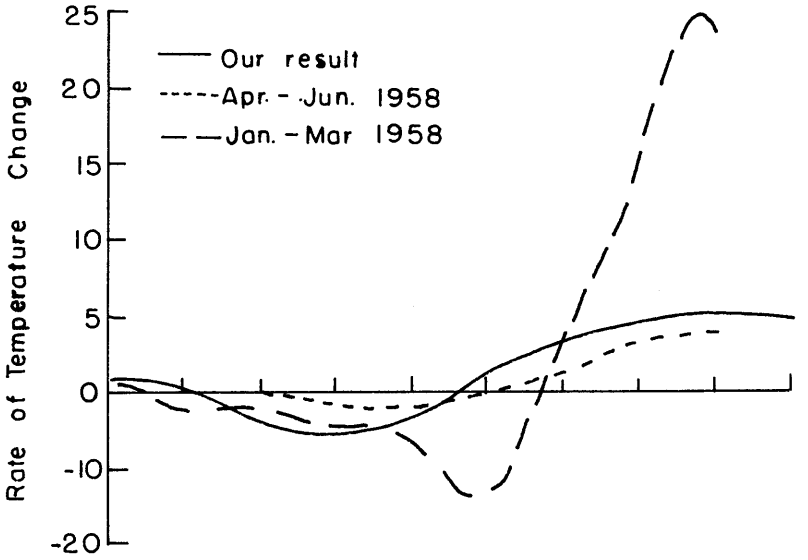

Figure 12. A comparison of heating rate at 50 mb due to eddy transport with actual estimates (Oort, 1964b). Units: 10^{-6} °C sec^{-1}.

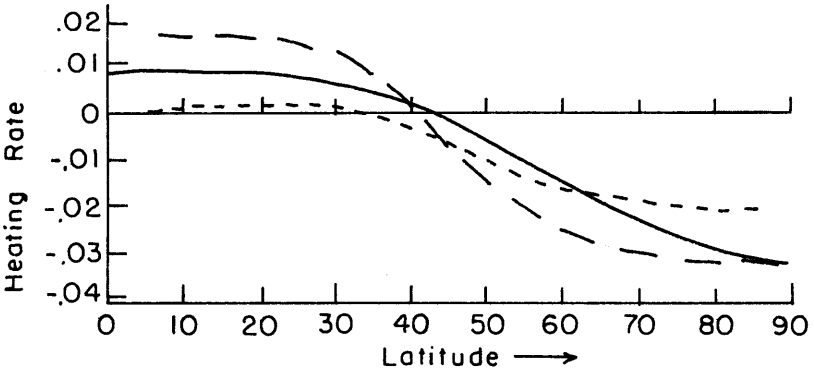

Figure 13. A comparison of net heating in the upper layer with actual estimates (dotted line, Manabe; dashed line, Ohring). Units: ly min^{-1}.

Table 23. Estimates of hemispheric energy transformations.*

Units: 10^{20} ergs sec^{-1}

	$[\bar{Q}\cdot\bar{A}]$	$[Q'\cdot A']$	$[\bar{A}\cdot\bar{A}']$	$[\bar{A}\cdot\bar{K}]$	$[A'\cdot K']$	$[K'\cdot\bar{K}]$
	Upper layer only					
Present Study			-.798	-1.040		.360
Study by Oort (1964)			-.531	-.254		.221
	Total atmosphere					
Present Study	35.1	-4.7	27.8	5.7	22.8	3.5
	W S	W S	W S	W S	W S	W S
Wiin-Nielsen & Brown (1960)	72.4	-40.8				
Wiin-Nielsen (1959)				2.6 -2.8	37.4 28.2	
Wiin-Nielsen, Brown & Drake (1963)			116.4 50.3			-.08 10.13
Brown (1964)	72.4 27.6	-40.8 -8.0				

*W and S indicate respectively winter and summer half year in which the estimates are made. For exact period of each estimate see individual paper listed in the references.

not agree very well with the actual observations, the overall increase of temperature from the equator to the pole is in good agreement with the observations. In view of the simplicity of the model such an agreement is satisfactory. We would like to point out here that at no time in our computation was a quasi-equilibrium state of the entire model atmosphere reached. The lower layer seems almost settled, but in the upper layer, oscillations still go on strongly. (see Figure 8). This probably implies that the vertical coupling of our model is not adequate. We intuitively expect that the overall temperature difference between the equator and the pole in the upper layer would reduce somewhat if the oscillations in the upper layer settled down to some kind of quasi-equilibrium.

b) In Figure 12 the meridional distribution of heating rate due to horizontal eddy heat transport at 50 mb is compared with the corresponding atmospheric values computed by Oort (1964) for the periods January - March and April - June 1958. Our result agrees rather well with the April - June distribution but is much smaller than the January - March values.

c) As a justification of the chosen function of the imposed heating the distribution of mean non-adiabatic heating rate in the upper layer is compared with the results of Ohring (1958) and Manabe et al (1961) in Figure 13. The agreement is rather surprising.

d) The directions of energy flow shown in Figure 6 and Figure 9 are in good agreement with the actual estimates by Oort and others except the conversion from zonal available potential energy to zonal kinetic energy in the lower layer. The active role of the troposphere and the passive nature of the lower stratosphere are well portrayed in the model. A quantitative comparison of our results with the observational estimates by Oort and Wiin-Nelson et al is given in Table 23. It shows that our results are comparable with the actual estimates.

e) The distribution of meridional momentum convergence due to horizontal eddy transports shown in Figure 10 is qualitatively in agreement with observed data. The distribution of zonal wind also agrees fairly well with observed data except that no polar jet exists at the upper most level and the maximum zonal wind appears at 100 mb instead of 200 mb because of limited vertical resolution. The zonal flow and the eddy motions are too weak at the lowest level because the low-level active eddies whose scales are smaller than wave number 6 are not included in the model.

f) The three-cell pattern of the mean meridional circulation, shown in Tables 20 and 21, has a weaker indirect cell than that deduced indirectly from observed data.

g) Both the increase in intensity of wave number 2 and the

decrease in intensity of wave number 6 with increasing height are qualitatively in agreement with our synoptic experience.

The discrepancies in the energy conversion $[\hat{A}_2 \cdot \bar{K}_2]$ and in the intensity of the indirect meridional cell may be attributed to the fact that in representing zonal flow profile, we use more modes than are allowed for the eddies. More specifically, three modes are included in the expansion of zonal flow (P_1^0 , P_3^0 and P_5^0) and its corresponding thermal structure (P_2^0 , P_4^0 and P_6^0), while only two modes are included in the expansion of eddy flow (P_{m+1}^m and P_{m+3}^m) and its corresponding thermal structure (P_m^m and P_{m+2}^m) for each wave number m . The purpose of such a selection of harmonics was to broaden the interaction spectra without increasing too much the work in the computation. However, in so doing we enhanced relatively the importance of symmetric effects, e. g., we enhanced the effect of symmetric baroclinicity relative to the effect of asymmetric baroclinicity. Consequently we over-emphasized the role of meridional overturning in producing kinetic energy and increased the intensity of the direct meridional cells relative to the intensity of the indirect cell, and this would in turn modify the zonal flow. Fortunately, our conclusion will not be affected by such errors. On the contrary, to include one more mode in the eddy expansions would intensify the eddy activity and hence would further favor the conclusions.

In our model the energy in the upper layer is dissipated through two processes, namely, small-scale frictional dissipation and radiative loss to the space. Both these losses are directly or indirectly compensated by vertical transport of eddy kinetic energy from below. The possibility of upward propagation of kinetic energy by large-scale disturbances has been theoretically studied (e. g., Charney and Drazen, 1961; Eliassen and Palm 1961). According to Charney and Drazen, vertical energy propagation in planetary standing waves can occur only when the mean zonal velocity is positive but smaller than approximately 38 m sec^{-1}; unstable waves are external and cannot penetrate very far into the upper atmosphere. According to Eliassen and Palm, planetary stationary waves in the westerlies transport wave energy upward if the waves tilt westward with height. In our experiment the forced longer wave is not stationary so that the above theoretical results do not apply. The major portion of the vertical energy transport $[K_T' \cdot K_S']_A$ given in Table 18 is actually due to the longer wave. The shorter wave in our experiment also transports wave energy upward across the 200 mb level; the amount transported by the shorter wave is almost as much as that by the longer wave. However, strong trapping of wave energy in the shorter wave occurs directly above the 100 mb level so that the energy of the short

wave becomes very small at the level 25 mb (see Figure 8). This is in good agreement with Charney and Drazen's result. Although the result of our experiment indicates the capability of large-scale waves in transporting energy into the lower stratosphere, the mean rate of the upward transport of kinetic energy due to the waves may not be taken faithfully in a quantitative sense when it is compared with the case in the real atmosphere. For in our model no downward propagation of kinetic energy into the lower stratosphere from above is allowed, and the upward energy flux across the 200 mb level due to small-scale eddies happens to be negative mainly as a result of the vertical finite resolution. In the real atmosphere the upward energy flux due to small-scale eddies is generally positive, and there is evidence that kinetic energy propagates from the upper stratosphere down to the lower stratosphere during certain short periods (e. g., Reed et al, 1963).

7. FURTHER EXPERIMENTS -- The Dependence of the Equator-to-pole Temperature Difference on the Vertical Distribution of Latitudinal Differential Heating

In the previous sections we have succeeded fairly well in explaining the observed latitudinal temperature profile in the lower stratosphere and its connection with energy transformation by performing a numerical experiment. In that experiment it has been seen how the generalized thermal wind equation and the linear divergence term in the vorticity equation were truncated. We may ask: "Would a different method of truncation of those terms change the main conclusion?" or, "Did the method of truncation of those terms crucially alter the statistical behavior of the dynamical system as far as the purpose of our study is concerned?" To test this it would be better to carry out another similar numerical experiment completely avoiding such kinds of truncation rather than just changing the way of truncation. We shall in this section perform an experiment in which we adopt the β -plane geometry, and then compare the results of the two experiments in connection with the major points with which we are concerned.

Another major purpose of the following experiment is to throw some light on the dependence of the equator-to-pole temperature difference on the vertical distribution of forcing. We might expect that the

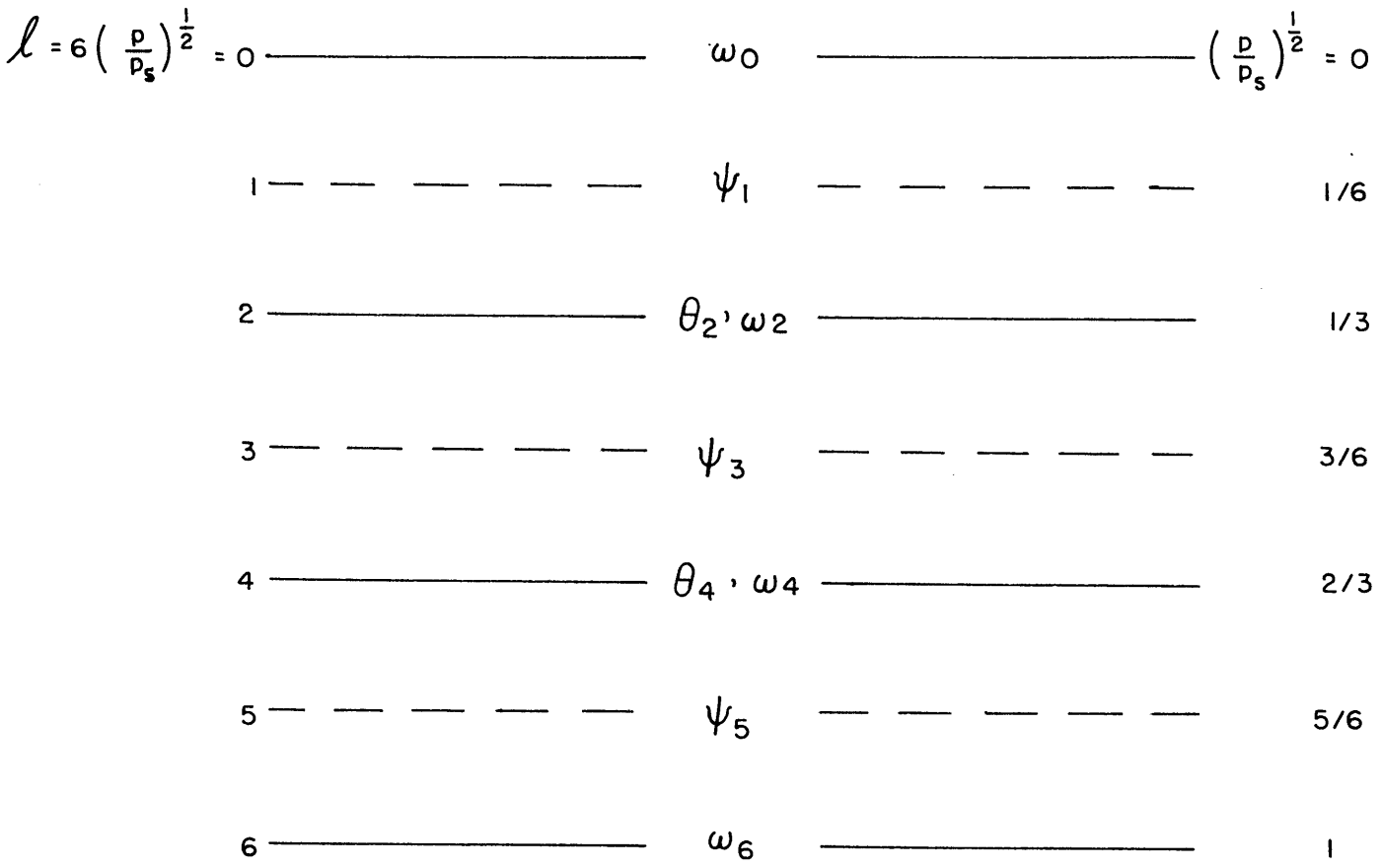

Figure 14. Vertical finite resolution for further experiments.

relative intensity of the upper and lower forcing would, in principle, determine the degree of passivity of the more stable layer.

We shall use equations (1) - (3) instead of (4) - (6), i.e., f and β will be held constant. The vertical resolution and the designation of variables is shown in Figure 14. The atmosphere is divided into six equal intervals of $(p/p_s)^{\frac{1}{2}}$, one level less than before so that the ratio of upper and lower thermal forcing may be conveniently defined.

We now parameterize the forcing function and dissipative processes in the same manner as before, and write the vertical difference equation as follows:

$$\frac{\partial}{\partial t}\nabla^2\psi_\ell = -J(\psi_\ell, \nabla^2\psi_\ell) - \beta\frac{\partial\psi_\ell}{\partial x} + \frac{gf}{\ell p_s}(\omega_{\ell+1} - \omega_{\ell-1}) + A\nabla^4\psi_\ell - k_\ell\nabla^2(\psi_\ell - \psi_{\ell+2}) - \frac{\ell-2}{\ell}k_{\ell-2}\nabla^2(\psi_\ell - \psi_{\ell-2}), \quad \ell = 1,3,5. \tag{108}$$

$$\frac{\partial}{\partial t}\theta_\ell = -J(\psi_\ell, \theta_\ell) + \sigma_\ell\omega_\ell + k_\ell(\theta_\ell^* - \theta_\ell), \quad \ell = 2,4 \tag{109}$$

$$\nabla^2\theta_\ell = -\frac{f}{c_p}\frac{6^{2\kappa}}{(\ell+1)^{2\kappa} - (\ell-1)^{2\kappa}}\nabla^2(\psi_{\ell+1} - \psi_{\ell-1}), \quad \ell = 2,4 \tag{110}$$

and

$$\psi_\ell = \frac{1}{2}(\psi_{\ell+1} + \psi_{\ell-1}), \quad \ell = 2,4 \tag{111}$$

where $k_{-1} = 0$

$$k_\ell = \frac{9}{4} \frac{g^2 \mu_{\ell+1}}{p_s R T_{\ell+1}} \frac{\ell+1}{\ell} \qquad \ell = 1, 3 \tag{112}$$

The boundary conditions at the top and bottom of the atmosphere are

$$\omega_0 = 0 \quad , \quad \omega_6 = 0 \tag{113}$$

For simplicity we shall deal with a square region limited by "walls" at $y = 0$ and πL, but open at the sides $x = 0$ and πL where we impose the so called cyclic condition that the flow at $x = 0$ is identical with that at $x = \pi L$. The boundary condition at the walls $y = 0$ and πL are heuristically assigned as are those in Phillips' numerical experiment, namely, on the walls, the zonally averaged flow, the perturbation part of streamfunctions, and the perturbation part of vorticity are always zero. A suitable set of orthogonal functions for this region and the associated boundary conditions is then the set

$$F_{0m} = \sqrt{2} \cos \frac{my}{L} \qquad m = 1, 2, \cdots,$$

$$F_{nm} = 2 \sin \frac{my}{L} \cos \frac{nx}{L} \qquad m = 1, 2, \cdots; \; n = 1, 2, \cdots,$$

$$\bar{F}_{nm} = 2 \sin \frac{my}{L} \sin \frac{nx}{L} \qquad m = 1, 2, \cdots; \; n = 1, 2, \cdots.$$

We shall only select the following subset of the above set,

namely,

$$\left\{ F_{0m}, F_{nm}, \bar{F}_{nm} \;\middle|\; m = 1, 2 \right\}$$

where $n = 3$ approximately corresponds to wave number 4 or 5 at 40° latitude if we take the length πL of the square region to be the distance between the pole and the equator.

Now we introduce the expansions

$$\psi_l = L^2 f \sum_{m=1,2} \left\{ \psi_{l0m} F_{0m} + \psi_{lnm} F_{nm} + \bar{\psi}_{lnm} \bar{F}_{nm} \right\}, \quad l = 1, 3, 5,$$

$$\theta_l = \frac{L^2 f^2}{g} \sum_{m=1,2} \left\{ \theta_{l0m} F_{0m} + \theta_{lnm} F_{nm} + \bar{\theta}_{lnm} \bar{F}_{nm} \right\}, \quad l = 2, 4,$$

and

$$\omega_l = f p_a \sum_{m=1,2} \left\{ \omega_{l0m} F_{0m} + \omega_{lnm} F_{nm} + \bar{\omega}_{lnm} \bar{F}_{nm} \right\}, \quad l = 2, 4.$$

When the expansions are substituted into (108) - (111), and coefficients of like orthogonal functions are equated, we have the following non-dimensional spectral equations.

$$\begin{aligned} \frac{d}{dt} \psi_{l01} = {} & \frac{9}{l} (\omega_{l+1\,01} - \omega_{l-1\,01}) - C_{01} \psi_{l01} \\ & - D_l (\psi_{l01} - \psi_{l+2\,01}) - \frac{l-2}{l} D_{l-2} (\psi_{l01} - \psi_{l-2\,01}) \\ & l = 1, 3, 5. \end{aligned} \tag{114}$$

$$\frac{d}{dt}\psi_{\ell 02} = \frac{1}{4}(a_{n2}^2 - a_{n1}^2) n \gamma_{221} (\psi_{\ell n1}\bar{\psi}_{\ell n2} - \psi_{\ell n2}\bar{\psi}_{\ell n1})$$

$$- \frac{q}{4\ell}(\omega_{\ell+1\,02} - \omega_{\ell-1\,02}) - C_{02}\psi_{\ell 02}$$

$$- D_\ell(\psi_{\ell 02} - \psi_{\ell+2\,02}) - \frac{\ell-2}{\ell} D_{\ell-2}(\psi_{\ell 02} - \psi_{\ell-2\,02})$$

$$\ell = 1, 3, 5. \qquad (115)$$

$$\frac{d}{dt}\psi_{\ell n1} = \frac{-n}{a_{n1}^2}\left\{(a_{n2}^2 - a_{02}^2)\gamma_{212}\psi_{\ell 02}\bar{\psi}_{\ell n2} + (a_{n1}^2 - a_{01}^2)\gamma_{111}\psi_{\ell 01}\bar{\psi}_{\ell n1}\right\}$$

$$+ \frac{nB}{a_{n1}^2}\bar{\psi}_{\ell n1} - \frac{q}{\ell a_{n1}^2}(\omega_{\ell+1\,n1} - \omega_{\ell-1\,n1}) - C_{n1}\psi_{\ell n1}$$

$$- D_\ell(\psi_{\ell n1} - \psi_{\ell+2\,n1}) - \frac{\ell-2}{\ell} D_{\ell-2}(\psi_{\ell n1} - \psi_{\ell-2\,n1}) \qquad (116)$$

$$\ell = 1, 3, 5,$$

$$\frac{d}{dt}\bar{\psi}_{\ell n1} = \frac{n}{a_{n1}^2}\left\{(a_{n2}^2 - a_{02}^2)\gamma_{212}\psi_{\ell 02}\psi_{\ell n2} + (a_{n1}^2 - a_{01}^2)\gamma_{111}\psi_{\ell 01}\psi_{\ell n1}\right\}$$

$$- \frac{nB}{a_{n1}^2}\psi_{\ell n1} - \frac{q}{\ell a_{n1}^2}(\bar{\omega}_{\ell+1\,n1} - \bar{\omega}_{\ell-1\,n1}) - C_{n1}\bar{\psi}_{\ell n1}$$

$$- D_\ell(\bar{\psi}_{\ell n1} - \bar{\psi}_{\ell+2\,n1}) - \frac{\ell-2}{\ell} D_{\ell-2}(\bar{\psi}_{\ell n1} - \bar{\psi}_{\ell-2\,n1}) \qquad (117)$$

$$\ell = 1, 3, 5.$$

$$\frac{d}{dt}\psi_{\ell n2} = -\frac{n}{a_{n2}^2}\left\{(a_{n2}^2 - a_{01}^2)\gamma_{122}\psi_{\ell 01}\bar{\psi}_{\ell n2} + (a_{n1}^2 - a_{02}^2)\gamma_{221}\psi_{\ell 02}\bar{\psi}_{\ell n2}\right\}$$

$$- \frac{q}{\ell a_{n2}^2}(\omega_{\ell+1\, n2} - \omega_{\ell-1\, n2}) - C_{n2}\psi_{\ell n2} + \frac{nB}{a_{n2}^2}\bar{\psi}_{\ell n2}$$

$$- D_\ell(\psi_{\ell n2} - \psi_{\ell+2\, n2}) - \frac{\ell-2}{\ell}D_{\ell-2}(\psi_{\ell n2} - \psi_{\ell-2\, n2}),$$

$$\ell = 1, 3, 5, \qquad (118)$$

$$\frac{d}{dt}\bar{\psi}_{\ell n2} = \frac{n}{a_{n2}^2}\left\{(a_{n2}^2 - a_{01}^2)\gamma_{122}\psi_{\ell 01}\psi_{\ell n2} + (a_{n1}^2 - a_{02}^2)\gamma_{221}\psi_{\ell 01}\psi_{\ell n2}\right\}$$

$$- \frac{q}{\ell a_{n2}^2}(\bar{\omega}_{\ell+1\, n2} - \bar{\omega}_{\ell-1\, n2}) - C_{n2}\bar{\psi}_{\ell n2} - \frac{nB}{a_{n2}^2}\psi_{\ell n2}$$

$$- D_\ell(\bar{\psi}_{\ell n2} - \bar{\psi}_{\ell+2\, n2}) - \frac{\ell-2}{\ell}D_{\ell-2}(\bar{\psi}_{\ell n2} - \bar{\psi}_{\ell-2\, n1}),$$

$$\ell = 1, 3, 5, \qquad (119)$$

$$\frac{d}{dt}\theta_{\ell 01} = n\gamma_{122}(\psi_{\ell n2}\bar{\theta}_{\ell n2} - \bar{\psi}_{\ell n2}\theta_{\ell n2}) + n\gamma_{111}(\psi_{\ell n1}\bar{\theta}_{\ell n1} - \bar{\psi}_{\ell n1}\theta_{\ell n1})$$

$$+ S_\ell\omega_{\ell 01} + g_\ell(\theta_{\ell 01}^* - \theta_{\ell 01})$$

$$\ell = 2, 4, \qquad (120)$$

$$\frac{d}{dt}\theta_{\ell o2} = n\gamma_{221}\left\{\psi_{\ell n1}\bar{\theta}_{\ell n2} - \bar{\psi}_{\ell n2}\theta_{\ell n1} + \psi_{\ell n2}\bar{\theta}_{\ell n1} - \bar{\psi}_{\ell n1}\theta_{\ell n2}\right\}$$

$$+ S_\ell \omega_{\ell o2} + g_\ell(\theta^*_{\ell o2} - \theta_{\ell o2}), \quad \ell = 2,4, \tag{121}$$

$$\frac{d}{dt}\theta_{\ell n1} = -n\gamma_{212}(\psi_{\ell o2}\bar{\theta}_{\ell n2} - \bar{\psi}_{\ell n2}\theta_{\ell o2}) - n\gamma_{111}(\psi_{\ell o1}\bar{\theta}_{\ell n1} - \bar{\psi}_{\ell n1}\theta_{\ell o1})$$

$$+ S_\ell \omega_{\ell n1} + g_\ell(\theta^*_{\ell n1} - \theta_{\ell n1}), \quad \ell = 2,4, \tag{122}$$

$$\frac{d}{dt}\bar{\theta}_{\ell n1} = n\gamma_{212}(\psi_{\ell o2}\theta_{\ell n2} - \psi_{\ell n2}\theta_{\ell o2}) + n\gamma_{111}(\psi_{\ell o1}\theta_{\ell n1} - \psi_{\ell n1}\theta_{\ell o1})$$

$$+ S_\ell \bar{\omega}_{\ell n1} + g_\ell(\bar{\theta}^*_{\ell n1} - \bar{\theta}_{\ell n1}), \quad \ell = 2,4 \tag{123}$$

$$\frac{d}{dt}\theta_{\ell n2} = -n\gamma_{122}(\psi_{\ell o1}\bar{\theta}_{\ell n2} - \bar{\psi}_{\ell n2}\theta_{\ell o1}) - n\gamma_{221}(\psi_{\ell o2}\bar{\theta}_{\ell n1} - \bar{\psi}_{\ell n1}\theta_{\ell o2})$$

$$+ S_\ell \omega_{\ell n2} + g_\ell(\theta^*_{\ell n2} - \theta_{\ell n2}), \quad \ell = 2,4 \tag{124}$$

$$\frac{d}{dt}\bar{\theta}_{\ell n2} = n\gamma_{122}(\psi_{\ell o1}\theta_{\ell n2} - \psi_{\ell n2}\theta_{\ell o1}) + n\gamma_{221}(\psi_{\ell o2}\theta_{\ell n1} - \psi_{\ell n1}\theta_{\ell o2})$$

$$+ S_\ell \bar{\omega}_{\ell n2} + g_\ell(\bar{\theta}^*_{\ell n2} - \bar{\theta}_{\ell n2}), \quad \ell = 2,4, \tag{125}$$

$$\theta_{l0m} = b_l(\psi_{l-1\,0m} - \psi_{l+1\,0m}), \quad l = 2,4;\ m = 1,2, \tag{126}$$

$$\theta_{lnm} = b_l(\psi_{l-1\,nm} - \psi_{l+1\,nm}), \quad l = 2,4;\ m = 1,2, \tag{127}$$

$$\bar{\theta}_{lnm} = b_l(\bar{\psi}_{l-1\,nm} - \bar{\psi}_{l+1\,nm}), \quad l = 2,4;\ m = 1,2, \tag{128}$$

and

$$\psi_{l0m} = \tfrac{1}{2}(\psi_{l+1\,0m} + \psi_{l-1\,0m}), \quad l = 2,4;\ m = 1,2,$$

$$\psi_{lnm} = \tfrac{1}{2}(\psi_{l+1\,nm} + \psi_{l-1\,nm}), \quad l = 2,4;\ m = 1,2,$$

$$\bar{\psi}_{lnm} = \tfrac{1}{2}(\bar{\psi}_{l+1\,nm} + \bar{\psi}_{l-1\,nm}), \quad l = 2,4;\ m = 1,2,$$

where

$$a_{nm}^2 = n^2 + m^2$$

$$b_l = 6^{2k}/[(l+1)^{2k} - (l-1)^{2k}]$$

$$\gamma_{jnm} = \frac{\sqrt{2}}{\pi} j\left(\frac{1}{j+n-m} + \frac{1}{j-n+m} + \frac{1}{-j+n+m} - \frac{1}{j+n+m}\right)$$

$$B = \beta \angle f^{-1}$$

$$C_{nm} = A \angle^{-2} f^{-1} a_{nm}^2$$

$$S_\ell = \sigma_\ell \rho_s c_p L^{-2} f^{-2}$$

$$D_5 = k_5 f^{-1}$$

$$D_{-1} = 0$$

$$D_\ell = k_\ell f^{-1} = \frac{9 g^2}{4 R \rho_s f} \frac{\mu_{\ell+1}}{T_{\ell+1}} \frac{\ell+1}{\ell}, \quad \ell = 1, 3$$

$$q_\ell = h_\ell f^{-1}$$

and $\psi_{1nm} = \psi_{7nm} = 0$ for all n and m.

Series A

In the following we shall take

L = 3185 km

n = 3

f = .9374 x 10^{-4} sec^{-1}

β = .5959

S_2 = 11.22

S_4 = .6173

A = 5 x 10^{-5}

D_1 = .7542 x 10^{-4}

D_3 = .6360 x 10^{-2}

D_5 = .2135 x 10^{-1}

(μ_4 = 150 gm cm^{-1} sec^{-1} ; $\mu_2 = \mu_4 S_4 / S_2$; k_5 = 2 x 10^{-6} sec^{-1})

q_4 = .4900 x 10^{-2}

q_2 = .1667 x 10^{-2}

θ^*_{1nm} = 0 for $n \neq 0$, or $m \neq 1$

and θ^*_{401} = .3504

The value of θ^*_{201} will change from one experiment to another. The ratio $\theta^*_{201}/\theta^*_{401}$ may be regarded as the ratio of the imposed thermal Rossby number in the upper layer to the imposed thermal Rossby number in the lower layers. By changing this ratio we hope to get some understanding of how the equator-to-pole temperature difference in the lower stratosphere (corresponding to $2\sqrt{2}L^2f^2\theta_{201}/c_p$ in our model) depends upon the vertical distribution of meridional differential heating.

The method of solution will be the same as the previous experiment except that the steady symmetric solution will be taken as the initial basic flow in each case.

It should be mentioned here that the statistics of the dynamic system (114) - (128) without thermal forcing in the second mode, i.e., $\theta^*_{\ell n2} = 0$ for all ℓ and n, is not unique. Two intransitive circulations, one different from the other only in the sign of the second mode, may develop, the choice between them is determined by the initial conditions (Lorenz, 1963b). However, this causes no trouble to us since in the following we are only concerned with the overall temperature difference from the equator to pole disregarding the detail in between.

Case 1. $\theta^*_{201} = \theta^*_{401}/3 = .1168$

This case roughly corresponds to the previous experiments. Therefore it will be qualitatively compared with the previous experiment

concerning the following major points:

a) the equator-to-pole temperature difference in the upper layer

b) the major mechanism responsible for the equator-to-pole temperature difference

c) the relationship between eddy heat transport and the energy conversion $[A' \cdot K']$, and

d) the interaction between the upper and lower layers revealed by the constrast of the energy conversion $[A' \cdot K']$ in the two layers.

The steady-state symmetric solution in this case

$$\psi_{501} = -.1531 \times 10^{-2}$$

$$\psi_{301} = .7358 \times 10^{-1}$$

$$\psi_{101} = 0.9778 \times 10^{-1}$$

$$\theta_{401} = .3280$$

$$\theta_{201} = .7699 \times 10^{-1}$$

$$\theta_{l02} = \psi_{l02} = 0 \quad \text{for all } l$$

One notices that the meridional temperature profiles in both layers are monotonically decreasing from the equator to the pole. The initial condition of the experiment consists of the steady symmetric solution and a very small perturbation part which is independent of height. The time increment for numerical integration is so chosen that the solu-

tion does not blow up at the end of the total time interval of 50 days and that a smaller time increment will not give a significantly different result. The chosen time increment is $.1013\, f^{-1}$ or 1/80 day. This implies 4000 time steps for 50 days.

The time sequences of the non-dimensional equator-to-pole potential temperature differences in the upper and lower layers, θ_{201} and θ_{401}, are shown in Figure 15. Both θ_{201} and θ_{401} oscillate rather regularly. In the lower layer the oscillation of θ_{401} settles down quickly to a value about .250 which corresponds to an equator-to-pole temperature difference about 50°C. The minimum value of θ_{401} is .170 corresponding to a temperature difference about 34°C. In the upper layer, the temperature oscillation lags 2 - 5 days behind that of the lower layer. Before the 10th day the θ_{201} changes very slowly. Then it decreases rapidly as the waves grow and transport heat northwards. The temperature difference θ_{201} reduces to zero at the time when θ_{401} reaches its minimum. Then θ_{201} becomes negative and oscillates between -.060 and -.170 with no apparent sign of settling. However, the mean value of θ_{201} in a complete cycle approaches a value of -.125, corresponding to an equator-to-pole temperature increase of 16.8°C. This value is in good agreement with the value in the previous experiment. It is very interesting to notice that there

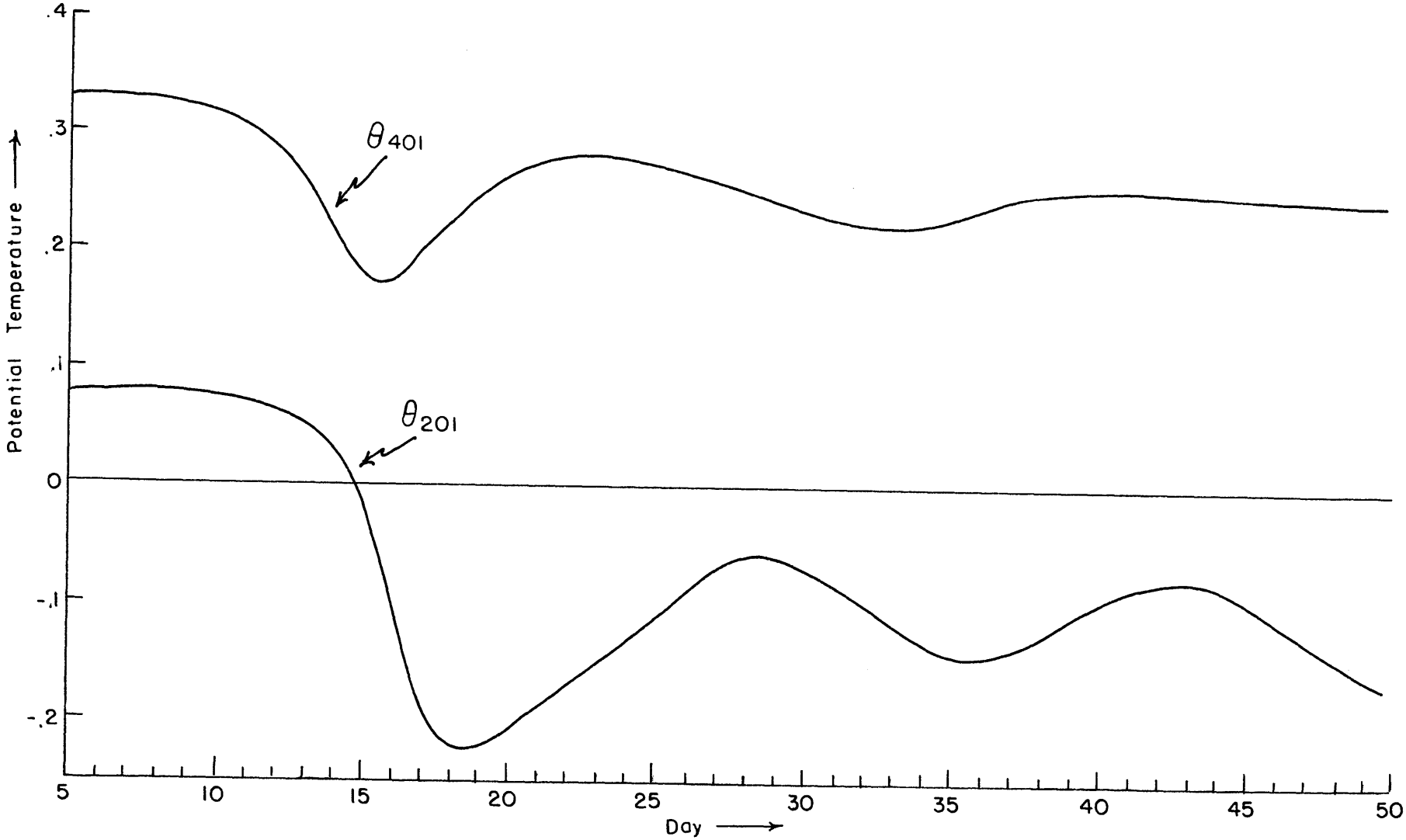

Figure 15. Time sequences of θ_{401} and θ_{201} (Series A, case 1) ; non-dimensional units.

is a small equator-to-pole temperature increase in the initial flow of the previous experiment but in the case here we have a monotonic equator-to-pole temperature decrease instead, yet a large equator-to-pole temperature increase is obtained. A careful scrutiny shows the following. Almost from the very beginning to the 14th day eddy available potential energy is converted into eddy kinetic energy both in the lower layer and in the upper layer (see Figure 17). The baroclinic production of eddy kinetic energy in the upper layer is likely stimulated by the production of energy in the lower layer. The eddy heat transport associated with the production of kinetic energy is poleward in both layers. The original meridional temperature gradient, proportional to θ_{201}, is gradually reduced and is completely washed away before the 15th day. As a result of the vanishing of zonal baroclinicity in mode 1, the energy conversion process $[A' \cdot K']$ in the upper layer reverses its direction. Meanwhile, an overshoot of poleward heat transport sets up a slight equator-to-pole temperature increase in the upper layer -- a negative θ_{201}. Now the eddy heat transport associated with the reversed energy conversion, $[A' \cdot K'] < 0$, is up-gradient, that is, still northward, the establishment of a strong equator-to-pole temperature increase is then on the move.

In order to further see the importance of the horizontal eddy

process to the equator-to-pole temperature increase, the change of θ_{201} due to the effects of horizontal eddy transport, meridional circulation and non-adiabatic heating are given in Figure 16. Is is clear that the effect of horizontal eddy transport is always opposite to the effect of mean meridional circulation, and generally the former is much bigger than the latter. The effect of non-adiabatic heating is momentarily much smaller than the other two. However, its long term mean is important as one expects. A comparison between the actual change of θ_{201} and the rate of change due to eddy heat transport only leads us to the conclusion that horizontal eddy heat transport is the controlling process of the equator-to-pole temperature difference. All these are in good agreement with the results of the previous experiment.

Shown in Figure 17 are the time sequences of the energy conversions $[A_2' \cdot \bar{A}_2]$, $[A_2' \cdot K_2']$ and $[A_4' \cdot K_4']$. The complete out of phase condition between $[A_2' \cdot \bar{A}_2]$ and $[A_2' \cdot K_2']$ is precisely what we postulated in the introduction and what we have found in the previous experiment. It supports the follwoing idea. No matter how complicated a hydrodynamic system is, the quasi-geostrophy constrains the system in such a way that baroclinic production of kinetic energy is generally accompanied by down-gradient horizontal heat flow and baroclinic consumption of kinetic energy is generally accompanied by up-gradient

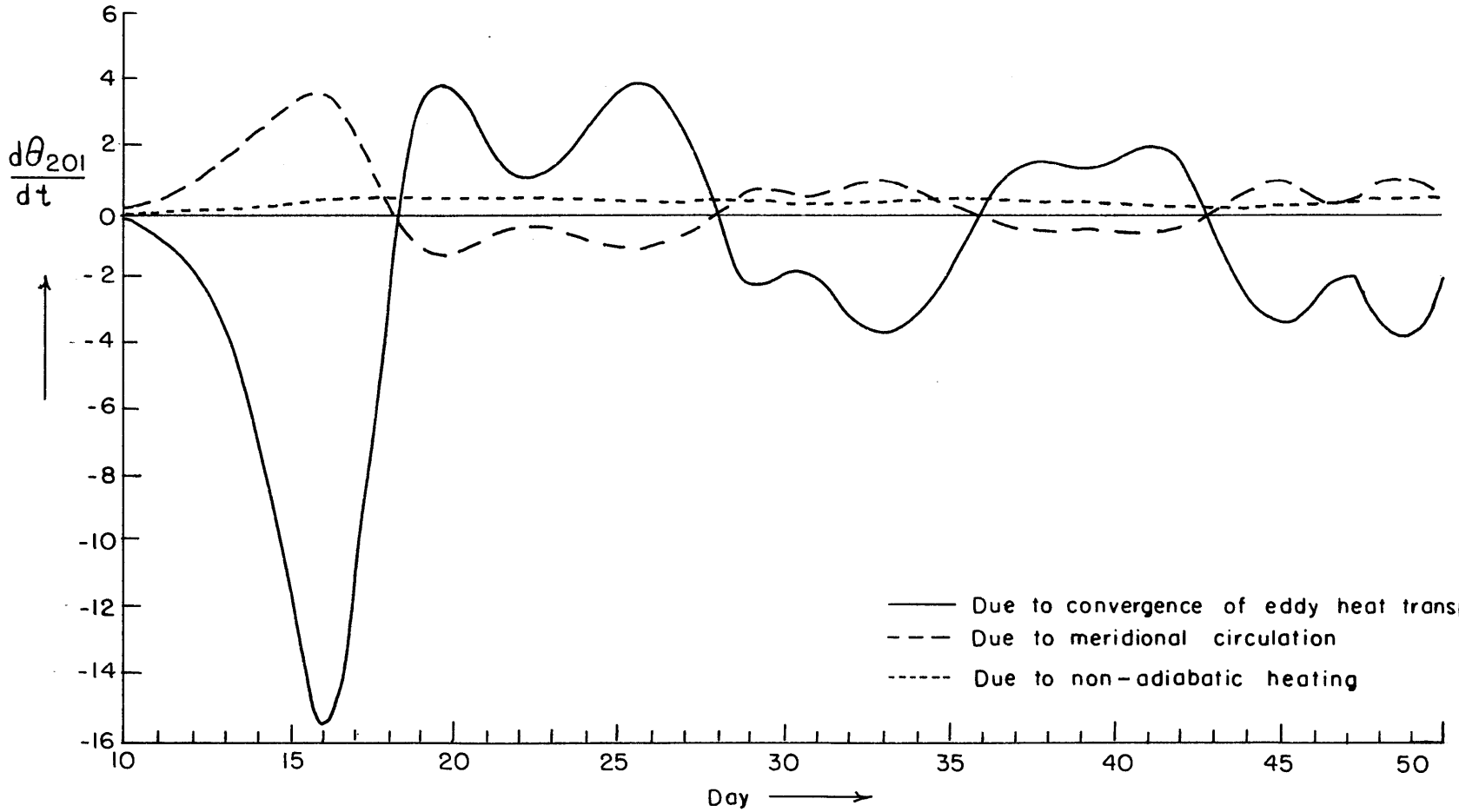

Figure 16. Time sequences of the components of $\frac{d\theta_{201}}{dt}$ in Series A, case 1 (10^{-3} non-dimensional units).

horizontal heat flow. We have just mentioned in this case the northward heat flow before the 18th day, first down-gradient before the 14th, then up-gradient from the 14th to the 18th, actually destroying the initial monotonic equator-to-pole temperature decrease and building the equator-to-pole temperature increase. The subsequent alternation of the heat flow was tending to maintain the equator-to-pole temperature increase.

The phase relation between $[A_2' \cdot K_2']$ and $[A_4' \cdot K_4']$ shown in Figure 17 is very interesting. Before the reversal of the equator-to-pole temperature difference the conversions $[A_2' \cdot K_2']$ and $[A_4' \cdot K_4']$ are in phase; a few days after the reversal, $[A_2' \cdot K_2']$ accomplishes a remarkable phase adjustment so that $[A_2' \cdot K_2']$ and $[A_4' \cdot K_4']$ thereafter are generally more than 90° out of phase. To the lower layer the upper layer first behaves like a subordinate before the reversal of the equator-to-pole temperature difference, then becomes a resistant or a compensator after the reversal. The latter part of the role of the upper layer was known in the previous experiment (see Tables 15, 17 and 18 and Figures 5 and 6).

Case 2. $\theta^*_{201} = 0$

The steady state symmetric solution in this case is

$\psi_{501} = -.1380 \times 10^{-2}$

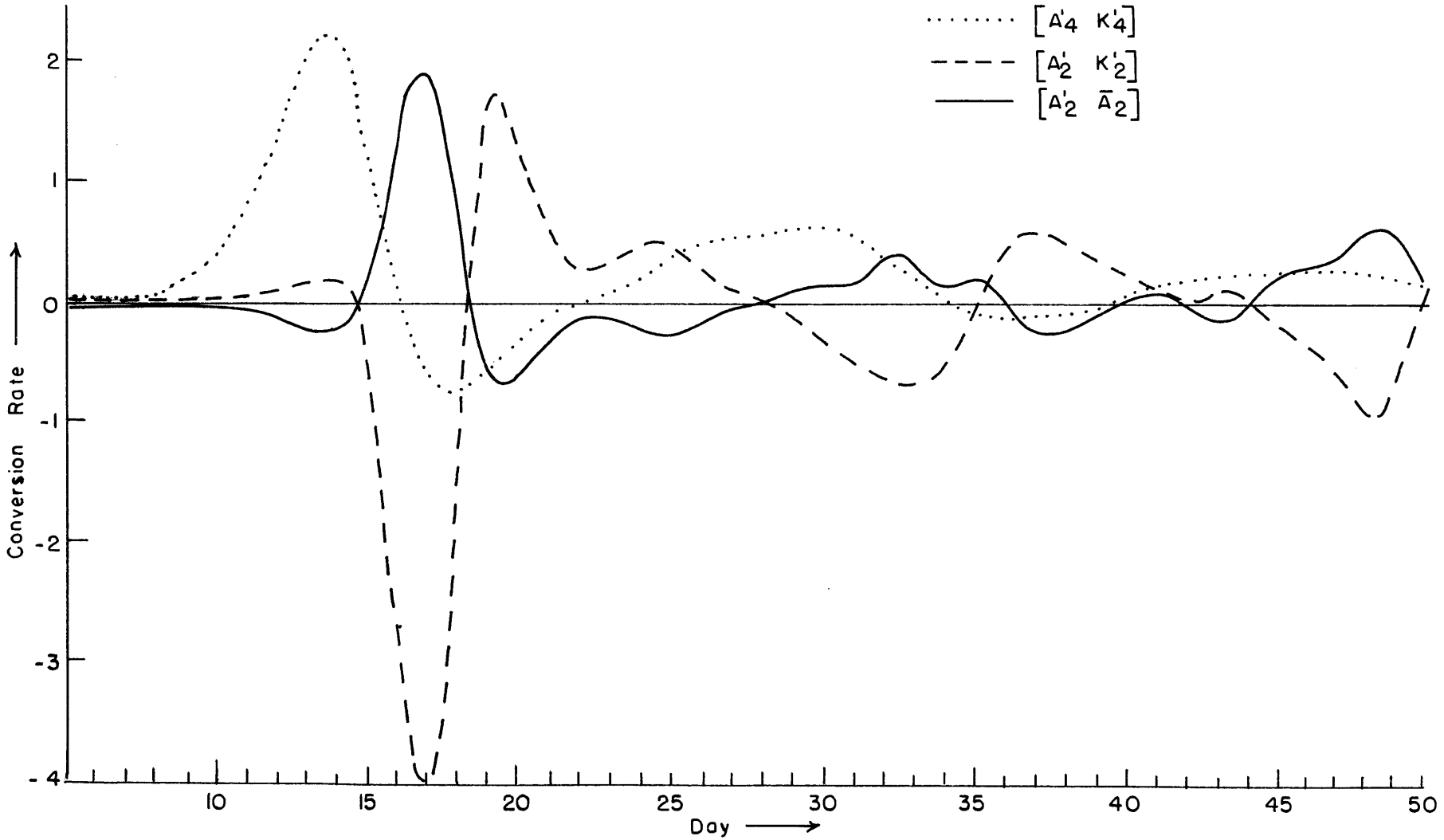

Figure 17. Time sequences of energy conversions $[A_2' \cdot \bar{A}_2]$, $[A_2' \cdot K_2']$, and $[A_4' \cdot K_4']$ (Case 1).

Units: $[A_2' \bar{A}_2]$, $[A_2' \cdot K_2']$ $.31 \times 10^{-4}$ non-dimensional units;
$[A_4' \cdot K_4]$ $.23 \times 10^{-3}$ non-dimensional units.

$\psi_{301} = .7378 \times 10^{-1}$

$\psi_{101} = .6580 \times 10^{-1}$

$\theta_{401} = .3282$

$\theta_{201} = -.2542 \times 10^{-1}$

$\theta_{l02} = \psi_{l02} = 0$ for all l .

It is noticed that the upper-layer meridional circulation forced by the lower layer sets up a slight equator-to-pole temperature increase of about $3.4^{\circ}C$. This symmetric solution plus the same perturbation part as in Case 1 will be the initial flow. Because of the equator-to-pole temperature increase the upper layer is characteristically different from the lower layer from the very beginning of the integration of the wave regime. The symmetric flow is supercritical to the distrubances. The disturbances immediately start to release kinetic energy from available potential energy and grow. Since the sense of baroclinicity is different in the upper layer, the waves in the upper layer do not go along with their lower part in the lower layer in the production of eddy kinetic energy. Instead, they convert eddy kinetic energy into eddy available potential energy and build a strong equator-to-pole temperature increase within the upper layer. The sequence of the events are exactly the same as in the first experiment discussed in Chapter 6. The time sequences of θ_{201} and θ_{401} are shown in Figure 18. Both θ_{401} and θ_{201} oscillate quite regularly and apparently settle down to the

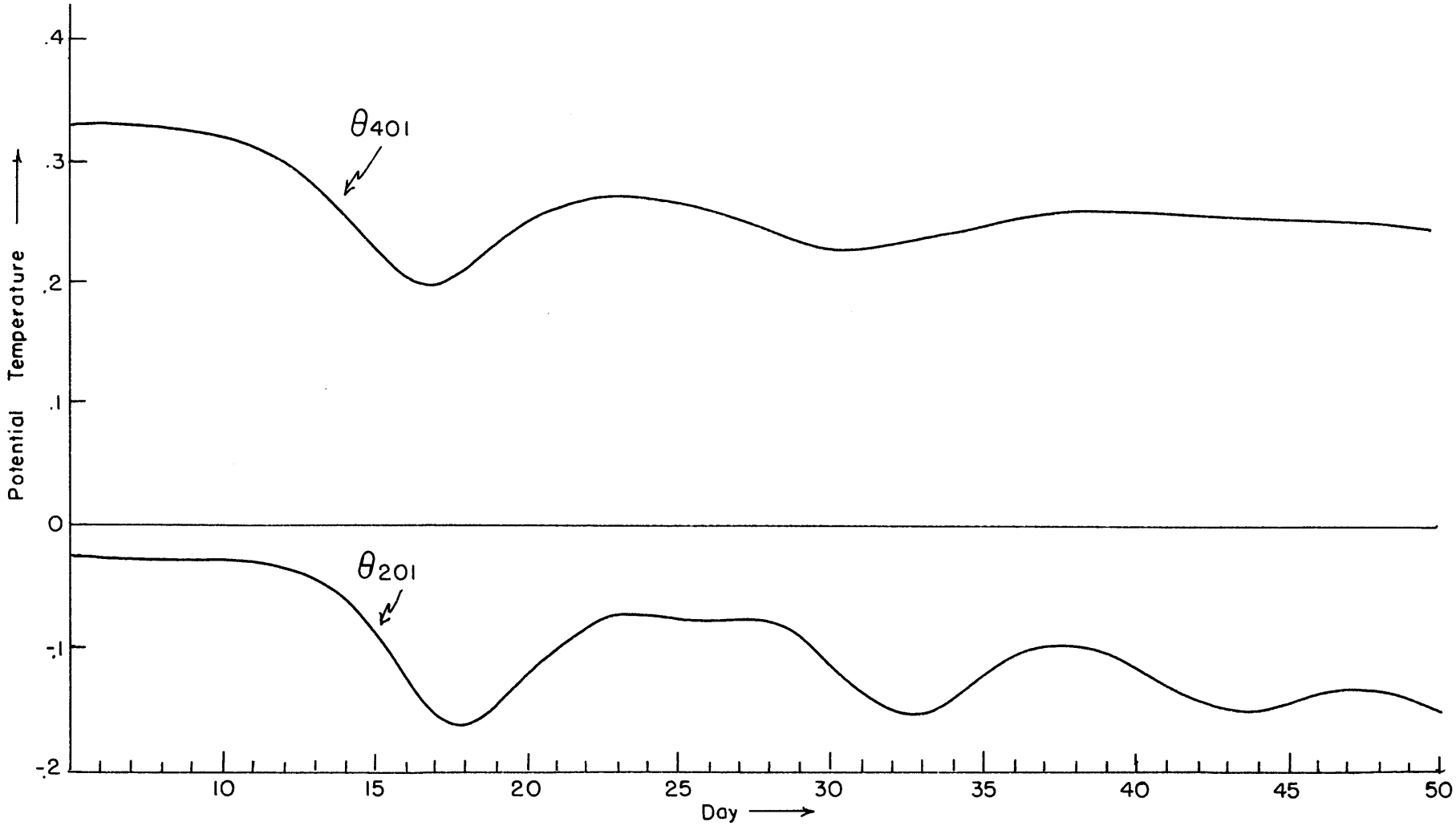

Figure 18. Time sequences of θ_{401} and θ_{201} (Series A, case 2); non-dimensional units.

values .250 and -.145 respectively. The time sequences of the energy conversions $[A_2' \cdot K_2']$, $[A_2' \cdot \tilde{A}_2]$ and $[A_4' \cdot K_4']$ are given in Figure 19. The phase relationship between them is the same as in the first experiment (see Figure 5 and Tables 15, 17 and 18).

Case 3. $\theta^*_{201} = \frac{3}{4}\theta^*_{401} = .2628$

The steady-state symmetric solution in this case is

$\psi_{501} = -.1720 \times 10^{-2}$

$\psi_{301} = .7333 \times 10^{-1}$

$\psi_{101} = .1378$

$\theta_{401} = .3277$

$\theta_{201} = .2050$

$\theta_{l02} = \psi_{l02} = 0$ for all l.

It is noticed that the increase of the imposed differential heating in the upper layer has a practically undetectable influence on the steady symmetric solution of the lower part while it is very important to the upper part of the solution.

The results of the time integration of the wave regime in this case is briefly given in Figures 20 and 21. Because of the larger baroclinicity existing in the upper layer than the previous cases, the lower layer baroclinic activity increases relative to the previous cases and its effect shows up in the fact that θ_{401} in this case approaches to a

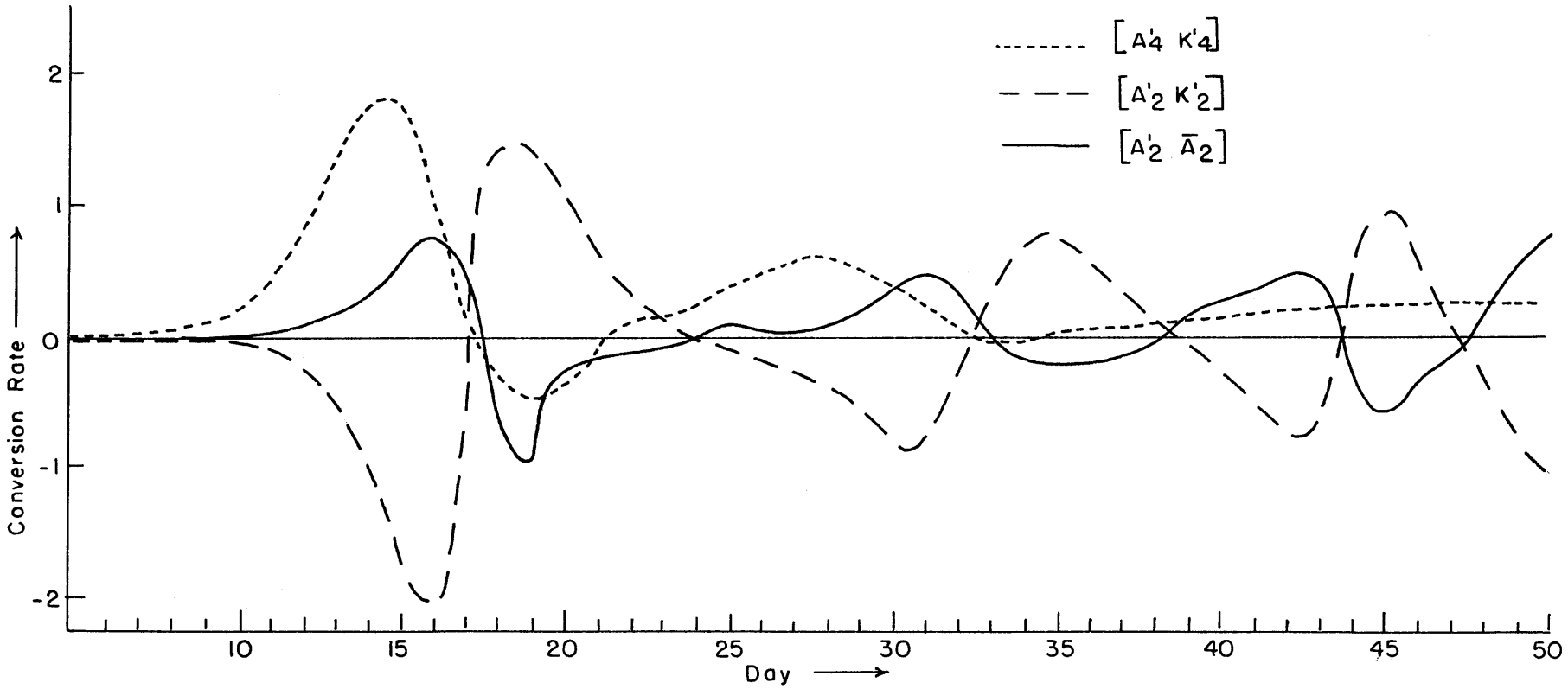

Figure 19. Time sequences of energy conversions $[A_2' \cdot \bar{A}_2]$, $[A_2' \cdot K_2']$ and $[A_4' \cdot K_4']$ (Case 2).

Units: $[A_2' \cdot \bar{A}_2]$, $[A_2' \cdot K_2']$ .31 x 10^{-4} non-dimensional units;

$[A_4' \cdot K_4']$ .23 x 10^{-3} non-dimensional units.

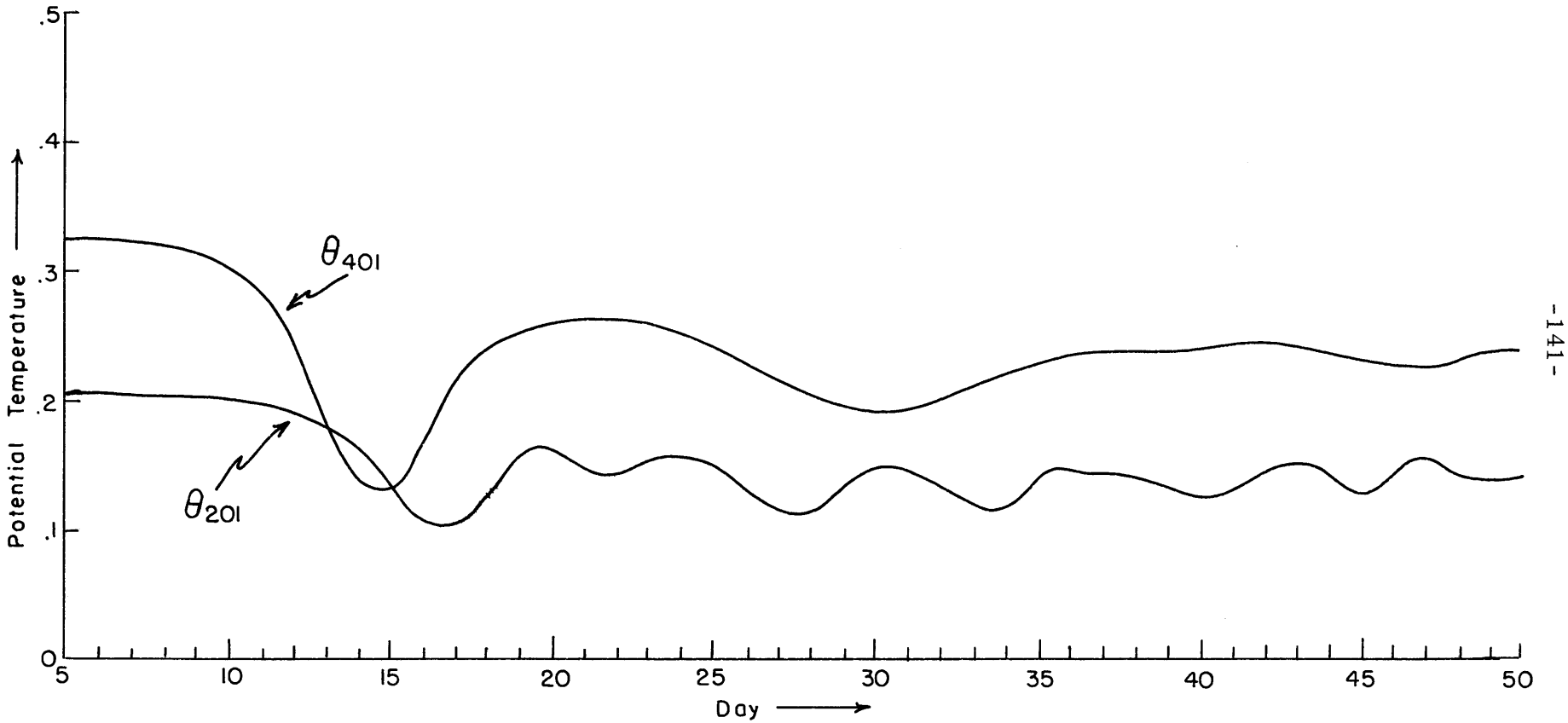

Figure 20. Time sequence of θ_{401} and θ_{201} (Series A, case 3); non-dimensional units.

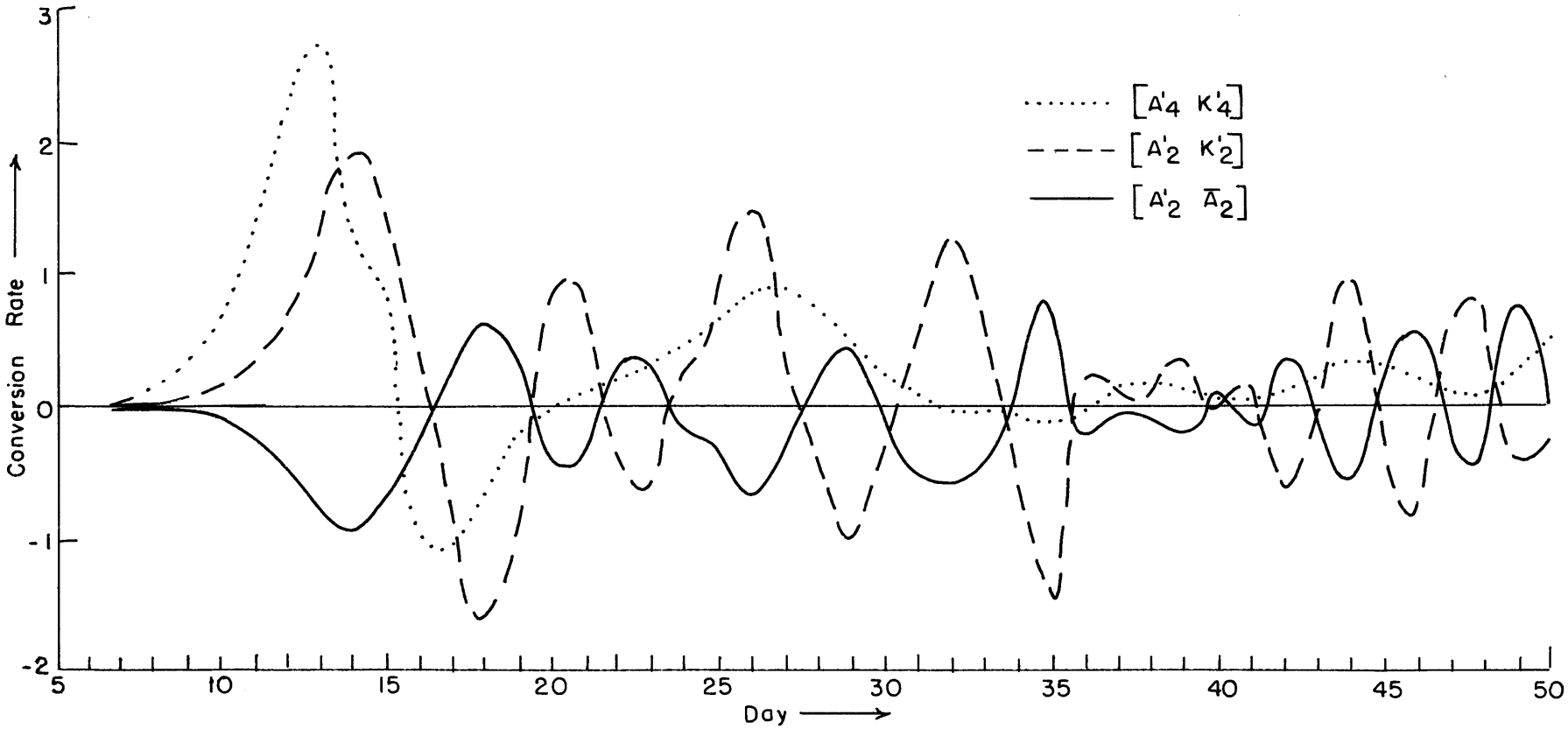

Figure 21. Time sequences of energy conversions $[A_2' \bar{A}_2]$, $[A_2' \cdot K_2']$ and $[\acute{A}_4 \cdot \acute{K}_4]$ (Case 3).

Units: $[A_2' \bar{A}_4]$, $[A_2' \cdot K_2']$ $.31 \times 10^{-4}$ non-dimensional units;

$[A_4' \cdot K_4']$ $.23 \times 10^{-3}$ non-dimensional units.

smaller value, .230, than the previous cases. Even though the baroclinic activity in the lower layer and consequently its influence on the upper layer increase relative to the previous cases, the northward heat transport associated with the production of eddy kinetic energy fails to upset the increase of temperature from the equator to the pole. The minimum value of θ_{201} is no less than .100 which corresponds to a equator-to-pole temperature decrease about 13.4°C. The oscillations of θ_{201}, $[A_2' \cdot K_2']$ and $[A_1' \cdot \bar{A}_1]$ are more frequent and irregular than the previous cases and exhibit a kind of interference of two different frequencies. $[A_1' \bar{A}_1]$ and $[A_2' \cdot K_2']$ are always completely out of phase as in the previous cases. However, the phase relationship between $[A_2' \cdot K_2']$ and $[A_4' \cdot K_4']$ are quite different. It seems that they both are composed of two oscillations with different frequencies (not subharmonic) but the one with higher frequency only clearly shows up in the upper layer wherein its amplitude is at least comparable to the one of lower frequency. A comparison between this case and the previous cases almost certainly concludes that the higher frequency oscillation of baroclinic energy conversion is enhanced by the increase of differential heating in the upper layer.

In summary, the results of the above cases have shown the following.

a) For the case corresponding to the first experiment, the magnitude of total temperature increase from the equator to pole in the upper layer, the relationship between the energy conversions $\{A'K'\}$ and $\{\bar{A}\cdot A'\}$, and the inter-layer interaction exhibited by the relation between $\{A_4'\cdot K_4'\}$ and $\{A_2'\cdot K_2'\}$ are in good agreement with those in the first experiment.

b) The increase of the ratio of the thermal forcing $\theta_{201}^*/\theta_{401}^*$ (θ_{201}^* and θ_{401}^* both positive, no other thermal forcing) relatively increases the potential of the active baroclinical activity in the upper layer or reduces the passivity of the upper layer. There likely exists a critical ratio of $\theta_{201}^*/\theta_{401}^*$, which may be a function of other parameters such as the static stability ratio S_2/S_4, the ratio of Prandl number etc., above which the value of θ_{201} can not statistically be negative. Below the critical ratio of thermal forcing the magnitude of θ_{201} would be in control of the lower-layer themal forcing θ_{401}^* and the lower-layer parameters such as $\mathcal{D}_5$. The change of θ_{201}^* would make no significant difference.

Series B

In order to verify the above conclusion about the dependence of θ_{201} on the ratio $\theta_{201}^*/\theta_{401}^*$ another series of experiments will be briefly presented in this section. In this series everything is the

same as in Series A except that the eddy part of the initial condition is changed and a small thermal forcing in the second mode is imposed on the flow. Namely,

$$\theta^*_{202} = -.0584 = \theta^*_{401} \ /6$$

The results of temperature oscillation in both layers are shown in Figure 22. The general character of the curves is the same as the corresponding cases in Series A except in the case $\theta^*_{201} / \theta^*_{401} = \frac{3}{4}$ which seems to be the critical value of the present series. This further supports the above conclusion b.

An additional case

In this case we attempt to get some idea about the sensibility of θ_{201} to the change of Austausch coefficient μ_2 in the upper layer. All the parameters are the same as in Case 1 of Series A except that μ_2 and consequently $\mathcal{D}_1$ here are ten times as big as in Case 1 of Series A. The time sequences of θ_{201} and θ_{401} in this case are shown in Figure 23 together with those in Case 1 of Series A. Clearly, the change of Austausch coefficient in the upper layer is insignificant to the value of θ_{201} as far as μ_2 is smaller than the Austausch coefficient μ_4 in the lower layer.

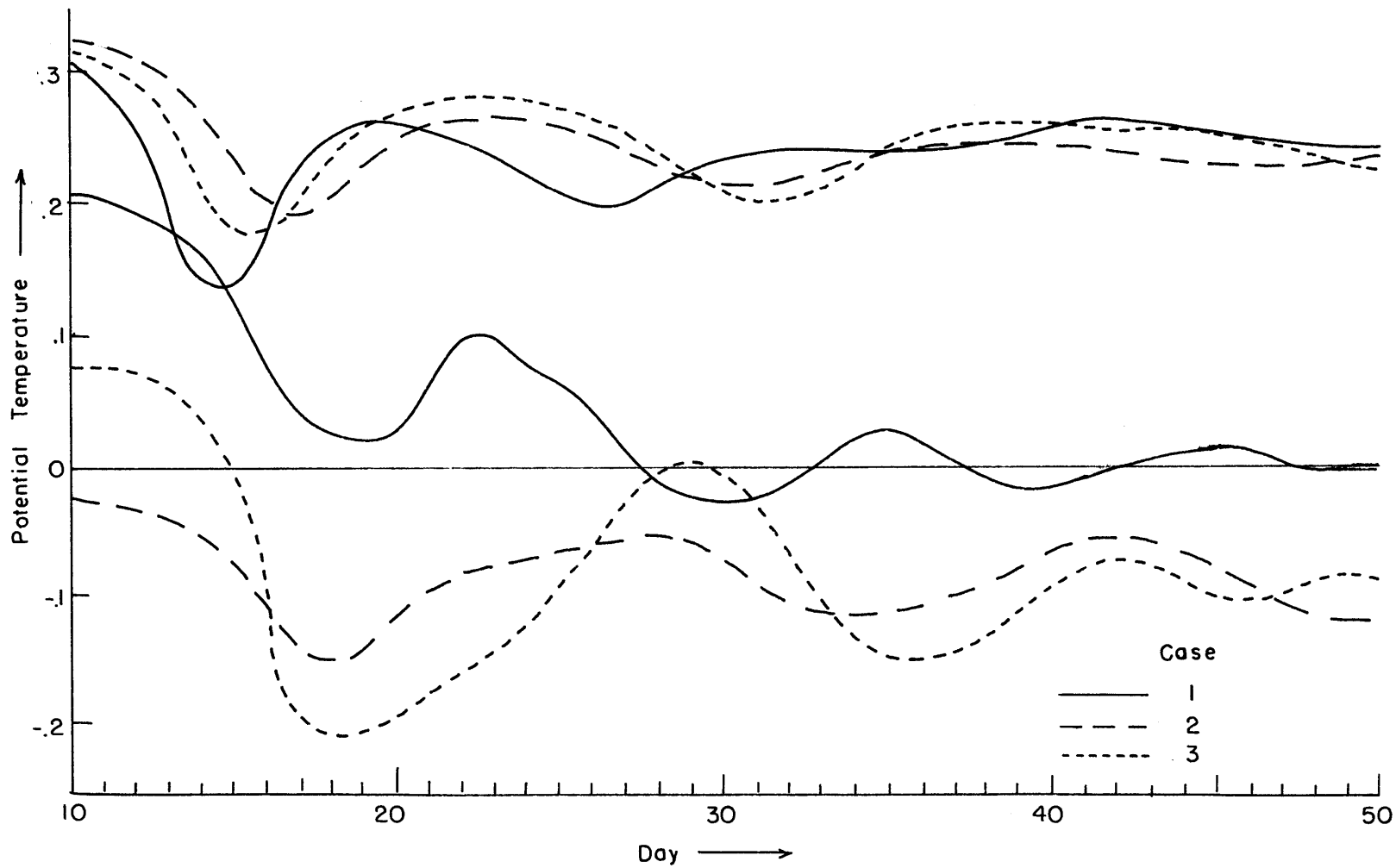

Figure 22. Time sequences of θ_{401} (upper curves) and θ_{201} (lower curves) in Series B.

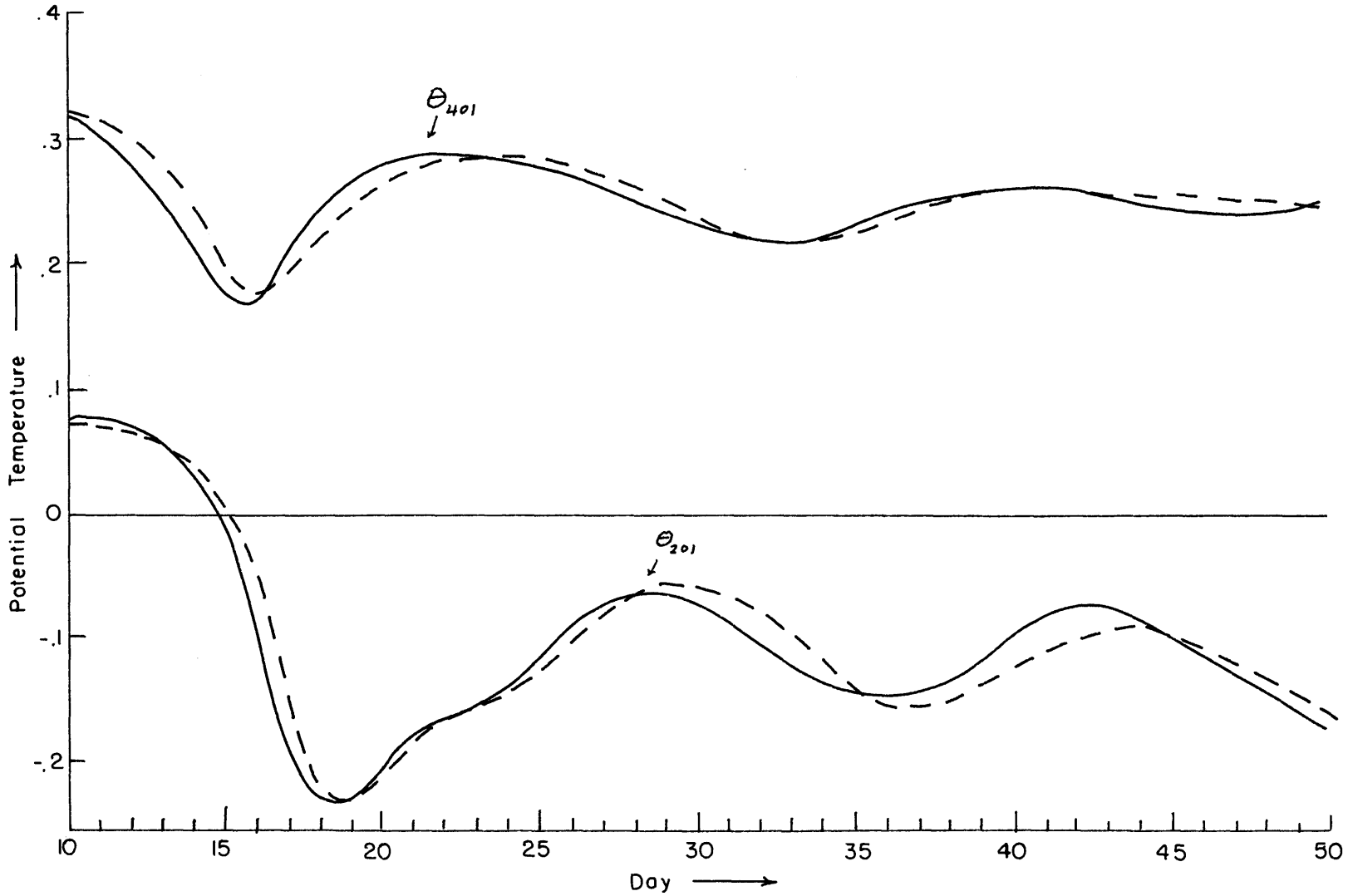

Figure 23. Time sequences of θ_{401} and θ_{201} in the case μ_2 = 82.5 gm cm sec^{-1} (solid lines). The dashed lines are reproduced from Figure 15.

8. SUMMARY AND CONCLUDING REMARKS

The object of this study has been to account for the observed equator-to-pole temperature increase in the lower stratosphere from the hydrodynamic point of view. To do this, simplifications of the hydrodynamic equations have been made and the atmosphere is represented by a nearly quasi-geostrophic model with static stability increasing upward rapidly and latitudinal differential heating increasing downward which heats the atmosphere in low latitudes and cools the atmosphere in high latitudes.

We have suceeded in reproducing the temperature increase from the equator to pole in the model. The magnitude of the equator-to-pole temperature increase is found to fluctuate between a few degrees centigrade and the lower thirties. The mean value is quite comparable to the observation. Northward eddy heat transport is found to be the direct cause for the temperature increase from the middle to high latitudes, while the tropical direct meridional cell seems responsible for the northward temperature increase in the tropical region.

It is found in the model that a baroclinic production of eddy kinetic energy, i.e., $[A' \cdot K'] > 0$, is accompanied by a down-gradient eddy heat transport, and a baroclinic consumption of eddy kinetic energy, i.e., $[A' \cdot K'] < 0$, is accompanied by an up-gradient eddy heat transport. This is in fact due to the quasi-geostrophic constraint on

large-scale motions.

The northward eddy heat transport in the upper layer is found to be a necessary result of the quasi-geostrophic constraint and the passive nature of the upper layer which is predetermined by the combined vertical distribution of latitudinal differential heating and hydrostatic stability. To be more precise, it is found in the model that when the baroclinicity of the upper layer, although weak, is in the same sense as the lower layer, i.e., temperature decreasing northwards, the upper part of an energy-generating wave also converts eddy available potential energy into eddy kinetic energy under the stimulation of the lower major part, the eddy heat transport in the upper layer is then northward, or down-gradient, to reduce the latitudinal temperature gradient. When the baroclinicity of the upper layer is in the sense opposite to the lower layer, i.e., temperature increasing northwards, the upper part of an energy-generating wave consumes the wave energy supplied from below by the lower major part, eddy heat transport in the upper layer is then up-gradient, also northward, to enhance the latitudinal temperature gradient. In those experiments where the initial upper-layer temperature decreases northward (e.g., Case 1 of Series A and B) the northward eddy heat transport in the upper layer, first down-gradient as temperature decreases northward then up-gra-

ient as temperature increases northward, actually builds up a big equator-to-pole temperature increase in the upper layer from the initial monotonically northward-decreasing temperature distribution. Should the same thing happen if the vertical distribution of latitudinal differential heating and static stability be arbitrarily assigned in the model? The answer is no. One may consider the case in which static stability increases upwards and latitudinal differential heating in the upper layer is intense enough to set up supercritical baroclinicity in the layer; the down-gradient eddy heat transport associated with eddy kinetic energy production should then never be able to reduce the latitudinal temperature difference far below the critical value which presumably is quite different from zero. Hence, intuitively, there may exist a critical case for a layer to be forced by its neighboring layers such that the overall temperature gradient in the layer is opposite to the sense of the latitudinal differential heating. This possibility has been partially investigated with all parameters fixed except the upper-layer latitudinal differential heating, or the ratio of the latitudinal differential heating in the upper layer to the latitudinal differential heating in the lower layer. Here we assume that horizontal differential heating can be to some extent independent of vertical differential heating. Although we have not determined it numerically,

there is clearly indicated the existence of a critical value of the ratio above which the equator-to-pole temperature difference in the upper layer can no longer be opposite to the latitudinal differential heating i in the layer. Below the critical ratio the magnitude of the reversed equator-to-pole temperature difference seems not significantly depending upon the ratio (or the upper differential heating).

For the existing atmospheric conditions the energy aspects of the model have been examined. The energy distribution and transformations are generally in good agreement with the observations in the real atmosphere. It is particularly interesting that the model is surprisingly successful in portraying the passive nature of the lower stratosphere. In the upper layer of the model both zonal and eddy available energy are dissipated by non-adiabatic heating or cooling. Eddy available potential energy supplies a large amount to zonal available potential energy to compensate the radiation loss and gets a supply from eddy kinetic energy to compensate its own loss. Eddy kinetic energy is reinforced by the lower layer.

It is quite interesting to notice that in this simple model upward energy transport due to large-scale waves supplies almost all the energy the upper layer needs. Care must be exercised in considering its reality though. It is also noticed that our model may be used to reveal certain aspects of the interaction between the lower stratosphere

and the upper stratosphere simply by reversing the vertical distribution of latitudinal differential heating, i.e., latitudinal differential heating increases with increasing height.

It is quite surprising that the oscillation in energy transformation persists in the upper layer after the lower-layer oscillation apparently tends to settle. It seems to be an unreal feature which might either result from the lack of sufficient coupling or the distortion of the movement of planetary long waves by the governing equations. This perhaps indicates that a multi-layer quasi-geostrophic model is still not good enough for synoptic studies of planetary long waves.

It is also interesting to notice that the argument in this study may equally well apply to any planetary atmosphere characterized by quasi-geostrophic motion and within the domain of wave regime. For that kind of application it may be of value to carry the investigation over a wide range of static stability and horizontal differential heating.

REFERENCES

Barnes, A.A., 1962: The Energy Balance of the Stratosphere During the IGY. Ph.D. Thesis, Mass. Inst. of Tech.

Brewer, A.W., 1949: Evidence for a World Circulation Provided by the Measurements of Helium and Water Vapour Distribution in the Stratosphere. Quart. J. R. Meteor. Soc. 75, 351-363.

Brown, J.A., 1964: A Diagnostic Study of Tropospheric Diabatic Heating and the Generation of Available Potential Energy. Tellus 16, 371-387.

Bryan, K., 1959: A Numerical Investigation of Certain Features of the General Circulation. Tellus 11, 163-174.

Charney, J.G., 1959: On the Theory of the General Circulation of the Atmosphere. The Rossby Memorial Volume, New York, Rockefeller Institute Press, pp. 178-193.

Charney, J.G. and P.G. Drazin, 1961: Propagation of Planetary-Scale Disturbances from the Lower Into the Upper Atmosphere. J. Geoph. Res. 66, pp. 83-109.

Charney, J.G. and A. Eliassen, 1949: A Numerical Method for Predicting the Perturbations of the Middle Latitude Westerlies, Tellus 1, 38-54.

Clapp, P.F., 1961: Normal Heat Sources and Sinks in the Lower Troposphere in Winter. Mon. Wea. Rev. 89, 147-162.

Dobson, G.M.B., A.W. Brewer and B.M. Cwilong, 1946: Meteorology of the Lower Stratosphere. Proc. Royal Soc. London, Ser. A. 185, 144-175.

Eady, E.T., 1949: Long Waves and Cyclone Waves. Tellus 1, 33-52.

Eliassen, A. and E. Palm, 1961: On the Transfer of Energy in Stationary Mountain Waves, Geofysiske Publikasjoner, Geophysica Norvegica, 12, 1-23.

Fjørtoft, R., 1960: On the Control of Kinetic Energy of the Atmosphere by External Heat Sources and Surface Friction. Quart. J.R. Meteor. Soc 86, 437-453.

Fultz, D., 1953: A Survey of Certain Thermally and Mechanically Driven Fluid Systems of Meteorological Interest. Fluid Models in Geophysics. Proc. 1st Sympos. on the Use of Models in Geophys. Fluid Dynamics, Baltimore 27-63.

Gates, W.L., 1961: Static Stability Measures in the Atmosphere. J. Meteor., 18, 526-533.

Goody, R.M., 1949: The Thermal Equilibrium at the Tropopause and the Temperature of the Lower Stratosphere. Proc. Royal Soc., London, Ser. A. 487-505.

Hide, R., 1958: An Experimental Study of Thermal Convection in a Rotating Liquid. Phil. Trans. Royal Soc. London, Ser. A., 250, 441-478.

Houghton, H.G., 1954: On the Annual Heat Balance of Northern Hemisphere. J. Meteor. 11, 1-9.

Kuo, H.L., 1952: Three Dimensional Disturbances in a Baroclinic Zonal Current. J. Meteor., 9, 260-278.

Kuo, H.L., 1953: The Stability Properties and Structure of Disturbances in a Baroclinic Atmosphere. J. Meteor., 10, 235-243.

Kuo, H.L., 1956: Energy - Releasing Processes and Stability of Thermally Driven Motions in a Rotating Fluid. J. Meteor., 13, 82-101.

Lorenz, E.N., 1960: Energy and Numerical Weather Production. Tellus 12, 364-373.

Lorenz, E.N., 1962: Simplified Dynamical Equations Applied to the Rotating - Basin Experiments. J. Atmos. Sci. 19, 39-51.

Lorenz, E.N., 1963: Deterministic Nonperiodic Flow. J. Atmos. Sci. 20, 130-141.

Lorenz, E.N., 1963b: The Mechanics of Vacillation. J. Atmos. Sci. 20, 448-464.

Manabe, S. and F. Moller, 1961: On the Radiative Equilibrium and Heat Balance of the Atmosphere. Mon. Wea. Rev. 89, 509-532.

Manabe, S. and R.F. Strickler, 1964: Thermal Equilbrium of the Atmosphere with a Convective Adjustment. J. Atmos. Sci. 21, 361-385.

Moller, F., 1943: Zur Erklärung der Stratosphären temperatur. Naturwissenschaften 31, 148.

Murakami, T., 1962: Stratospheric Wind Temperature and Isobaric Height Conditions During the IGY Period. Part I. Report No. 5, Planetary Circulation Project, Dept. of Meteor., Mass. Inst. Tech. pp. 1-213.

Newell, R.E., 1962: Transfer Through the Tropopause and Within the Stratosphere. Quart. J.R. Meteor. Soc. 89, 167-204.

Ohring, G., 1958: The Radiation Budget of the Stratosphere. J. Meteor., 15, 440-451.

Oort, A. H., 1962: Direct Measurement of the Meridional Circulation in the Stratosphere During the IGY. Report No. 6, Planetary Circulation Project, Dept. of Meteor., Mass. Inst. of Tech.

Oort, A.H., 1964b: On the Energy Cycle in the Lower Stratosphere. Doctor Thesis, University of Utrecht, pp. 110.

Oort, A.H., 1964a: On the Energetics of the Mean and Eddy Circulations in the Lower Stratosphere. Tellus 16, 309-327.

Peixoto, J.P., 1960: Hemispheric Temperature Conditions During the Year 1950. Sci. Report No. 4, Planetary Circulation Project, Dept. of Meteor., Mass. Inst. of Tech., pp. 1-211.

Peng, L., 1963: Stratospheric Wind Temperature and Isobaric Height Conditions During the IGY Period: Part II. Report No. 10, Planetary Circulation Project, Dept. of Meteor., Mass. Inst. of Tech. pp. 1-208.

Phillips, N.A., 1956: The General Circulation of the Atmosphere: A Numerical Experiment. Quart. J. R. Meteor. Soc. 82, 123-164.

Reed, R. J., J. L. Wolfe and H. Nishimoto, 1963: A Spectral Analysis of the Energetics of the Stratospheric Sudden Warming of Early 1957. J. Atmos. Sci., 20, 256-275.

Smagorinsky, J., 1963: General Circulation Experiments with the Primitive Equations. Mon. Wea. Rev. 91, 99-164.

Stackpole, J. D., 1964: Some Properties of A Low Order Model of Atmospheric Circulation. Ph. D. Thesis, Mass. Inst. of Tech.

Starr, V. P., 1960: Questions Concerning the Energy of Stratospheric Motions. Arch. Met. Geoph. Biobl. A, 12, 1-7.

Thompson, P.D., 1961: Numerical Weather Analysis and Predication. The Macmillan Co., N.Y., pp. 170.

Ward, F., and R. Shapiro, 1961: Meteorological Periodicities. J. Meteor. 18, 635-656.

White, R.M., 1954: The Counter-Gradient Flux of Sensible Heat in the Lower Stratosphere. Tellus 6, 177-178.

Wiin-Nielsen, A., 1959: A Study of Energy Conversion and Meridional Circulation for the Large-Scale Motion in the Atmosphere. Mon. Wea. Rev. 87, 319-332.

Wiin-Nielsen, A. and J.A. Brown, 1960: On Diagnostic Computations of Atmospheric Heat Sources and Sinks and the Generation of Available Potential Energy. Proc. Internat. Symposium on Numerical Weather Predication, Meteor. Soc. Japan, 593-613.

Wiin-Nielsen, A., J.A. Brown and M. Drake, 1963: On Atmospheric Energy Conversions Between the Zonal Flow and the Eddies. Tellus 15, 261-279.

APPENDIX

Define

$$Y_n^m = P_n^m(\mu)\, e^{im\lambda}$$

where $\mu = \sin\phi$, $P_n^m(\mu)$ is the associated Legendre function of order m and degree n (m, n integers $n \geq |m|$) and $P_n^m(\mu)$ is normalized so that

$$\int_{-1}^{1} P_{n_1}^m P_{n_2}^m \, d\mu = \begin{cases} 0 & n_1 \neq n_2 \\ 1 & n_1 = n_2 \end{cases} \qquad (A1)$$

and

$$P_n^{-m} = (-1)^m P_n^m \qquad (A2)$$

$Y_n^m(\mu,\lambda)$ is called a surface sperical harmonic of order m and degree n since it satisfies the equation

$$\frac{d}{d\mu}\left[(1-\mu^2)\frac{dG}{d\mu}\right] + \frac{1}{1-\mu^2}\frac{d^2G}{d\lambda^2} = -n(n+1)G$$

or

$$a^2 \nabla^2 G = -n(n+1)G \qquad (A3)$$

Here ∇^2 is the sperical two dimensional Laplacian operator and a is the radius of the sphere.

The following recurrence formulas will be useful.

$$(2n+1)\mu P_n^m N_n^m = (n-m+1) P_{n+1}^m N_{n+1}^m + (n+m) P_{n-1}^m N_{n-1}^m \qquad (A4)$$

$$(\mu^2-1)\frac{dP_n^m}{d\mu} N_n^m = (n-m+1) P_{n+1}^m N_{n+1}^m - (n+1)\mu P_n^m N_n^m \qquad (A5)$$

where

$$N_n^m = \left(\frac{2}{2n+1}\frac{(n+m)!}{(n-m)!}\right)^{\frac{1}{2}} \qquad (A6)$$

Now supposing

$$\nabla^2\psi(\lambda,\mu) = \sum_{n=|m|}^{\infty}\sum_{m=-\infty}^{\infty} \zeta_n^m Y_n^m \qquad (A7)$$

$$\theta(\lambda,\mu) = \sum_{n=|m|}^{\infty}\sum_{m=-\infty}^{\infty} \theta_n^m Y_n^m \qquad (A8)$$

and

$$\nabla^2 X(\lambda,\mu) = \sum_{n=|m|}^{\infty}\sum_{m=-\infty}^{\infty} \omega_n^m Y_n^m \qquad (A9)$$

are known and writting

$$J(\psi,\nabla^2\psi) = \sum_{n=|m|}^{\infty}\sum_{m=-\infty}^{\infty} A_n^m Y_n^m$$

$$J(\psi,\theta) = \sum_{n=|m|}^{\infty}\sum_{m=-\infty}^{\infty} B_n^m Y_n^m$$

$$\nabla\cdot\mu\nabla\psi = \sum_{n=|m|}^{\infty}\sum_{m=-\infty}^{\infty} C_n^m Y_n^m$$

$$\nabla\cdot\mu\nabla X = \sum_{n=|m|}^{\infty}\sum_{m=-\infty}^{\infty} D_n^m Y_n^m$$

iting

let us find A_n^m, B_n^m, C_n^m and D_n^m in terms of ζ_n^m, θ_n^m and ω_n^m.

By (A3) we have immdeiately

$$\psi = -a^2 \sum_{n=|m|}^{\infty} \sum_{m=-\infty}^{\infty} \frac{\zeta_n^m}{n(n+1)} Y_n^m \qquad (A10)$$

Since

$$J(A,B) = \frac{1}{a^2}\left(\frac{\partial A}{\partial \lambda}\frac{\partial B}{\partial \mu} - \frac{\partial A}{\partial \mu}\frac{\partial B}{\partial \lambda} \right) \qquad (A11)$$

By (A7) and (A10) we have

$$\sum_{g=|h|}^{\infty} \sum_{h=-\infty}^{\infty} A_g^h P_g^h e^{ih\lambda} = \frac{i}{2} \sum_{\substack{l=|k|\\ s=|r|}}^{\infty} \sum_{k,r=-\infty}^{\infty} \left[\frac{1}{l(l+1)} - \frac{1}{s(s+1)} \right]$$

$$\times \zeta_l^k \zeta_s^r e^{i(k+r)\lambda} \left[r P_s^r \frac{dP_l^k}{d\mu} - k P_l^k \frac{dP_s^r}{d\mu} \right]$$

If both sides of the equation are multiplied by $P_n^{-m} e^{-im\lambda}$ and integrated over the entire sphere, we obtain

$$A_n^m = \frac{i}{2} \sum_{\substack{l=|k|\\ s=|r|}}^{\infty} \sum_{k,r=-\infty}^{\infty} \left[\frac{1}{l(l+1)} - \frac{1}{s(s+1)} \right] \zeta_l^k \zeta_s^r \int_{-1}^{1} P_n^m \left[r P_s^r \frac{dP_l^k}{d\mu} - k P_l^k \frac{dP_s^r}{d\mu} \right] d\mu \qquad (A12)$$

where $k + r = m$, and use of (A1) and (A2) have been made.

Similarly, by (A8), (A10) and (A11) we obtain

$$B_n^m = -i \sum_{\substack{l=|k|\\ s=|r|}}^{\infty} \sum_{k,r=-\infty}^{\infty} \frac{\zeta_s^r \theta_l^k}{s(s+1)} \int_{-1}^{1} P_n^m \left[r P_s^r \frac{dP_l^k}{d\mu} - k P_l^k \frac{dP_s^r}{d\mu} \right] d\mu \qquad (A13)$$

where

$$k + r = m$$

Since

$$\nabla\cdot\mu\nabla\psi = \mu\nabla^2\psi + \nabla\mu\cdot\nabla\psi$$

or

$$\nabla\cdot\mu\nabla\psi = \mu\nabla^2\psi + \frac{1}{a^2}(1-\mu^2)\frac{\partial\psi}{\partial\mu}$$

By (A9) we have

$$\sum_{g=|h|}^{\infty}\sum_{h=-\infty}^{\infty} C_g^h P_g^h e^{ih\lambda} = \sum_{d=|c|}^{\infty}\sum_{c=-\infty}^{\infty}\left(\mu P_d^c - \frac{1-\mu^2}{d(d+1)}\frac{dP_d^c}{d\mu}\right)\zeta_d^c e^{ic\lambda}$$

If both sides of the equation are multiplied by $P_n^{-m} e^{-im\lambda}$ and integrated over the entire sphere,

$$C_n^m = \sum_{d=|m|}^{\infty}\zeta_d^m \int_{-1}^{1} P_n^m\left[\mu P_d^m - \frac{(1-\mu^2)}{d(d+1)}\frac{dP_d^m}{d\mu}\right]d\mu$$

Use of (A1) and (A2) have been made.

Making use of (A4) and (A5) we have

$$C_n^m = \sum_{d=|m|}^{\infty}\zeta_d^m \times\left[\frac{(d-m+1)(d+2)}{(d+1)(2d+1)}\frac{N_{d+1}^m}{N_d^m}\int_{-1}^{1} P_{d+1}^m P_n^m d\mu + \frac{(d+m)(d-1)}{d(2d+1)}\frac{N_{d-1}^m}{N_d^m}\int_{-1}^{1} P_{d-1}^m P_n^m d\mu\right]$$

or

$$C_n^m = \zeta_{n-1}^m\frac{(n-m)(n+1)}{n(2n-1)}\frac{N_n^m}{N_{n-1}^m} + \zeta_{n+1}^m\frac{n(n+m+1)}{(n+1)(2n+3)}\frac{N_n^m}{N_{n+1}^m}$$

Making use of (A6) we have

$$C_n^m = \frac{n+1}{n}\left[\frac{(n+m)(n-m)}{(2n+3)(2n+1)}\right]^{\frac{1}{2}} \zeta_{n-1}^m + \frac{n}{n+1}\left[\frac{(n+m+1)(n-m+1)}{(2n+3)(2n+1)}\right]^{\frac{1}{2}} \zeta_{n+1}^m \quad (A14)$$

similarly

$$D_n^m = \frac{n+1}{n}\left[\frac{(n+m)(n-m)}{(2n+3)(2n+1)}\right]^{\frac{1}{2}} \omega_{n-1}^m + \frac{n}{n+1}\left[\frac{(n+m+1)(n-m+1)}{(2n+3)(2n+1)}\right]^{\frac{1}{2}} \omega_{n+1}^m \quad (A15)$$

In this study m, n are small numbers. The integrals

$$L_{n_1 n_2 n_3}^{m_1 m_2 m_3} \equiv \int_{-1}^{1} P_{n_1}^{m_1}\left[m_2 P_{n_2}^{m_2}\frac{dP_{n_3}^{m_3}}{d\mu} - m_3 P_{n_3}^{m_3}\frac{dP_{n_2}^{m_2}}{d\mu}\right] d\mu$$

are evaluated by direct integration.

BIOGRAPHICAL NOTE

The author was born at Chiyang, Hunan, China on the twenty-first of September 1925. After graduating from high school, he received basic meteorological training and served in the Chinese Air Force Weather Service from 1947 to 1956. He received a B. S. degree from the National Taiwan University in 1960 and a M. A. degree in Meteorology from the University of California in 1962.

He is a member of the Chinese Meteorological Society.